A MODEL STUDY ON THE EFFECTS OF WALL STIFFNESS AND SURCHARGE ON DYNAMIC LATERAL EARTH PRESSURES

A THESIS SUBMITTED TO
THE GRADUATE SCHOOL OF NATURAL AND APPLIED SCIENCES
OF
MIDDLE EAST TECHNICAL UNIVERSITY

BY

ULAŞ ÇİLİNGİR

IN PARTIAL FULFILLMENT OF THE REQUIREMENTS
FOR
THE DEGREE OF MASTER OF SCIENCE
IN
CIVIL ENGINEERING

JULY 2005

Approval of the Graduate School of Natural and Applied Sciences

Prof. Dr. Canan Özgen

Director

I certify that this thesis satisfies all the requirements as a thesis for the degree of Master of Science.

Prof. Dr. Erdal Çokça

Head of Department

This is to certify that we have read this thesis and that in our opinion it is fully adequate, in scope and quality, as a thesis for the degree of Master of Science.

Prof. Dr. M. Yener Özkan

Supervisor

Examining Committee Members

Prof. Dr. Orhan Erol	(METU,CE)	
Prof. Dr. Yener Özkan	(METU,CE)	
Prof. Dr. Erdal Çokça	(METU,CE)	
Assoc. Prof. Dr. K. Önder Çetin	(METU,CE)	
M.S. Gülru Saadet Yıldız	(DSİ)	

I hereby declare that all information in this document has been obtained and presented in accordance with academic rules and ethical conduct. I also declare that, as required by these rules and conduct, I have fully cited and referenced all material and results that are not original to this work.

Name, Last name :

Signature :

ABSTRACT

A MODEL STUDY ON THE EFFECTS OF WALL STIFFNESS AND SURCHARGE ON DYNAMIC LATERAL EARTH PRESSURES

ÇİLİNGİR, Ulaş
MSc., Department of Civil Engineering
Supervisor: Prof. Dr. M. Yener ÖZKAN

June 2005, 97 pages

A model study on laterally braced sheet pile walls retaining cohesionless soil was conducted using 1-g shaking table. Lateral dynamic earth pressures, backfill accelerations and dynamic displacement of walls were measured. Input accelerations were kept between 0.03g to 0.27g. A data acquisition system consisting of dynamic pressure transducers, accelerometers, displacement transducer, signal conditioning board and a data acquisition card compatible with a personal computer was used during the study. Three different walls with thicknesses of 6.6, 3.2 and 2.0 mm were used in order to investigate the effects of changing wall stiffness value on lateral seismic pressures developed on the wall. In addition to that, steel blocks were placed on top of the backfill in order to simulate a surcharge effect of 1.57 kPa to 3.14 kPa during shaking. Amplification of input acceleration, incremental seismic lateral thrusts and corresponding maximum dynamic pressures, application point of the resultant, effect of stiffness and surcharge on maximum seismic lateral thrust and dynamic wall deflections were calculated by processing raw data stored. The results were compared to previous model studies and some analytical methods available.

Keywords: Laterally Braced Sheet Pile Wall, Model Tests, Effect of Wall Stiffness, Effect of Surcharge, Seismic Lateral Thrust

ÖZ

SÜRŞARJIN VE DUVAR RİJİTLİĞİNİN DİNAMİK YANAL TOPRAK BASINÇLARINA OLAN ETKİSİ ÜZERİNE BİR MODEL ÇALIŞMASI

ÇİLİNGİR, Ulaş
Yüksek Lisans, İnşaat Mühendisliği Bölümü
Tez Yöneticisi: Prof. Dr. M. Yener ÖZKAN

Haziran 2005, 97 sayfa

1-g sarsma tablası kullanılarak yanal olarak desteklenmiş, dolgu malzemesi kohezyonsuz kuru kum olan model palplanş duvarları üzerinde testler yapılmıştır. Yanal dinamik basınç değerleri, dolgu ivmeleri ve duvarların dinamik deplasmanları ölçülmüştür. Yer ivmeleri 0.03g den 0.26g ye kadar değişen değerlerde tutulmuştur. Çalışma sırasında kullanılan veri toplama sistemi dinamik basınç ölçerler, ivmeölçerler, bir adet yer değiştirme ölçeri, sinyal işleme kutusu ve kişisel bilgisayarlarla uyumlu veri toplama kartından oluşmaktadır. Değişen duvar rijitliğinin yanal dinamik basınçlarına olan etkisini araştırmak amacıyla 6.6, 3.2 ve 2.0 mm kalınlığında üç değişik duvar modeli kullanılmıştır. Ayrıca, sarsma sırasında dolgu malzemesi üzerine etki eden sürşarjın yanal dinamik basınç değerlerine olan etkisini araştırmak amacıyla dolgu malzemesi üzerine yerleştirilen ve 1.57 kPa dan 3.14 kPa ya kadar sürşarj sağlayan çelik levhalar kullanılmıştır. Dinamik basınç artışları, dinamik duvar itkisi artışları ve bu itki değerlerine ait dinamik basınçlar, toplam itkinin etki noktası, duvar rijitliğinin ve sürşarjın maksimum yatay duvar itkisine olan etkisi ve duvarların dinamik yer değiştirmeleri depolanan ham veri işlenerek hesaplanmıştır. Sonuçlar daha önceki model çalışmalarla ve bazı analitik çözümlerle karşılaştırılmıştır.

Anahtar Kelimeler: Yanal Olarak Desteklenmiş Palplanş Duvar, Model Testler, Duvar Rijitliğinin Etkisi, Sürşarjın Etkisi, Sismik Yanal İtki

TO MY FAMILY

ACKNOWLEDGEMENTS

This dissertation could not have been written without invaluable support and guidance of my supervisor Prof. Dr. M. Yener ÖZKAN throughout the study. He and Anil Yunatcı patiently guided me through the research. I am also thankful to Yüksel Proje Uluslararası A.Ş. and Geoteknik Construction Company for both financial and technical support they provided. Mr. Ali BAL and all other Soil Mechanics Laboratory staff are also sincerely acknowledged.

Finally, I would like to express my deepest thanks to my family and friends for their endless patience and understanding.

TABLE OF CONTENTS

LIST OF TABLES

LIST OF FIGURES

CHAPTER 1

INTRODUCTION

1.1 General Considerations

Retaining walls are built in order to support the lateral forces created by earth materials. These lateral forces result from sudden changes in elevation of the earth surface. They have several fields of usage especially in geotechnical engineering applications, in coastal and harbor engineering and in highway projects (Kramer, 1996).

Retaining walls can be classified regarding their lateral restraining conditions:

1. Laterally restrained walls: These type of walls are constructed to minimize the lateral deflections. They generally fail by yielding or fracturing. These can be classified as force governed walls.
2. Walls which are not laterally restrained: This type fails by translation, rotation or a combination of both. These can be classified as displacement governed walls (Richards & Elms, 1979).

There are several methods used for the seismic design and analysis of the retaining walls. Most common method is the famous Mononobe – Okabe theory which is a pseudodynamic version of the Coulomb's theory where earthquake loading is the product of a seismic coefficient with the weight of the gravity wall.

In addition to the frequently used Mononobe - Okabe method, Nazarian and Hadjian (1979) state that there are three types of approach used in the dynamic analysis of retaining walls:

- Analytical Solutions
- Numerical Modeling
- Experiments and Field observations

Tens of analysis methods were proposed based on these approaches. In addition to these Nazarian and Hadjian (1979) also state that analytical solutions may be divided into three as follows:

- Fully Plastic Solutions
- Solutions based on Elastic Wave Theory
- Inelastic Dynamic Solutions

In every case the validity of these methods shall be verified by experimental data or field observations.

1.2 Aim of the Study

This model study on laterally braced sheet pile walls aims to highlight following main points concerning the dynamic behavior: (1) The extent to which dynamic earth pressures developed behind the retaining wall and the application point of the total thrust on the wall when the wall is subjected to different input motions. (2) The effect of changing surcharge on the dynamic earth pressures. (3) The effect of changing wall stiffness to the dynamic earth pressures.

A shake table in Middle East Technical University Soil Mechanics Laboratory with dimensions 1m*1m*2m was used in the experiments. Input motions having frequencies between 2.94 to 3.70 Hz and amplitudes between 0.68 to 2.94 mm were created. In the soil bin, three model walls having 65 cm height and 98 cm width with varying thicknesses from 2mm to 6.6 mm were used. Backfill material was dry sand. Dynamic pressure transducers were installed on the wall; accelerometer transducers were placed in the backfill, about 10cm behind the wall. A displacement transducer was placed at a point on the wall 47.5 cm high from the base of the soil bin. In order to create surcharge effect, four 4 cm thick plates were placed on the backfill material where three of them have dimensions of 20cm by 97cm and one with the dimensions of 15cm by 97cm. A rotating motor with gears having different sizes were used to create input motion. The amplitudes of the input motions were adjusted by using an eccentric disk system.

Chapter 2 introduces a summary of the chronological development and the state of the art of the subject. Chapter 3 presents the detailed description of the apparatus and procedure used in the experiments. In Chapter 4 the results are presented and Chapter 5 gives discussion of the results. Chapter 6 conludes the subject.

CHAPTER 2

LITERATURE SURVEY ON SEISMIC BEHAVIOR OF RETAINING WALLS

2.1. General

Seismic design of the retaining walls is a matter of interest since the beginning of this century. For designing retaining walls, which are resistant to earthquake loading, different ideas and methods were developed.

There are two important factors for the design of the retaining walls subjected to seismic loads: (1) The amount of earth pressures developed behind the wall (2) The distribution of this pressure for the calculation of the application point of the total thrust. For this reasons analytical solutions, solutions based on experiments and other numerical methods such as finite element applications were developed.

Kramer (1996) points out some important results, which are derived mainly from model tests and numerical analyses of the gravity retaining walls, as follows:

1. Movement of walls occurs by translation and/or rotation. The relative amounts of these movements depend on the type of wall and one or the other may dominate the type of movement.
2. The mode of wall movements is the main factor for the amount and distribution of the dynamic pressures developed on the back of the wall.
3. If the wall moves towards the backfill, maximum soil thrust develops. The minimum soil thrust occurs in the opposite case.
4. The shape of the dynamic earth pressure distribution is transient. It changes as the wall moves. Therefore the point of application also changes. The position of the application point of the total thrust goes up the wall as the wall moves towards backfill and down as the wall moves away from the backfill.

5. Dynamic wall pressures increase significantly near the natural frequency of the wall backfill system. Near these frequencies the permanent wall displacements are also highest. The deflections of the different parts of a wall may also be out of phase relative to each other.
6. After the strong shaking ends increased residual pressures may develop behind the wall.

Following section gives a brief summary of the chronological development of the subject. After that, frequently used design methods will be given. In the last section information about the State-of-the Art and the effects of the surcharge and stiffness on the wall behavior will be presented.

2.2. A Brief Summary about the Chronological Development of the Subject

As Nazarian and Hadjian (1979) stated, the solution methods used for the dynamic behavior of retaining walls can be divided into four categories:

1. Fully Plastic Solutions: This kind of analytical approach assumes that there is a definite failure surface developed behind the retaining wall. The pseudo-static analysis of the wedge behind the wall gives analytical expressions about the amount and the point of application of the total dynamic thrust. The most famous method is Mononobe – Okabe method.
2. Solutions based on Elastic Wave Theory: This approach assumes that the whole wall and backfill system moves in elastic range. Nazarian and Hadjian (1979) state that “the application of a design method using Elastic Wave Theory would only be suitable for the movements of wall-soil system in elastic range.” There are solutions developed by several researchers such as Wood (1973), Scott (1973). But almost all the papers dealing with elastic wave theory ignores the effects of surcharge on the backfill.
3. Inelastic Dynamic Solutions: These methods are based on the elasto-plastic models. The knowledge is still not enough. Solutions are complex and mostly based on Finite Element Methods. Several researchers such as Clough & Duncan (1971), Lee & Harrington (1972) and Subzeveri & Ghahramani (1974) tried to treat the dynamic behavior of retaining walls by the use of this approach (Nazarian and Hadjian, 1979).
4. Experiments and Field Observations: There are a number of methods available. They are given in this section briefly.

First attempt to calculate the magnitude of the dynamic earth pressure developed behind retaining walls during earthquakes was the famous Mononobe-Okabe (M-O) approach which formulates the problem by the use of Coulomb's active earth pressure theory. They considered that the point of application of the total thrust is H/3 above the base of the retaining wall. This method is still widely used for the design of the retaining walls. A detailed description of this method will be given in the following section. A model study performed by Mononobe & Matsuo in 1929 and Jacobsen in 1939 also showed reasonable agreement in the maximum pressure values with Mononobe – Okabe (M-O) method (Seed & Whitman, 1970). Jacobsen, in 1939, stated that for base accelerations lower than 0.4 g M-O formulation for the maximum dynamic earth pressures is realistic. Jacobsen also found that the application point of pressure is 2/3 H above the base (after Seed & Whitman, 1970).

Ishii, Arai and Tsuchida (1960) performed model studies on retaining walls and found that maximum lateral pressures are in good agreement or lower than the M-O values. In the paper it is stated that the point of application of the total thrust is between 0.33 H to 0.40 H above the base. They first introduced the fact that the lateral earth pressures change significantly during the wall movements. They also stated that for acceleration values up to 0.5 g the sand deposit behind the retaining wall behaves as rigid body as in the case of M-O formulation. They observed that sand consolidated, wall pressures increased residually and phase differences developed between base motions and wall pressures.

Matuo and Ohara (1960) performed model studies and analytical solutions on quay walls and found that the amplitude of maximum pressure decreases as the displacement increases. They stated that the dynamic pressure is larger at the top of the wall which is contrary to the idea that the application point of the total thrust is 1/3 H above the base. They derived an analytical model. But experimental values are significantly lower than the analytical calculations. They considered this as the effect of experimental apparatus.

Murphy (1960) conducted model tests on gravity walls supporting sand layers. These tests showed that retaining walls fail by sliding and tilting occurring at the same time. He showed that failure in these model tests occurred by outward rotation about the toe with a failure plane incline at 35° to the horizontal. The behavior was consistent with the results of M-O method.

First attempts to analyze the dynamic pressures using a model based on elastic wave theory are also dating back to 1960's. "Matuo and Ohara (1960) have found an approximate elastic solution for the dynamic soil pressure on a rigid wall for translational motions using a two-dimensional analytical model. However, they have simplified the problem by assuming no vertical displacement in the soil mass. The basic equations were derived using classical wave theory, assuming that the wall was stationary, with the waves traveling in the soil media and impinging on the surface of the wall creating resulting stresses. They have also included charts showing experimental verification of the theoretical results obtained". (Nazarian & Hadjian, 1979)

Another study, where elastic wave theory is used, was conducted by Scott in 1973. In this model one dimensional elastic shear beam is connected to the retaining wall by Winkler springs. The flexibility of the retaining wall is represented by a rigid wall which is hinged to the base. Figure 2.1 shows the details of the Scott's model. "An interesting finding indicates that, for a rigid wall and with soil stiffness properties increasing with depth, the solutions based on the first mode could give a triangular pressure distribution. Under these conditions (i.e. straight line first mode), no mode other than the first mode will develop a base moment. However higher modes will contribute additional pressures" (Nazarian & Hadjian, 1979).

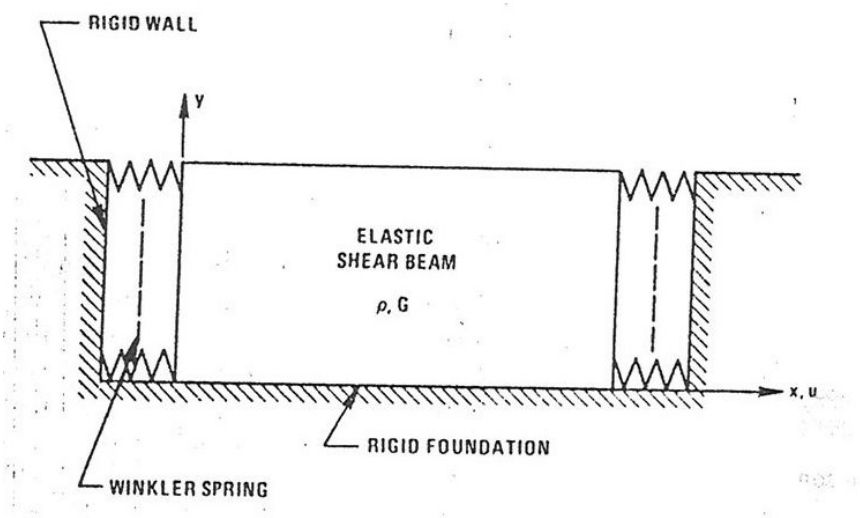

Figure 2.1 Scott's Elastic Model (after Nazarian & Hadjian, 1973)

"Wood (1973) has presented an extensive study of the behavior of rigid soil-retaining structures subjected to earthquake motions. The study is based on linear elastic theory and idealized representations of wall-soil systems. The static solutions were referred to earlier. The present analysis emphasizes the dynamic solutions. The normal mode solution has been derived for an

arbitrary time-dependent forcing of the rigid boundaries. However, results are given for modal forces and for harmonic forcing of the rigid boundaries. The modal responses are also used to compute the response by Response Spectrum method and statistical estimates of the maximum wall forces have been obtained by idealizing the earthquake forces as a stationary Gaussian random process" (Nazarian & Hadjian, 1973).

"Within assumptions made, Wood's solution is an important contribution to the understanding of the forces on retaining walls that do not displace sufficiently to develop failure planes. Disregarding any large strains due to the earthquake motions in the free field, in elastic analysis as given by Wood is considered appropriate. However, two important assumptions need to be evaluated: (1) The assumption of a finite layer of soil down to the base of wall is not a generally realizable situation, and thus a normal mode solution may not provide useful results; and (2) the treatment of damping in the solution. Soil-structure interaction studies indicate beyond any doubt that radiation effects could become important. The model does not have this property, and energy is dissipated only by an assumed modal damping mechanism. The cases where elastic solutions are appropriate would in all probability also exhibit significant radiation effects.

Wood further suggests that if relative displacements of building foundation are sufficient to produce plastic state of stresses in the backfill, the maximum pressure distributions may be controlled by passive earth pressures rather than active pressures" (Nazarian & Hadjian, 1979)

Table 2.1 shows a comparison between Wood's and Scott's methods that are used in the solution of the same problem in terms of forces, moments and moment arms.

Table 2.1 A comparison between Wood's and Scott's Solutions (after Nazarian & Hadjian, 1979)

Author	**Moment arm**	**Force, in pounds**	**Moment, in foot-pounds**	**Remarks**
Wood	0.6 H	19,000	230,000	Elastic, body force 1500 fps (460 m/s) shear wave velocity
Scott	0.62 H	11,000	137,000	

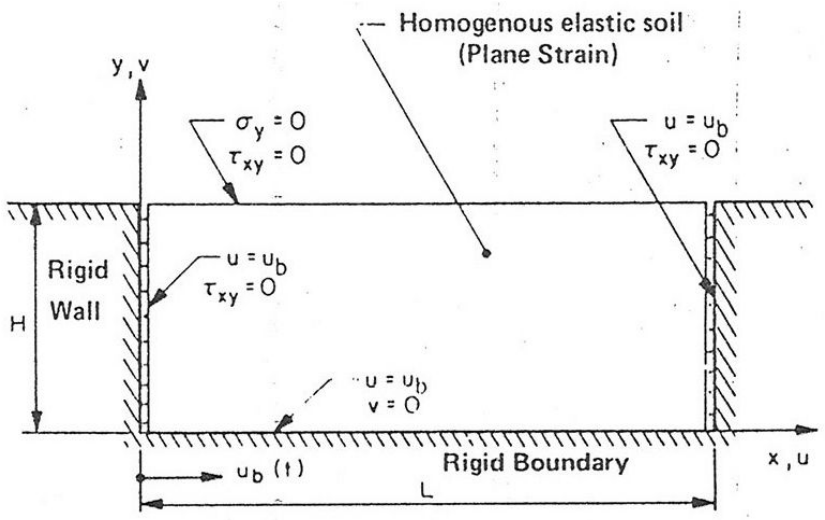

Figure 2.2 Wood's Model (after Nazarian & Hadjian, 1979)

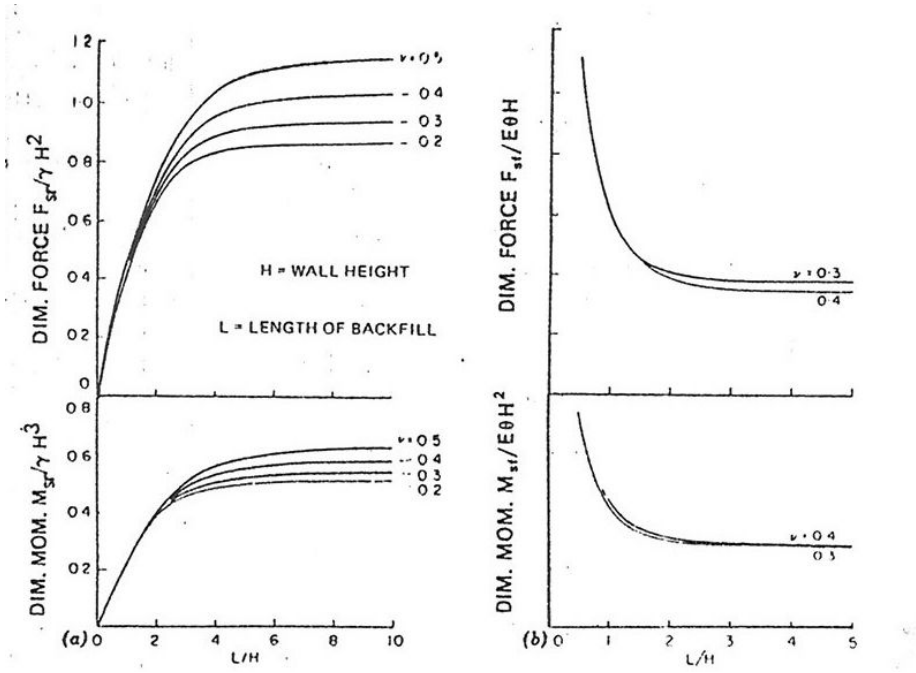

Figure 2.3 Wood's Elastic Model. Force and Moment on: (a) Smooth Rigid Wall for One-g Static Horizontal Body Force; (b) Statically Forced Smooth Rotating Wall (after Nazarian & Hadjian, 1973)

Seed and Whitman published a State-of-the Art research paper in 1970 and recommended that "for seismic design of retaining walls and bridge abutments above water table the factor of safety provided in static case would be adequate to prevent damage during earthquakes." They also stated that "it is apparent that most walls with horizontal backfill and no surcharge can withstand substantial earthquake shaking and conservatively designed walls can withstand very strong motions without detrimental translation."

They listed blasting effects and effects of explosions on earth retaining structures and give examples about protective construction.

Prakash and Basavanna stated in their paper in 1969 that the earth pressure distribution behind a gravity retaining wall is nonlinear. They concluded that this distribution is a function of wall friction angle, angle of internal friction of the backfill and vertical and horizontal earthquake accelerations. They concluded that the application point of the total seismic thrust is higher than 1/3 H. They described the height of the application point with the following formula:

$$h_a = c_{ha} * H / 3 \qquad (2.1)$$

where H is the height of the wall and C_{ha} is a factor depending on coefficient of horizontal acceleration k_h. Figure 2.4 shows the relationship between C_{ha} and k_h (Seed and Whitman, 1970).

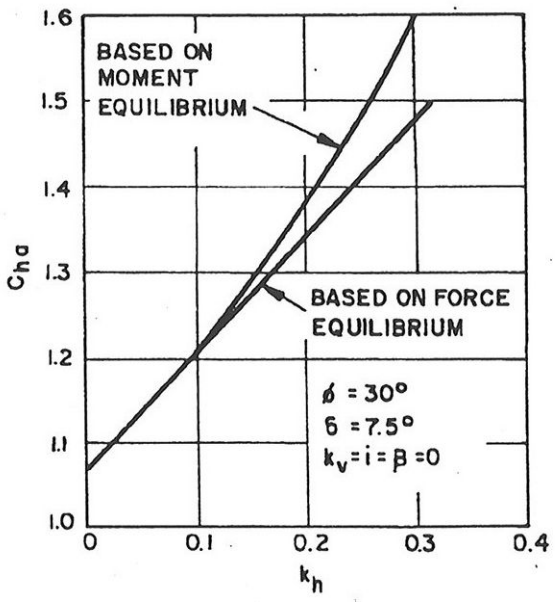

Figure 2.4 C_{ha} versus horizontal acceleration coefficient k_h (after Seed and Whitman, 1970)

In 1970 Saran and Prakash published a paper on mathematical derivations considering a slice of a failure wedge. They stated that the application point of the dynamic thrust shifts towards the base if the equilibrium forces are considered. This effects increases with increasing accelerations. Two other publications of Saran and Prakash were on the combined effects of sliding, overturning, and bearing pressures. The second paper is an improvement to the M-O method. It gives solutions to the dynamic active and passive pressures for three modes of wall movement: translation, rotation about the bottom, rotation about the top.

Nandakumaran and Joshi (1973) state that the height of point of application of dynamic thrust from the bottom of the wall increases with increasing surcharge.

Ichihara and Matsuzawa (1973) conducted model tests on shaking table with a bin having dimensions 200*100*75 cm. They observed that the application point of total thrust shifts upward with increasing accelerations and becomes 0.45H at approximately 0.3 g. They derived an empirical equation for the application point.

Richards and Elms (1979) summarized a series of theoretical and experimental investigations on the seismic behavior of gravity, tied-back and reinforced-earth retaining walls. They stated that

“the Newmark sliding-block model is shown to be appropriate for displacement-controlled design, though modifications and limitation are discussed” within that paper. Their test results show that “sliding block behavior only takes place after a high limiting acceleration has been passed. Where rotational failure is expected, walls will be stronger than anticipated. Elastic resonance effects are likely to be significant for full-size walls.” They also state three important conclusions on seismic behavior of gravity retaining walls: (1) “The dynamic soil pressures on gravity retaining walls are greater than those found by M-O method due to the effect of wall inertia.” Note that the inertial effects were first introduced in this paper. (2) It is wise to assume that the point of application of dynamic thrust is at H/2 with uniform distribution of pressure. (3) It is important to design the walls considering the wall displacements.

Sherif, Ishibashi and Lee (1982) conducted model tests on rigid retaining walls and found that the dynamic total active earth pressures are approximately 30% higher than those predicted by M-O method. In addition to this observation they concluded that those dynamic incremental pressures are considerably smaller than the elastic solution of Wood (1973).

Measurements on a prototype, full scale wall conducted by Fukuoka & Imamura (1984) also showed that the pressures developed are higher than those predicted by M-O method.

With the introduction of the computers, complex numerical solutions like finite element method were introduced into the subject. Nadim and Whitman (1983) found after their finite element solutions that there is considerable amplification of acceleration in the backfill in the case of dynamic loading.

2.3. Frequently Used Design Methods

Seismic design methods for the construction of retaining walls can be classified into two: (1) Methods based on allowable seismic pressures. (2) Design methods based on maximum allowable displacements. More detailed descriptions of the two elastic methods - Wood’s and Scott’s Methods – will be given in the last section.

2.3.1. Design Methods based on Seismic Pressures

2.3.1.1. Mononobe – Okabe Method

As previously stated Mononobe – Okabe method is an extension of Coulomb's active earth pressure theory. Forces acting on the wedge behind a gravity retaining wall are illustrated in Figure 2.5.

In Mononobe – Okabe method, the total seismic active thrust is given by the following expression:

$$P_{AE} = \frac{1}{2} \cdot K_{AE} \cdot \gamma \cdot H^2 \cdot (1 - k_v) \tag{2.2}$$

where,

K_{AE} = dynamic active earth pressure coefficient

γ = unit weight of the backfill

H = height of the retaining wall

K_v = coefficient of vertical acceleration

The dynamic active earth pressure coefficient K_{AE} is found using following formula:

$$K_{AE} = \frac{\cos^2(\phi - \theta - \beta)}{\cos\theta \cdot \cos^2\beta \cdot \cos(\delta + \beta + \theta)\left[1 + \sqrt{\frac{\sin(\phi + \delta) \cdot \sin(\phi - \theta - i)}{\cos(\delta + \beta + \theta) \cdot \cos(i - \beta)}}\right]^2} \tag{2.3}$$

where,

$$\theta = \tan^{-1}\left(\frac{k_h}{1 - k_v}\right) \tag{2.4}$$

For the definitions of the angles i, β, ϕ, δ see figure 2.5.

Total seismic thrust P_{AE} is the sum of the static earth pressure P_A and dynamic increment ΔP_{AE} as follows:

$$P_{AE} = P_A + \Delta P_{AE} \tag{2.5}$$

The static component of this equation is the same as the Coulomb's active earth pressure formula as stated below.

$$P_A = \frac{1}{2} \cdot K_A \cdot \gamma \cdot H^2 \tag{2.6}$$

where,

$$K_A = \frac{\cos^2(\phi - \beta)}{\cos^2 \beta \cdot \cos(\delta + \beta)\left[1 + \sqrt{\frac{\sin(\phi + \delta) \cdot \sin(\theta - i)}{\cos(\delta + \beta) \cdot \cos(i - \beta)}}\right]^2} \tag{2.7}$$

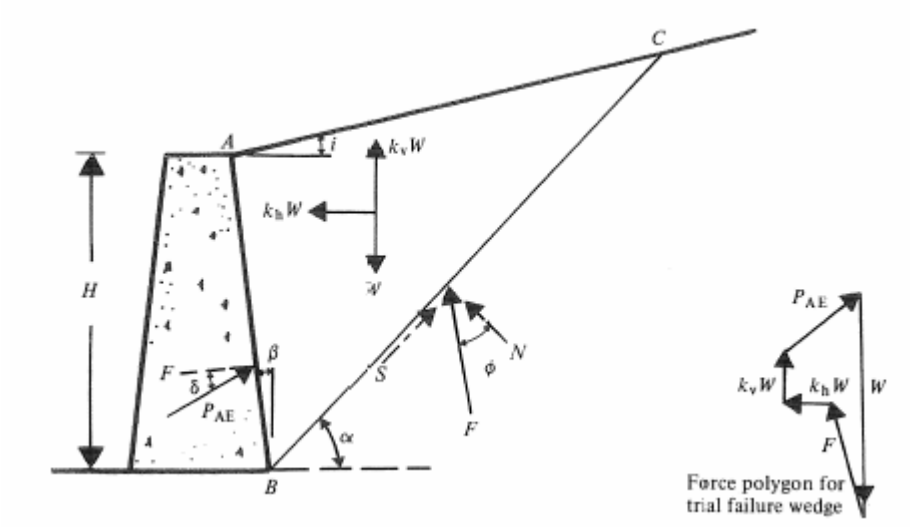

Figure 2.5 Forces for M-O method in active case (after Das,1983)

Wall shape and dimensions are calculated using above formulae, where total seismic active thrust acts 0.33 H above the base. If the stability against overturning and sliding is within the allowable limits considering the factor of safety, the design is adequate. If not, wall dimensions are changed and calculations are conducted again until a safe design is at hand.

2.3.1.2. Steedman and Zeng Method

Steedman – Zeng method is a pseudodynamic analysis which accounts for phase differences and amplification effects developing during an earthquake (Kramer,1996).

If the active wedge shown in Figure 2.6 is considered, acceleration at a depth z can be expressed as follows:

$$a(z,t) = a_h \sin\left[\omega\left(t - \frac{H-z}{v_s}\right)\right] \tag{2.8}$$

where

a_h = amplitude of harmonic horizontal input acceleration

ω = cyclic frequency of harmonic input motion

t = time

v_s = velocity of vertically propagating harmonic shear wave

H = height of the wall

Z = depth

The mass of a thin element in the active wedge is:

$$m(z) = \frac{\gamma}{g} \cdot \frac{H-z}{\tan\alpha} dz \tag{2.9}$$

where

γ = unit weight of the backfill material

g = gravitational acceleration

For δ, ϕ and α refer to figure 2.6.

The total inertial force acting on the wall can therefore be given as:

$$Q_h(t) = \int_0^H m(z) \cdot a(z,t) \cdot dz = \frac{\lambda \gamma a_h}{4\pi^2 g \tan\alpha}\left[2\pi H \cos\omega\zeta + \lambda(\sin\omega\zeta - \sin\omega t)\right] \tag{2.10}$$

where

$$\lambda = 2\pi v_s / \omega \tag{2.11}$$

and

$$\zeta = t - \frac{H}{v_s} \tag{2.12}$$

By resolving the forces on the wedge we can obtain the total soil thrust as follows:

$$P_{AE}(t) = \frac{Q_h(t)\cos(\alpha - \phi) + W\sin(\alpha - \phi)}{\cos(\delta + \phi - \alpha)} \tag{2.13}$$

If we differentiate the total soil thrust we can obtain the total earth pressure distribution as follows:

$$P_{AE}(t) = \frac{\delta P_{AE}(t)}{\delta z} = \frac{\gamma z}{\tan\alpha}\frac{\sin(\alpha - \phi)}{\cos(\delta + \phi - \alpha)} + \frac{k_h \gamma z}{\tan\alpha}\frac{\cos(\alpha - \phi)}{\cos(\delta + \phi - \alpha)}\sin\left[\omega\left(t - \frac{z}{v_s}\right)\right] \tag{2.14}$$

The height of application of total thrust varies with time according to the following formula:

$$h_d = H - \frac{2\pi^2 H^2 \cos\omega\zeta + 2\pi\lambda H \sin\omega\zeta - \lambda^2(\cos\omega\zeta - \cos\omega t)}{2\pi H \cos\omega\zeta + \pi\lambda(\sin\omega\zeta - \sin\omega t)} \tag{2.15}$$

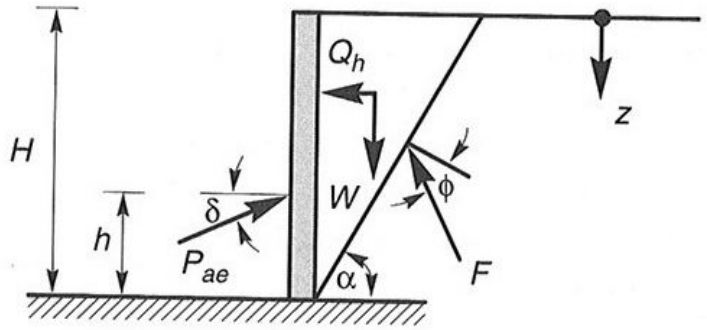

Figure 2.6 Forces acting on Steedman-Zeng wedge and their notations (after Kramer,1996)

2.3.2. Displacement Based Design Methods

2.3.2.1. Richard and Elms Method

This method considers the wall inertia effect and therefore suitable for gravity type retaining walls. For no wall movement the required weight of the wall is expressed as follows:

$$W_w = \frac{1}{2}\gamma H^2 K_{AE}\left[\frac{\cos(\delta+\beta)-\sin(\delta+\beta)\tan\phi_b}{(\tan\phi_b-\tan\theta)}\right] \tag{2.16}$$

where

γ = unit weight of the wall material

H = height of the wall

$$\tan\theta = \frac{k_h}{(1-k_{v)}} \tag{2.17}$$

For δ and β please refer figure 2.5. ϕ_b is the base friction angle.

Richard and Elms (1979) state that for the use of K_{AE} considering the maximum ground acceleration leads to uneconomical design of wall. Therefore using smaller wall dimensions is more feasible where the wall is allowed to move for a small amount.

For the calculation of the total relative displacement of a wall following relation is given:

$$D = 0.087 \frac{V^2}{Ag} \left(\frac{N}{A} \right)^{-4} \tag{2.18}$$

where

A=maximum acceleration coefficient
V=maximum velocity
N=maximum critical acceleration coefficient and defined as follows:

$$N = A \left(\frac{0.087 V^2}{DAg} \right)^{\frac{1}{4}} \tag{2.19}$$

Following steps are followed in the design of gravity retaining walls by using Richards and Elms method:

1. An allowable design displacement D is chosen.
2. N is calculated for known values of A and V from Equation 2.19
3. K_{AE} is calculated from Mononobe-Okabe formulation (See Equation 2.3). Instead of k_h, N is used for the calculation of θ.
4. The required wall weight is computed from Equation 2.16.

2.3.2.2. Nadim and Whitman Method

The method proposed by Nadim and Whitman takes the effect of amplification of motion in the backfill into account. It consists of following steps:

1. Fundemental frequency f_1 of the backfill for the design earthquake is calculated as follows:

$$f_1 = \frac{V_s}{4H} \tag{2.20}$$

where

V_s= shear wave velocity
H = thickness of the backfill

2. $\frac{f}{f_1}$ ratio is calculated where f is the estimated dominant frequency of the expected ground motion. If this ratio is smaller than 0.25, the effect of ground motion amplification is neglected. If it is in the vicinity of 0.5 then the peak acceleration, A, and the peak velocity, V, of the design earthquake is increased by 25%-30%. If it is between 0.7 and 1.0 increase A and V by 50%.

3. Then using the new values of A and V retaining wall design is utilized based on a rigid plastic method. (e.g. Richards and Elms method) (Nadim and Whitman, 1983).

2.3.3. Elastic Methods and Methods Based on Elastic Wave Theory

These methods are mainly applicable for non-yielding walls where displacements do not cause plastic deformations. Therefore, as the range of input accelerations and amplitude of the motions are considered, elastic methods are more suitable in analyzing model test conducted in this study.

There are two important elastic methods developed by Wood (1973) and Scott (1973) which will be presented in this section.

2.3.3.1 Wood's Model

Wood's model considers a homogenous linear elastic soil body trapped between two rigid walls as shown in Figure 2.2. The walls are in such a distance that the pressure developed on one wall does not influence the pressure values on the other one. Wood's study clearly showed that for low frequency input motions the amplification effects are negligible [i.e. for motions less than the fundamental frequency of unrestrained backfill ($f_0 = \upsilon_s / 4H$)]. For this range of frequencies wall pressures can be obtained using elastic methods. Wood suggested that the maximum seismic thrust is at a height of 0.63 H from the base. Following equations are used for

the calculation of incremental seismic thrust for a uniform, constant, horizontal acceleration (after Kramer, 1996).

$$\Delta P_{eq} = \gamma \cdot H^2 \cdot \frac{a_h}{g} \cdot F_p \tag{2.21}$$

where

ΔP_{eq} = Seismic incremental thrust

γ = Unit weight of the backfill

a_h =maximum horizontal acceleration

g =gravitational acceleration

F_p =Dimensionless thrust factor as given in Figure 2.7 for different Poisson's ratio (v) values.

Wood expressed the dynamic overturning model as follows:

$$\Delta M_{eq} = \gamma \cdot H^3 \cdot \frac{a_h}{g} \cdot F_m \tag{2.22}$$

where

ΔM_{eq} = Seismic incremental overturning moment

γ = Unit weight of the backfill

a_h =maximum horizontal acceleration

g =gravitational acceleration

F_m =Dimensionless moment factor as given in Figure 2.8 for different Poisson's ratio (v) values.

Then, the point of application of the dynamic thrust can be found using the following formula:

$$h_{eq} = \frac{\Delta M_{eq}}{\Delta P_{eq}} \tag{2.23}$$

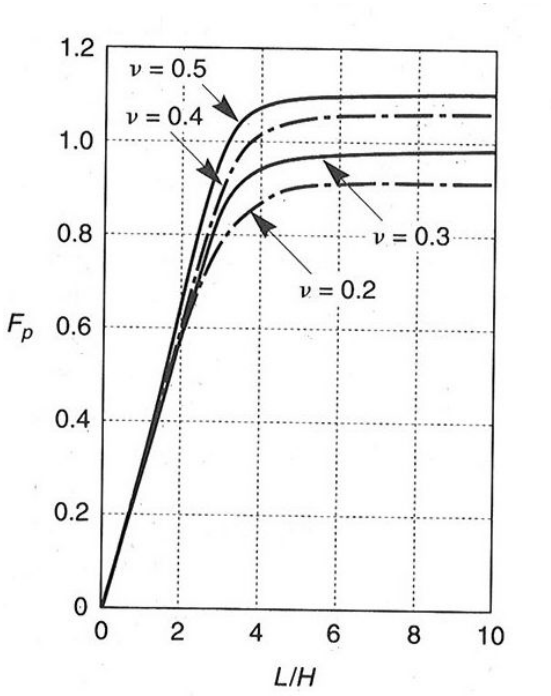

Figure 2.7 Dimensionless thrust factor for different Poisson's ratio (v) values (after Kramer,1996)

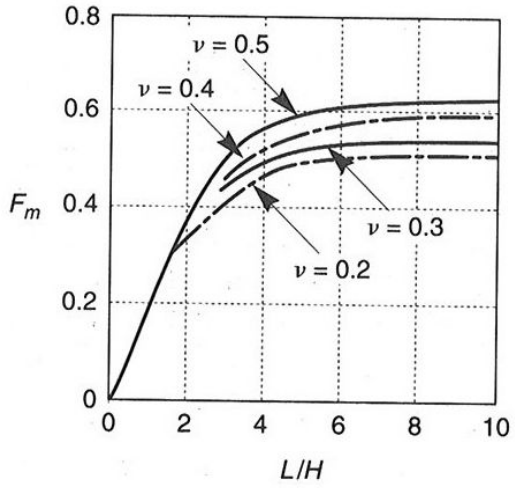

Figure 2.8 Dimensionless moment factor for different Poisson's ratio (v) values (after Kramer,1996)

2.3.3.2. Scott's Model

Scott considered a one-dimensional elastic shear beam connected to the wall by Winkler springs as shown in Figure 2.1. Closed form solution for the maximum seismic force on the wall is obtained as follows:

$$p_{m1} = \frac{2}{\pi} \cdot p_0 \cdot H \tag{2.24}$$

$$p_0 = \frac{32 \cdot G \cdot S_{v1} \cdot (1-\nu)}{\pi \cdot \omega_1 \cdot L \cdot (1-2\nu)} \tag{2.25}$$

$$\omega_1 = \frac{\pi \cdot V_s}{2 \cdot H} \cdot \left[1 + \frac{64}{\pi^2} \cdot \frac{(1-\nu)}{(1-2\nu)} \left(\frac{H}{L} \right)^2 \right]^{\frac{1}{2}} \tag{2.26}$$

where

p_{m1}=maximum total seismic pressure on the wall

p_0 = maximum pressure at the ground surface

ω_1 = fundamental frequency of the system

V_s= shear wave velocity

G = shear modulus

ν = Poisson's ratio

H = height of the wall

L = distance to the problem boundary

The height of the point of application of total seismic thrust is given as 0.64H above the base of the wall (Scott, 1973).

"Velestos and Younan (1994) and Velestos, Parikh and Younan (1995) provided approximate solutions to the seismic pressure problem and concluded that Scott's model (1975) which does not consider the radiational damping capacity of the medium may lead to large errors (after Çalışan, 1999)."

2.4. State-of-the Art

2.4.1. General

In this section the State-of-the Art regarding the research on the effect of wall stiffness and surcharge on seismic pressures developed on the wall in the case of low frequencies (elastic case) will be presented.

2.4.2. Effect of Wall Stiffness

Velestos and Younan (1997) states that “the existing elastic solutions are limited to nondeflecting rigid walls and do not provide for the important effect of wall flexibility.” According their research on rigid walls which are elastically constrained against rotation at their base, both the magnitudes and distributions of the dynamic wall pressures and forces are quite sensitive to the flexibility of the base constraint. They conclude that “for the soil-wall system examined, both the distributions of the wall-displacements, wall pressures, and associated forces induced by horizontal ground shaking are quite sensitive to the flexibilities of the wall and its base. Increasing either flexibility reduces the horizontal extensional stiffness of the retained medium relative to its shearing stiffness, and this reduction decreases the proportion of the soil inertia forces that gets transferred to the wall and, hence, the forces developed in it.

For realistic wall flexibilities the total wall force or base shear is one-half or less that obtained for a fixed-based, rigid wall, and the corresponding reduction in the overturning base moment is even larger. With the information that has been presented, the precise dependence of these critical forces on the flexibilities of the wall and its base may be evaluated readily (Velestos and Younan, 1997).”

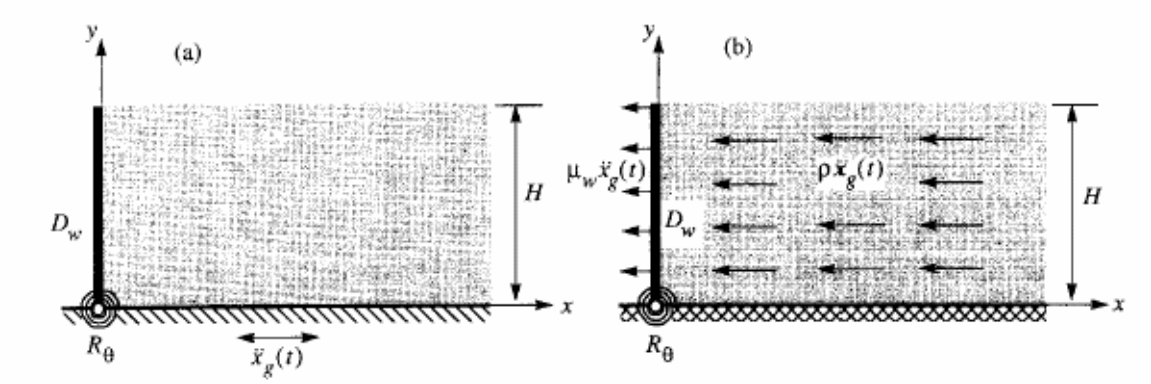

Figure 2.9 Soil Wall System investigated by Velestos and Younan (1997) (a) Base-Excited System (b) Force – Excited System (after Velestos and Younan, 1997)

Figure 2.10 shows the distributions of wall pressures for statically excited systems with different wall and base flexibilities. For statically excited systems the authors refers to such systems where the dominant frequency of the excitations are extremely small compared to the fundamental frequency of the soil wall system.

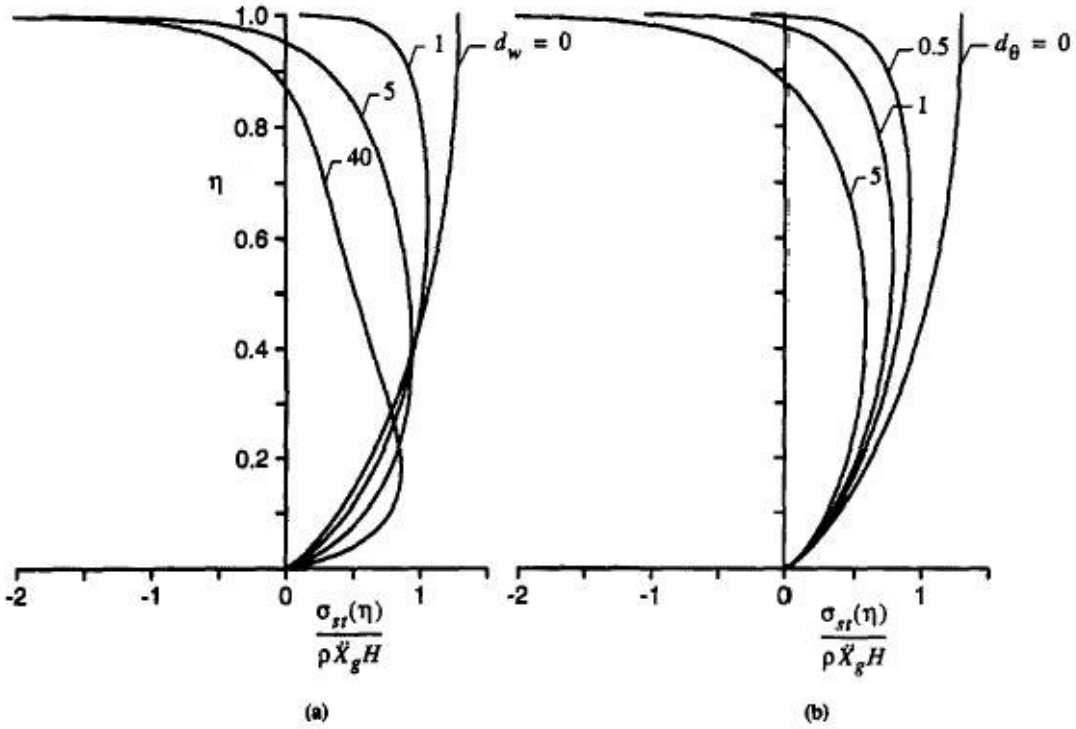

Figure 2.10 Distributions of Wall Pressure for Statically Excited Systems with Different Wall and Base Flexibilities (a) for $d_\theta = 0$ (b) for $d_w = 0$ (after Velestos and Younan, 1997)

In the above figure:

$\eta = y / H$ = dimensionless vertical position coordinate

d_θ = relative flexibility of the rotational base constrained and retained medium

d_w =relative flexibility of the wall and the retained medium

ρ = mass density of the soil medium

H = height of the wall

$\ddot{X}_g$ = maximum ground acceleration

$\sigma_{st}(\eta)$ = wall pressure

Figure 2.11 shows the normalized effective heights for the statically excited systems with different wall and base flexibilities.

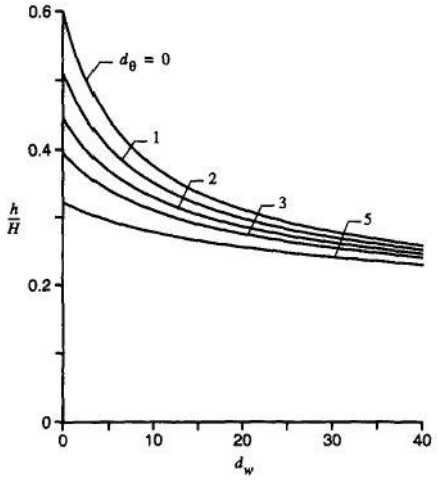

Figure 2.11 Normalized effective heights for the statically excited systems with different wall and base flexibilities (after Velestos and Younan, 1997)

Figure 2.12 shows the difference in pressure distributions between rigid and very-flexible non-sliding walls in pseudo-statically excited wall-backfill systems. As you can see Wood's solution gives considerably higher values.

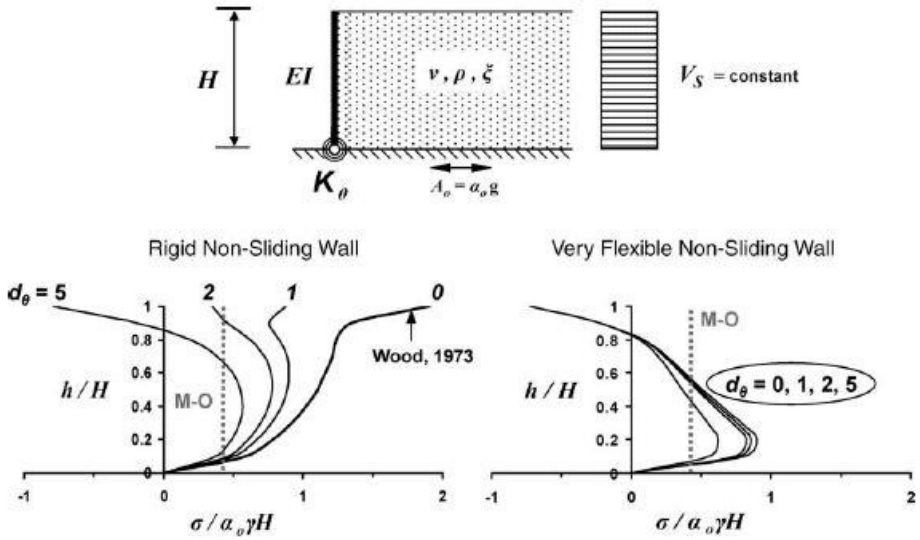

Figure 2.12 Elastic dynamic earth-pressure distribution of a pseudo-statically excited one-layer system for a non-sliding wall (after Gazetas et al., 2004)

2.4.3. Effect of Surcharge

Caltabiano et al. (2000) proposed a new method which is based on the pseudo-static equilibrium of the soil-wall systems with surcharge. But the formulas provided are only applicable to yielding systems with an inclined failure surface behind the wall. The effect of the intensity of the surcharge and of its distance from the wall is investigated and they are compared with the systems without surcharge.

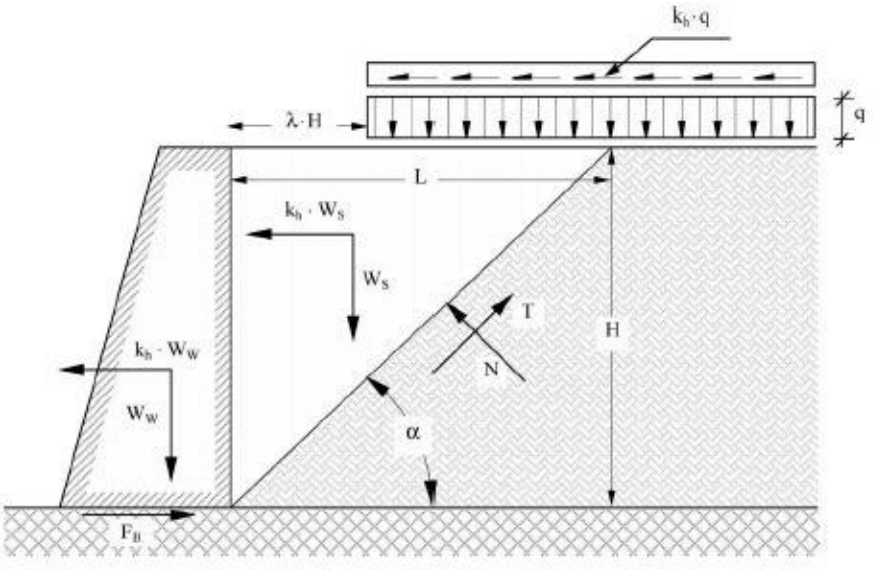

Figure 2.13 Soil-Wall System considered by Caltabiano et al. (2000)

For the system shown in Figure 2.13 the dynamic equilibrium condition is given by the following expression:

$$F_I + F_S + F_D = 0 \tag{2.27}$$

where F_I, F_s and F_D are, respectively, the resultant inertia forces acting on the system, the resultant of the lateral stresses acting on the wall and the resultant of the shear stresses acting at the base of the wall. The effect of the surcharge on the system is considered as a shear force acting on the top of the backfill which has a magnitude of $k_h \cdot q$ (See Figure 2.13).

After solving the system using limit equilibrium conditions the following expression for the critical acceleration is obtained:

$$k_h = \frac{-(2A_1 + A_2 A_3) + \sqrt{(2A_1 + A_2 A_3)^2 + A_0 (A_2{}^2 - 4A_4)}}{A_0} \tag{2.28}$$

where

$$A_0 = (Q\lambda - \Gamma + R\Phi)^2 \tag{2.29}$$

$$A_1 = \left[\Gamma\mu\Phi + Q\lambda - \Phi^2(Q\lambda - \Gamma)\right](1+Q) \tag{2.30}$$

$$A_2 = \Gamma\mu - \left[1 + Q(1+\lambda\Phi)\right] \tag{2.31}$$

$$A_3 = (\lambda - \Phi)Q - (\Gamma + \Phi) \tag{2.32}$$

$$A_4 = (1+Q)(\Gamma\mu\Phi + Q\lambda)\Phi \tag{2.33}$$

$$\Phi = \tan\varphi \tag{2.34}$$

$$Y = \tan\alpha \tag{2.35}$$

$$\Gamma = \frac{2W_w}{\gamma H^2} \tag{2.36}$$

$$Q = \frac{2q}{\gamma H} \tag{2.37}$$

$$\mu = \tan\varphi_B \tag{2.38}$$

In the above equations φ is the internal friction angle, φ_B is the base friction angle and γ is the unit weight of the soil. For q, H, α, λ, W_s and W_w please see Figure 2.13.

After finding k_h value the amount of dynamic pressure, the application point of the dynamic thrust can be found by solving the pseudo-static force equilibrium equations.

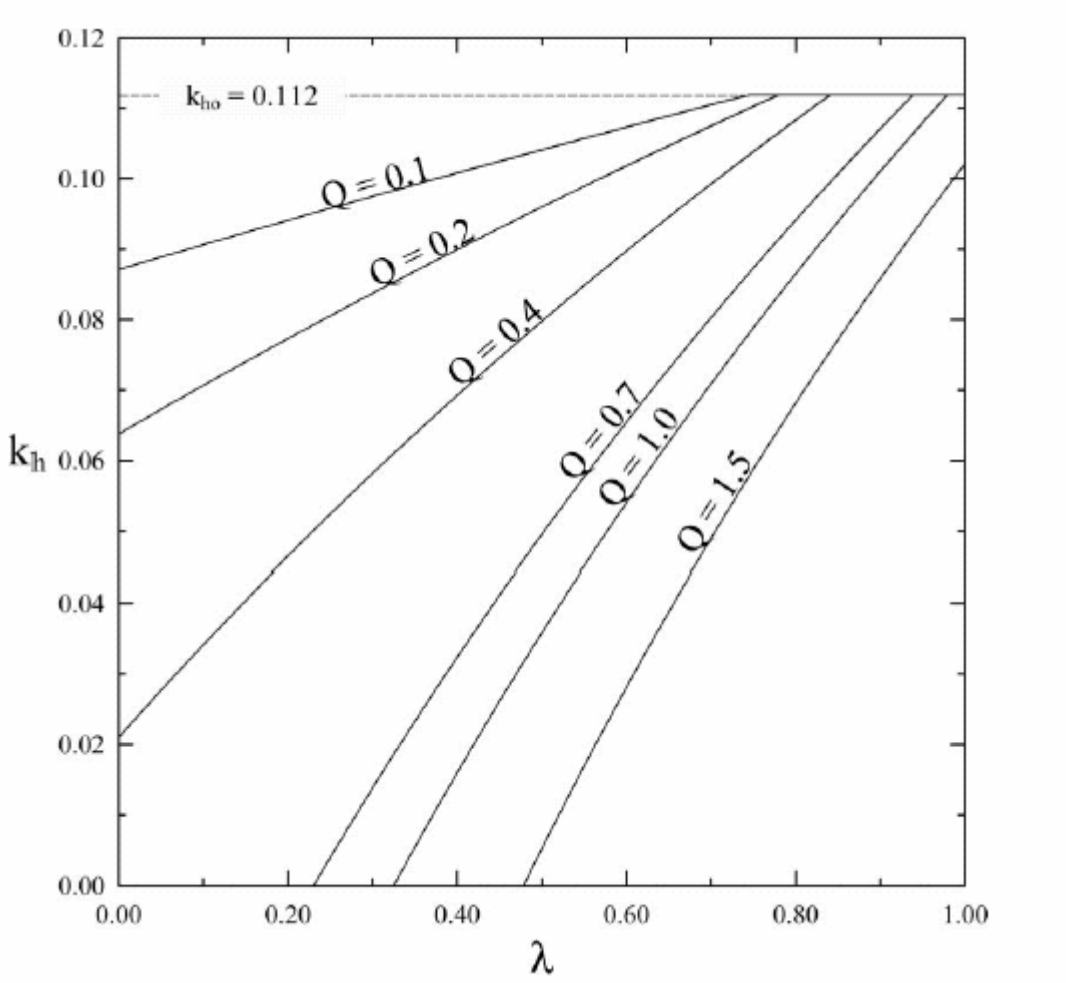

Figure 2.14 Critical acceleration coefficient k_h versus normalized surcharge distance λ (after Caltabiano et al., 2000)

CHAPTER 3

PROCEDURE FOR SHAKING TABLE TESTS CONDUCTED ON THE MODEL RETAINING WALLS

3.1 General

A total number of 54 shaking table test were conducted in order to determine the effects of harmonic input motion, stiffness of the retaining system, and the surcharge on dynamic pressures on the wall, displacement of the wall and backfill accelerations. Tests were conducted using three different vibration frequencies and three different amplitude values. In addition to that, two different surcharge values and three different wall types were used in the experiments. In each test input motion is applied by 15 seconds and earth pressure, acceleration and displacement values were recorded using a data acquisition system.

3.2 Apparatus

3.2.1 Shaking Table System

Tests were conducted by using a shaking table apparatus located at Soil Mechanics Laboratory at Middle East Technical University Department of Civil Engineering. The shaking table apparatus is consisting of two main parts: (1) Motion Generation System (2) Soil Bin resting on the shaking table. Whole system is resting on a 3.5m x 1.0m main steel frame lying on a reinforced concrete foundation constructed by Çalışan (1997) and having U shaped steel sections (See Figure 3.1).

The soil bin itself is located on four rubber bearings (See Figure 3.2) and rests on the main frame having dimensions of 2m x 1m in plan. The remaining part of the frame is reserved for the motion generating electric motor.

Figure 3.1 General View of the Shaking Table Apparatus

Figure 3.2 Rubber Bearings

3.2.1.1 Motion Generating System

The sinusoidal input motion is generated using an electric motor which is connected to the shaking table frame by a connection shaft. The motor is powered by AC outlet. The motion generated by electric motor is transmitted to the shaft by means of a chain as can be seen in Figure 3.3. The frequency of the input motion is adjusted by using gears of different diameters.

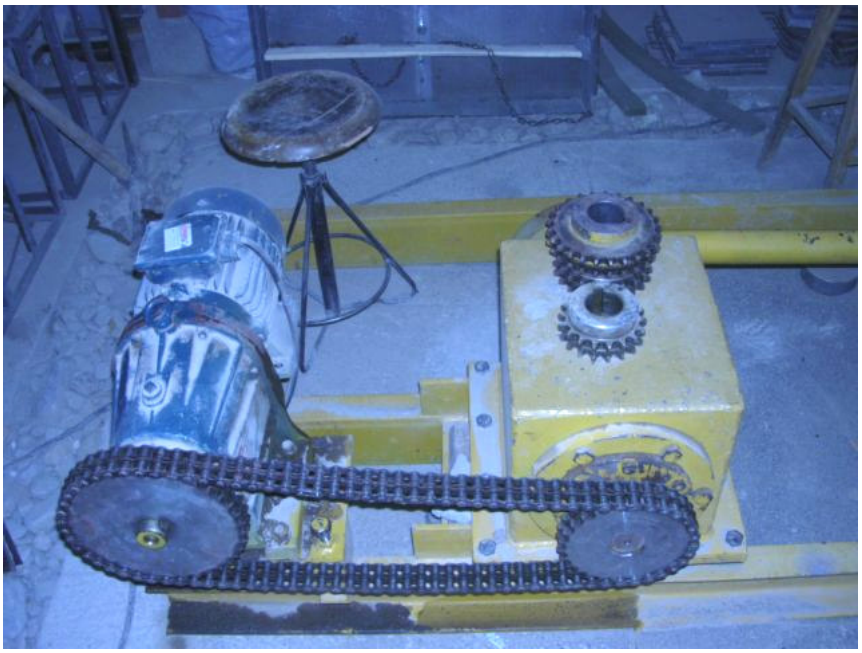

Figure 3.3 Electric motor, gearbox system, eccentric disks and the rigid shaft

The amplitude of the sinusoidal motion is adjusted by means of two eccentric disks which are connected to the gearbox at one end and to the main frame of the shaking table at the other end. Two disks are connected to each other by means of one fixed and five adjustable bolts. One disk is connected to gearbox and the other to the shaft. By changing the relative positions of the eccentric disks the amplitude of the input motion is adjusted.

The input motion can be represented by following formula:

$$x = x_0 \sin \omega t \tag{3.1}$$

where

x: displacement at time t
x_0: displacement amplitude
w: angular frequency of the motion
t: time

Taking the first derivative of this function gives us velocity and the second derivative is the acceleration:

$$\dot{x} = x_0 \cdot \omega \cdot \cos \omega t \tag{3.2}$$

and

$$\ddot{x} = -x_0 \cdot \omega^2 \cdot \sin \omega t \tag{3.3}$$

3.2.1.2 Soil Bin

The soil bin has dimensions of 2.0m x 1.0m x 1.0m. The inner face of the soil bin is covered by sand papers which simulates the friction behavior between sand particles. A plexiglass sliding window having dimensions of 90cm x 60cm is located on one face of the soil bin to enable visual inspection of the backfill (See Figure 3.4). It also makes operations easier during filling and emptying of the soil bin.

Figure 3.4 Plexiglass Sliding Window

3.2.2 Model Walls

Three different wall types having thicknesses of 2.0, 3.2 and 6.6 mm were used during the tests. These walls were previously manufactured by Yunatçı (2003), but only the one with the thickness of 3.2 mm was used during experiments. In order to use four dynamic earth pressure transducers instead of three – which is the number used by Yunatçı (2003) – one additional hole was drilled in the middle of the two lower one.

The surfaces of the plates are smooth in texture and they are all straight in geometry. The vertical alignment of the plates was attained by mounting the plate on the walls of the soil bin by

means of L shaped steel profiles. The wall is also braced at two layers by using thicker L shaped steel profiles which are attached to the wall and the free face of the soil bin in front of the wall (See Figure 3.5). No free space is left between the wall and the bracings to prevent undesirable bumping of the wooden bracings against the face of the wall. After mounting the wooden bracings and backfilling operation is complete the profiles which keep the wall in its vertical position were detached.

Figure 3.5 Top view of the wooden bracings

3.2.3 Sieving Mechanism

Backfilling operation was conducted by raining method in order to obtain a backfill of uniform density. Yunatci (2003) thoroughly describes the procedure for the backfilling operation. The falling height of the sand is tried to be kept at 65 cm during the backfilling operation in order to have the same density value at every depth of the backfill. The reason for choosing this height is mainly the operational difficulties in placing the sieve on the top of the soil bin. The 65cm high backfill is obtained by raining sand having 10cm accumulated height by free fall. According to Rad and Tümay (1985) the effect of falling height above 40cm has a minor influence on the density of the deposited fill. During the backfilling samples were collected at three level and their specific gravity values were obtained by laboratory tests. The results were shown on table 3.1.

Figure 3.6 Sieve used for the experiment

3.2.4 Blocks of Steel Weights for Simulating Surcharge Effects

In order to simulate the effect of surcharge on the dynamic behavior of retaining walls, blocks of steel weights were manufactured at a workshop of Geoteknik Construction Company in OSTİM –ANKARA. They are made of steel with a length of 97 cm and thickness of 20 mm. These blocks can be hinged to each other and also in one array we have two sets of blocks as shown in Figure 3.7 and 3.8. With the screws it is possible to keep two blocks on each other without any sliding taking place. Three blocks having 20 cm width and one block with a width of 15 cm were used during the experiments. They were placed on the backfill and sand particles were glued on the bottom of the blocks in order to keep them in place (to prevent sliding on top of the surface during experiments). 1 layer of these blocks weighs 114.5 kg. Two layers have a dead weight of 229.1 kg. They exert a surcharge of 1.57 kPa for one layer of blocks and 3.14 kPa for two layers.

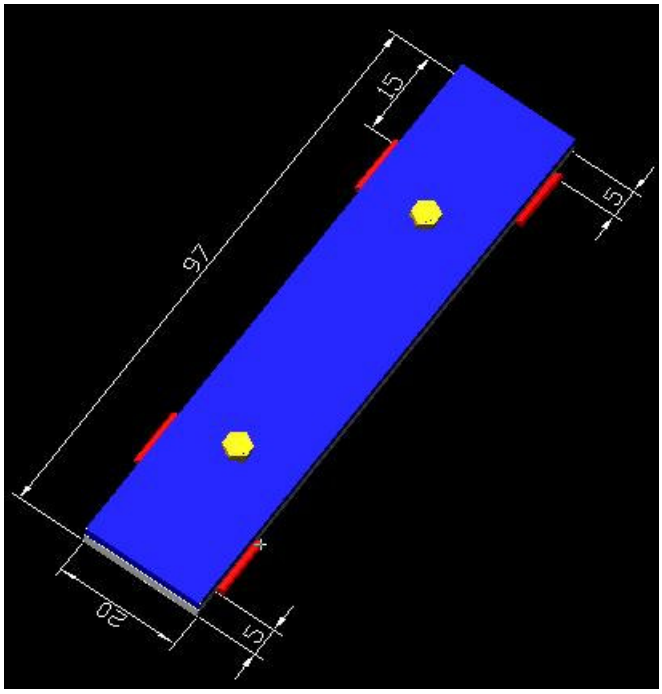

Figure 3.7 Graphical view of surcharge blocks

Figure 3.8 Surcharge blocks on top of the backfill

3.2.5 Data Acquisition System

Data acquisition system used for the experiment had been used by Çalışan (1999) and Yunatçı (2003) in their previous studies. The schematic representation of the system is shown in figure 3.9 below.

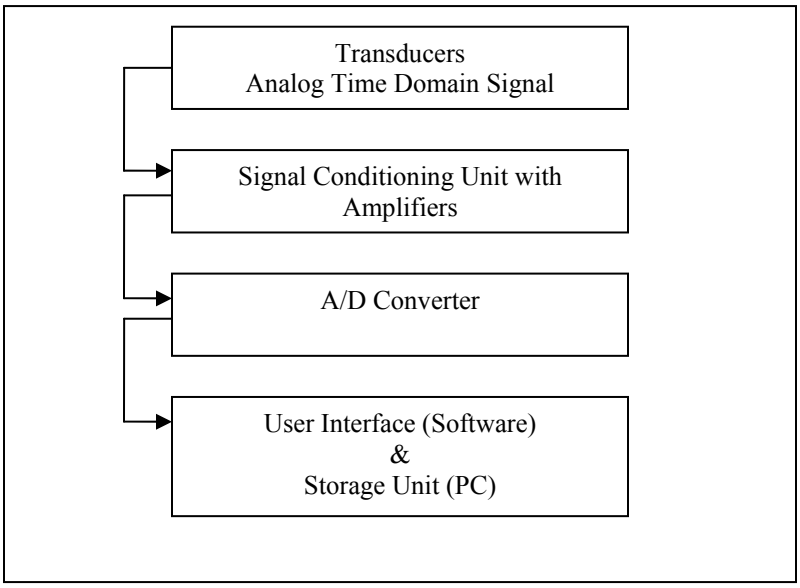

Figure 3.9 Schematic representation of the data acquisition system

Figure 3.10 General view of the data acquisition system

Data arriving from 8 channels is converted from analog to digital form using 200 Hz pacer frequency at each channel. If we consider that the largest frequency of the harmonic input motion does not exceed 4 Hz this rate of sampling is suitable enough for our further data analyses.

The signal conditioning unit has three purposes:

1. Capturing real world phenomena stimulated on transducers via its sockets
2. Amplifying the weak outputs by desired gain setting
3. Sending the signal to the analog to digital converter

In the experiments ADVANTECH® PCLD-770 signal conditioning board with eight PCLD-7702 amplifiers were used (See Figure 3.11). Table 3.2 shows the gain settings used in the experiments.

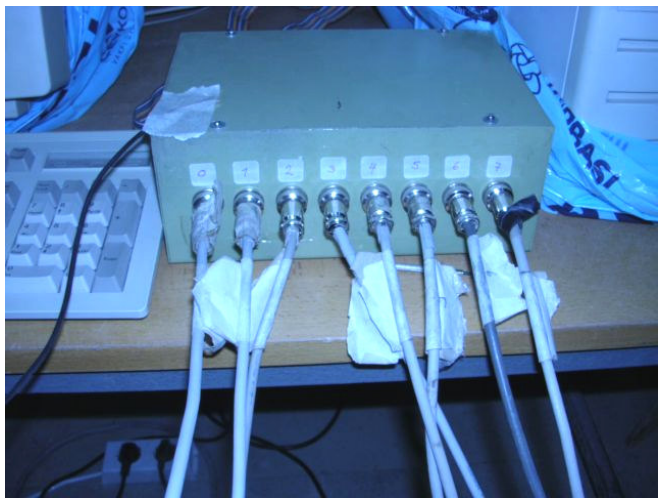

Figure 3.11 Signal Conditioning Board

Table 3.1 Signal gain settings used for each channel

	CH 0	CH 1	CH 2	CH 3	CH 4	CH 5	CH 6	CH 7
Gain Setting	100	200	200	100	1000	1000	1000	1000

In the experiments ADVANTECH® PCL-818 HD A/D plug-in card was used for digitizing analog signal. It supports 8 differential or 16 single ended inputs at 100 kHz sampling frequency. In this study +/-0.5 V differential input was applied in order to obtain the most precise measurement as in the previous studies conducted using this data acquisition system. PCL-818 HD has a 12-bit resolution which means that the voltage input is divided in 2^{12} grids and sampled accordingly.

PC-STREAMER® software was used to view and store the data which runs under DOS environment. Following are the settings used for this experiment.

Card Type	: PCL 818
Pacer Frequency	: 1600
Time Base	: 1 MHz
Polarity	: Bipolar
Input Voltage Range	: +/- 0.5 V
Trigger Mode	: Pacer
Trigger Condition	: Free Run
Start Scan Channel	: 0
Stop Scan Channel	: 7
Base I/O Address	: 200
Interrupt Level	: IRQ2
DMA Channel	: #3
File Size	: 100 kB

Required file size for one run is computed as follows:
2 bytes/channel x 8 channel x 200 Hz x 25 sec = 80000 bytes ≈ 80 kB

3.3 Instrument Layout

Figure 3.12 shows the layout of the experiments with the place and the type of transducer used. Following section explains the calibration of those transducers in order to obtain calibration coefficients which are used for converting voltage output into real physical quantities.

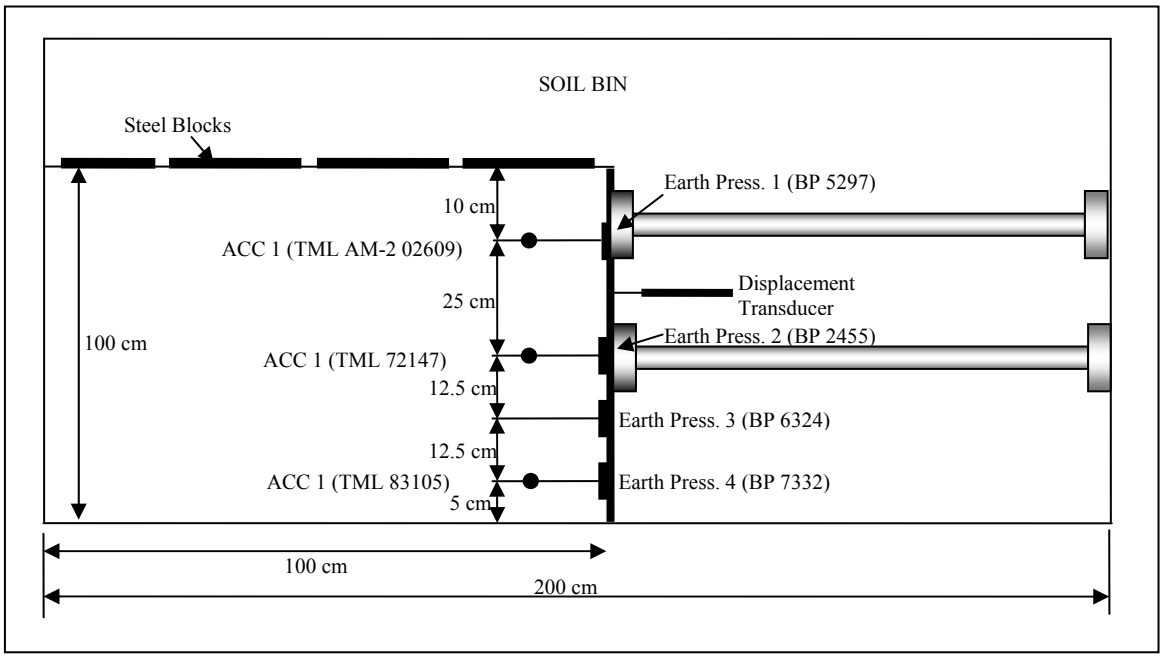

Figure 3.12 Schematic view of the instrumentation used in the experiment (not to scale)

3.4 Calibration of the Instruments used in the Experiments

3.4.1 Dynamic Earth Pressure Transducers

During the experiments TML type KDF-200 kPa were used to measure the dynamic earth pressures. These transducers are circular in shape and have an outer diameter of 50mm. Diameter of the sensing area is 34mm.

The calibration of these transducers were done by simply putting a standard dead weight on the top of the transducer and reading the voltage output by using data acquisition system. By changing the dead weight, different voltage values are obtained for different weights. After obtaining four or five data points the calibration coefficient is calculated. The procedure is explained by Çalışan (1999) and Yunatçı (2003) in detail.

3.4.2 Accelerometers

Three accelerometers having capacities of 1g, 5g and 200g were used during tests. Accelerometers were calibrated by rotating them exactly 90° along their sensing axes as can be seen on figure 3.13. This corresponds to 1g change in acceleration. Corresponding voltage value is read and recorded to calculate calibration coefficient.

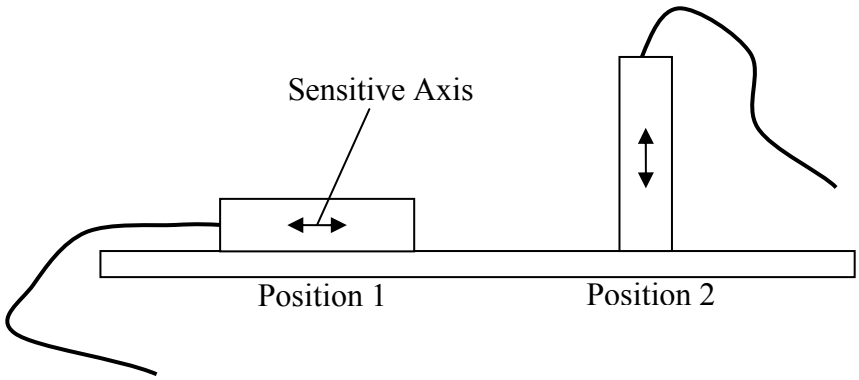

Figure 3.13 Calibration of accelerometers

3.4.3 Displacement Transducers

A displacement transducer having a 100 mm capacity is placed at a height of 42.5 cm from the bottom of the soil bin, between earth pressure transducers 1 and 2. Calibration procedure is exactly same as Çalışan (1999) and Yunatçı (2003). Displacement transducer is fixed by a stand in a vertical position and objects with known heights were put between flat surface and the sensing rod of the transducer. After taking off the object the change in voltage value is recorded. This procedure is repeated for different objects and then the calibration coefficient is calculated.

3.5 Properties of Soil

Air dried sand was used in the experiments as previously done by Çalışan (1999) and Yunatçı (2003). Some routine tests were conducted to find the properties of the sand. Following sections give further details about them.

3.5.1 Grain Size Distribution

Grain size distribution of the soil is found by using dry sieving method. Grain size distribution curve is given in Appendix C. Fines content was calculated as 3.29%. Coefficient of uniformity c_u and coefficient of curvature c_c were calculated as 4 and 1.17 respectively.

3.5.2 Water Content and Specific Gravity

Water content and specific gravity of the sand was calculated as 1.07 (%) and 2.668 respectively.

3.5.3 Density

Density values for the sand specimen are taken from the previous study conducted by Yunatci (2003) by considering that the same sand have been used. Values are tabulated below.

Table 3.2 Unit weight and void ratio values

Maximum Dry Unit Weight (kN/m^3)	18.3
Minimum Dry Unit Weight (kN/m^3)	14.93
Maximum Void Ratio	0.757
Minimum Void Ratio	0.434
Average Unit Weight (kN/m^3)	16.93
Relative Density	64%

3.5.4 Shear Strength Parameters

In order to verify results for the shear strength parameters obtained by previous studies conducted by Çalışan (1999) and Yunatçı (2003) a direct shear test was conducted. But due to

previously stated reasons by Çalışan (1999) the results obtained were not reliable enough. One is that the weight of the cap without any additional dead weight already exerts a normal stress of 14 kPa which is a far bigger value than our low confining stress conditions. Second reason is that the stiffness of the proving rings is not suitable to measure the shear force for relatively low stresses. The result of the direct shear test conducted gives an internal friction angle of 54°. Plot of the direct shear test results is given in Appendix C.

The value obtained by several triaxial tests carried out by both Çalışan (1999) and Yunatçı (2003) gives a value of 47° for internal friction angle for the sand.

3.6 Procedure for the Tests

The tests were performed on three different walls with thicknesses of 6.6, 3.2 and 2.0 mm respectively. Walls were 65cm in height and 99cm in width. Detailed description of the test apparatus is listed in Section 3.2. A total of 54 test were carried out. Tests are divided into three sets where in each set the thickness of the wall is changed. In each set there are 18 tests where the amplitude and frequency of the harmonic input motion and the intensity of the surcharge is changed. Each run lasts approximately 15 seconds. The exact procedure for the tests is same as previously explained by Yunatçı (2003):

1. The steel walls are fixed in the soil bin using “L” shaped small steel profiles. Profiles are screwed on the soil bin at two different levels on both sides leaving 6.6, 3.2 or 2.0mm space depending on the thickness of the wall used. Then the wall is inserted between the profiles by making sure that it stays vertical.

2. The sides and the bottom of the wall are isolated by using flexible rubber sheets and silicon isolators in order to prevent leakage of sand during shaking. A copper wire is attached to the metal wall. The other end will then be attached to the PC-chasis during the test to prevent induction of noise in the system due to static charges.

3. Dynamic earth pressure transducers are mounted on the wall and their sockets are covered temporarily by plastic films until the data acquisition system is brought to the laboratory. Data acquisition system is kept in another place until all backfilling operation is completed due to severe environmental conditions in the laboratory which might damage the system.

4. Two wooden lateral bracings are put between wall and opposite side of the soil bin by using thicker “L” shaped profiles. It is important that bracings are in full contact with the wall.

5. The sieve is placed 65cm above the base of the soil bin and chained to four metal sticks at the edges of the sieve. Two sliding lids are are attached to the bottom of the sieve and then the sand is placed on top of the sieve by forming a 10cm thick layer (Çalışan, 1999).

6. After leveling the sand poured on the top of the sieve the sliding lids are taken out allowing the free fall of the sand from a height of 65cm.

7. Operations 5 and 6 are repeated until a backfill of 65cm height is obtained. It is important that the falling height of the sand is kept constant during backfilling. During these operations accelerometers are placed in the backfill approximately 10 cm away from the face of the wall. It is important to adjust the orientations of the accelerometers by considering their sensitive axes. Sampling containers are placed in the backfill at three levels (10, 30 and 55cm from the bottom of the soil bin) to determine the density and/or specific gravity of the backfill. Density values at each level of the backfill shall be close to each other.

8. After backfilling is complete the sand surface is trimmed and leveled. Sieve is detached and taken away. Small “L” shaped profiles are also detached.

9. Displacement transducer is placed in the soil bin by fixing it using magnet stand. Its vertical and horizontal alignment is adjusted carefully.

10. Data acquisition system and the PC are brought to the laboratory after the dust during backfilling operation is settled down and the transducers are plugged. They are covered by plastic sheets to prevent hazard due to severe environmental conditions. The system is turned on and data monitoring software PC-SCOPE® is run to check whether the analog time signal is correct. Data acquisition system is left turned for 20 – 30 minutes for initial fluctuations in the signal to diminish (Çalışan, 1999)

11. Amplitude and frequency is brought to desired level by adjusting eccentric discs and changing the gear.

12. Static data is collected for 10 seconds and then the electric motor is turned on. Input motion is applied for 15 seconds and then the motor switch is turned off. Data collected by PC-STREAMER® is then saved on the hard disk.

54 separate runs were carried out in 6 days and then the raw data obtained was processed as explained in the following section.

3.7 Data Processing

To store the raw data obtained from the tests PC - STREAMER® software was used which runs under MS-DOS environment. Data stored by PC - STREAMER® has .DAT extension. However it is possible with this software to convert this data into ASCII text format which enables the user to process the data in common applications.

MATLAB® scientific computing software is used in the processing of time domain signal. There are several reasons for this:

1. MATLAB® is versatile and fast software allowing the user to process a huge amount of data in a very short time.
2. It has very useful tools, functions and packages to process time domain signals.
3. Due to the fact that wall – backfill system was excited using very small input accelerations the noise present in the data acquisition system can overwhelm the output of physical phenomenon as can be seen in Figure 3.14. This signal shall be filtered in order to obtain a more realistic data.
4. It has a very useful plotting function where statistical about the graph is calculated by using some simple applications.

After filtering the raw data, MS-EXCEL spreadsheet application was used to further analyze the time domain signal.

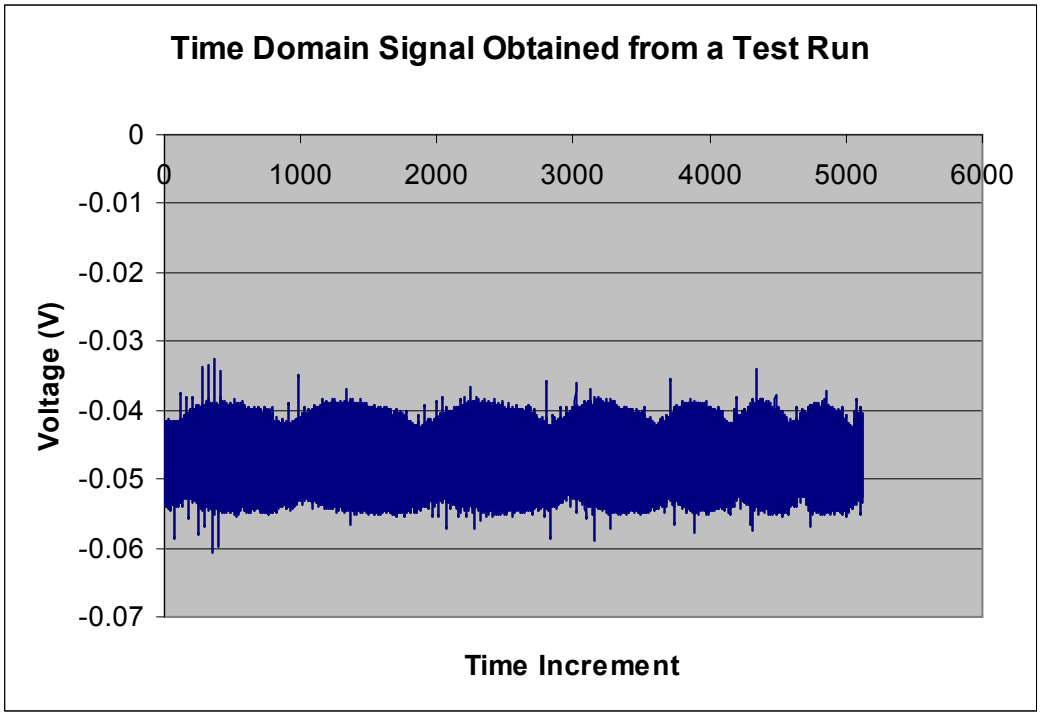

Figure 3.14 An example of time domain signal obtained from a test run. Note that the motion starts at 2000th time increment but it is almost impossible to find the intensity and/or the frequency of the signal coming from the transducer.

The time domain signal shall be first converted into frequency domain in order to filter the signal at desired frequencies. In order to do that, Discrete Cosine Transform (DCT) method was used. It is a Fourier- related transform method where only real numbers are used in contrary to Discrete Fourier Transform (DFT). Therefore there is no need to convert imaginary part of the signal by multiplying it with its conjugate. Therefore discrete data obtained by DCT is half the length of that obtained by DFT and the number of operations carried out by using DCT is less than that of DFT. It is also widely used in coding images like in standard JPEG compression (Bock, 1998).

One dimensional transform is defined as follows:

$$t(k) = c(k)\sum_{n=0}^{N-1} s(n)\cos\frac{\pi(2n+1)k}{2N} \tag{3.1}$$

where s is an array of N original numbers, t is the array of N transformed values, and the coefficient c is given by:

$$c(0) = \sqrt{1/N}, c(k) = \sqrt{2/N} \tag{3.2}$$

for $1 \le k \le N-1$

The DCT has an inverse and it is defined by:

$$s(n) = \sum_{k=0}^{N-1} c(k)t(k)\cos\frac{\pi(2n+1)k}{2N} \tag{3.3}$$

After converting time domain signal into frequency domain signal, upper and lower pass filtering (band filtering) is applied to the data where only the component at desired frequency is left and the other parts of the frequency domain signal is equated to zero. By using Inverse Discrete Cosine Transform the filtered data is converted back into time domain. Major steps of data filtering can be explained as follows:

1. Run MATLAB® and choose IMPORT DATA command from the FILE menu. Select the data you want to analyze in text format. You should see Import Wizard initializing. Select SPACE as column separator and press NEXT and FINISH buttons. You should see your input file as a double array in Workspace window.
2. Into the command window enter following commands (Say the name of the double array is INPUT):

a=INPUT(2500:5000,1:8) → Creates an 2500 to 8 array "a" from 2500th to 5000th time increment corresponding to 12.5 to 25 seconds. The motion is started at 10th second but there is an initial impact when the motor is turned on. It is wise to analyze the signal after the effect of initial impact diminishes.

b=dct(a) → This command creates an array consisting of transformed values.

plot(b) → This command plots the DCT graph (See Figure 3.15)

b(1:81,1:8)=0 → By this command high pass filtering is applied to the data (i.e. the values lower than 81st data point is deleted). Note that the value 81 is chosen for the sake of

example. It is important to know the frequency of the input motion in order to obtain correct frequency component.

b(84:2501,1:8)=0 → Low pass filtering

c=idct(b) → Creates an array “c” which is the inverse discrete cosine transform of array “b”.

plot(c) → Desired time domain signal to analyze (See Figure 3.16)

3. After filtering is complete, the time domain signal data can be saved as an ASCII file on the hard disk using DLMWRITE command.

A sensitivity analysis was conducted using a perfect sine curve and it is found that if the width of the filter band is taken as 0.05 seconds, its effect on the amplitude of the signal in the time domain does not exceed 5%.

After filtering operation is complete raw data is processed further by using MS-EXCEL spreadsheet application.

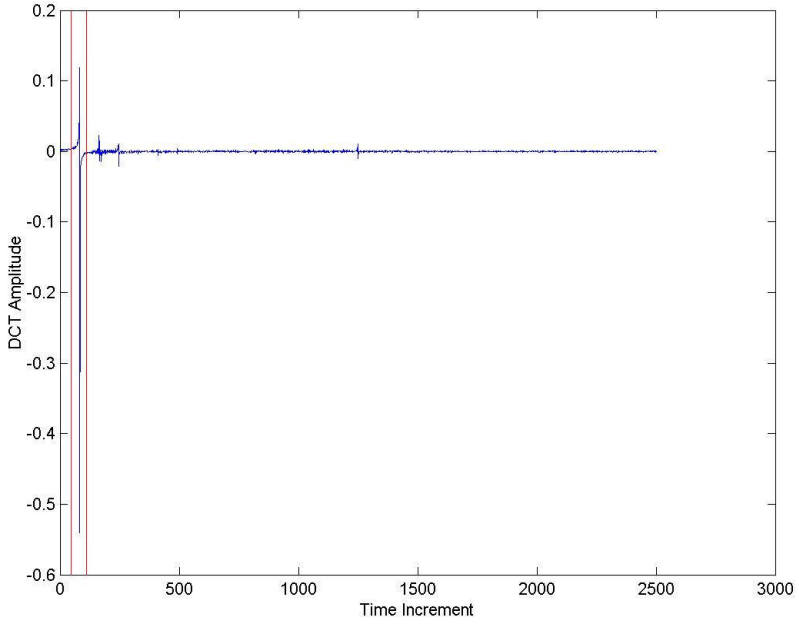

Figure 3.15 Plot of DCT transform. Two red lines shows the frequency band used in filtering operation. Upper and lower frequencies outside this domain are equated to zero.

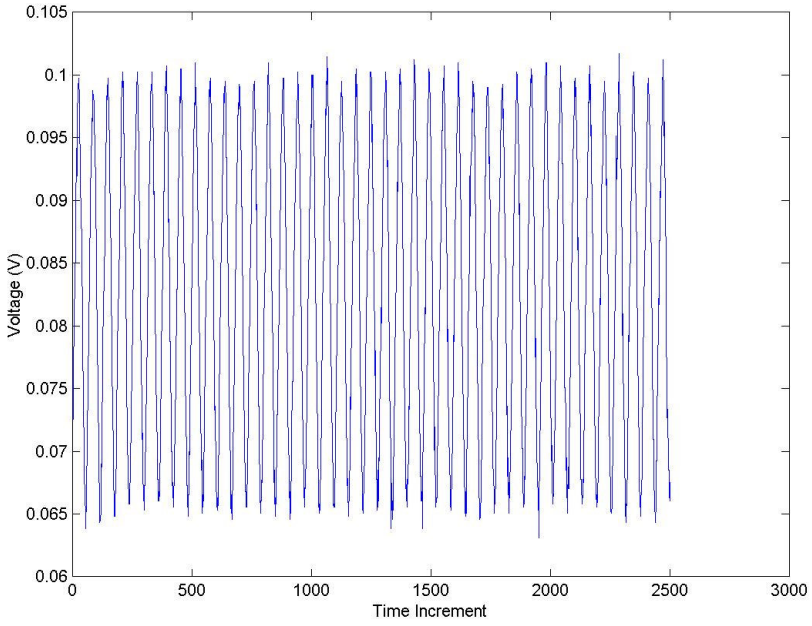

Figure 3.16 Time domain signal after filtering

CHAPTER 4

PRESENTATION OF RESULTS OBTAINED FROM SHAKING TABLE TESTS

4.1 General

A total 54 test was carried out with different wall thicknesses, surcharge amounts and different amplitudes and frequencies of the input motion. Each test lasted for approximately 15 seconds. The soil bin was emptied and filled again each time when the wall type was changed. Dynamic earth pressure measurements were taken at four different locations as explained before. Acceleration values were taken at three different levels and dynamic displacement was measured at a point 42.5 cm from the bottom of the soil bin.

4.2 Visual Inspections

During the tests it is observed that the steel blocks on top of the backfill did not slide on top of the backfill at any acceleration level of the input motion. In addition to that, the lateral bracings were remained fixed between the face of the wall and the soil bin; i.e. they move as a single piece with the wall backfill system.

It has been observed that no failure surface was developed right behind the wall. This indicated that whole wall – backfill system moved as a single piece as expected.

It was not possible to keep the surface of the backfill in its initial form because the steel blocks should be put and then removed away from the top of the backfill. Therefore it was not possible to measure the surface settlements. Note that in these test we dealt with very small input accelerations where the surface settlement amounts between two tests could not be observed visually.

4.3 Backfill Acceleration and Amplification of Accelerations

The accelerations were taken at three different levels. To investigate whether there was amplification of the input accelerations, registered peak accelerations at three levels (bottom, middle and top) were normalized with respect to maximum input acceleration values and then plotted against the input accelerations. These plots were drawn for three different wall types and 2 different surcharge values (a total of 6 plots). For the wall type 2 the amplification effect was also compared with the values obtained by Yunatçı (2003). Table 4.1 presents the properties of different walls, surcharge amounts and test layout used by Yunatçı (2003) in order to make comparisons easier. Figure 4.1 shows the instrument layout used by Yunatçı (2003). Please see Figure 3.12 for the instrument layout used in this study.

Table 4.1 Properties of the Test Layouts used in this study and in the study carried out by Yunatçı (2003)

This Study			
Wall Type	Wall Thickness (mm)	Number of Steel Block Layers	Surcharge Exerted (kPa)
1	6.6	1 Layer	1.57
2	3.2	2 Layers	3.14
3	2.0		
Note that wall is braced at two levels in current study			
Yunatçı (2003)			
In this study wall is braced at three levels. Wall thickness is 3.2 mm. There was no surcharge.			

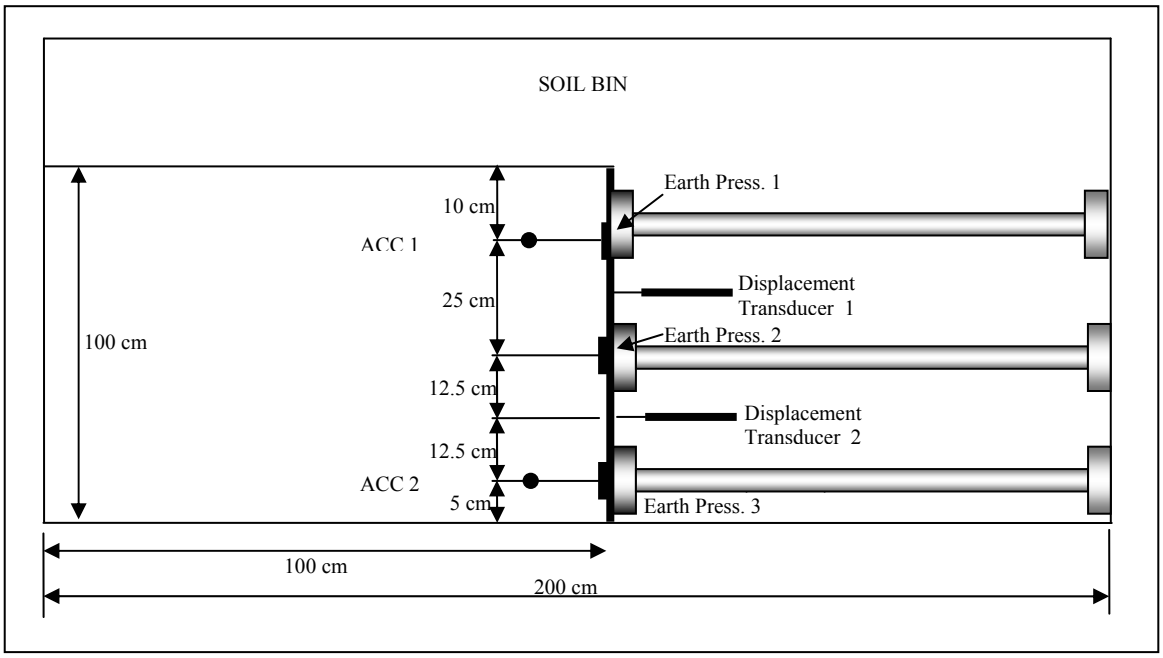

Figure 4.1 Instrument Layout used by Yunatçı (2003)

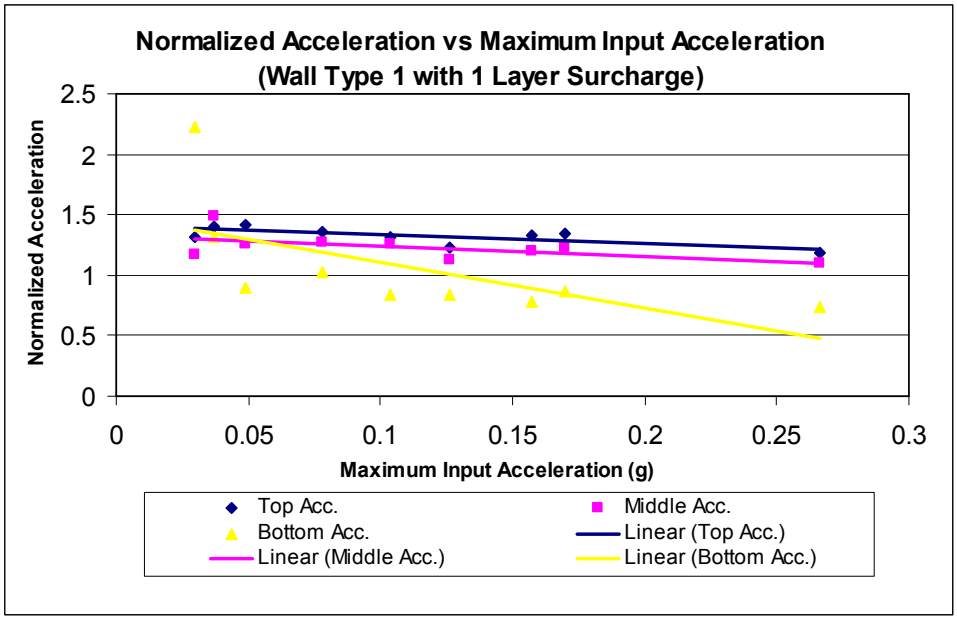

Figure 4.2 Normalized Acceleration versus Maximum Input Acceleration for Wall Type 1 with 1 Layer Surcharge

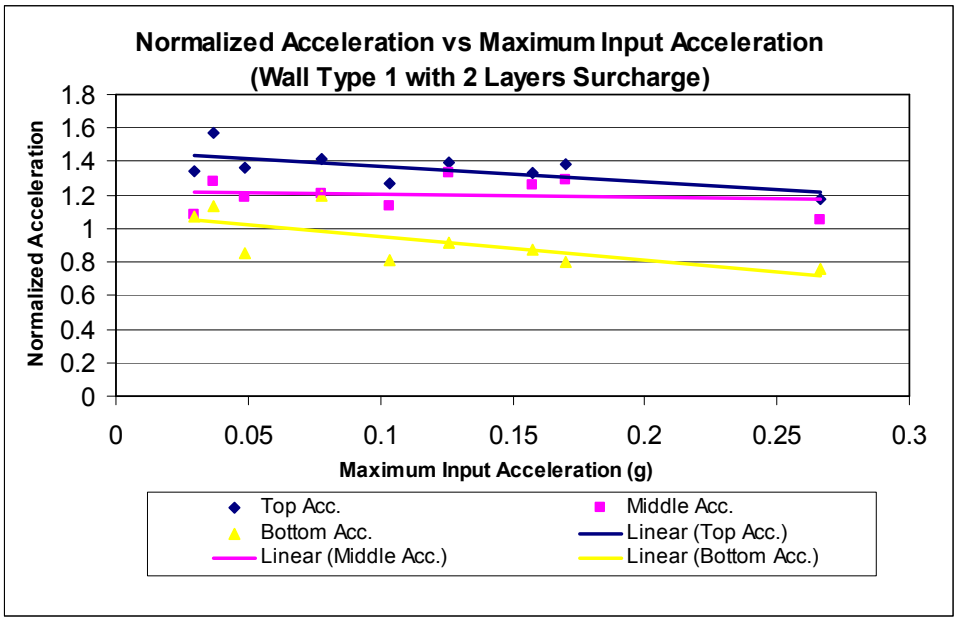

Figure 4.3 Normalized Acceleration versus Maximum Input Acceleration for Wall Type 1 with 2 Layers Surcharge

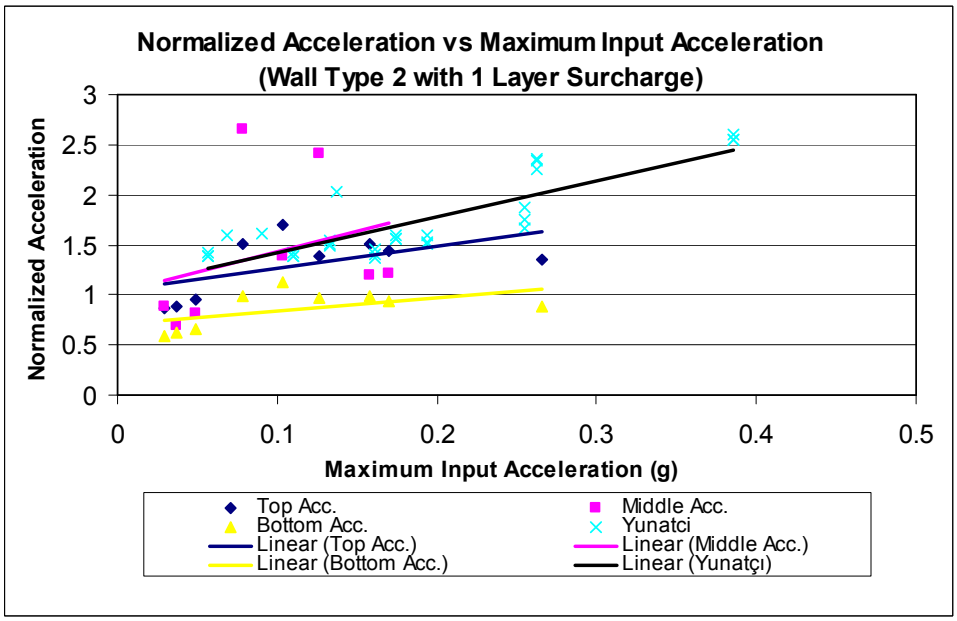

Figure 4.4 Normalized Acceleration versus Maximum Input Acceleration for Wall Type 2 with 1 Layer Surcharge

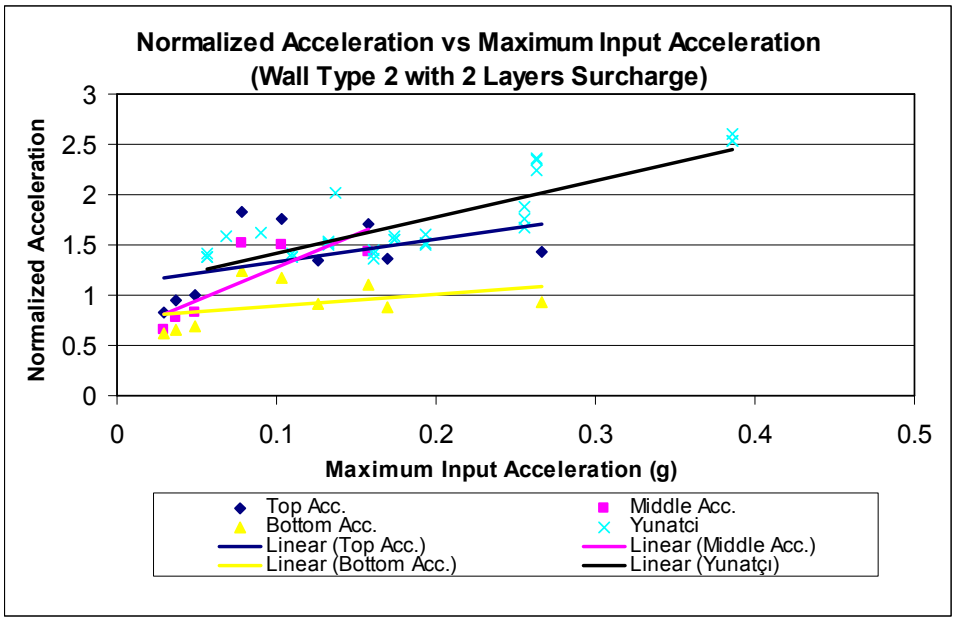

Figure 4.5 Normalized Acceleration versus Maximum Input Acceleration for Wall Type 2 with 2 Layers Surcharge

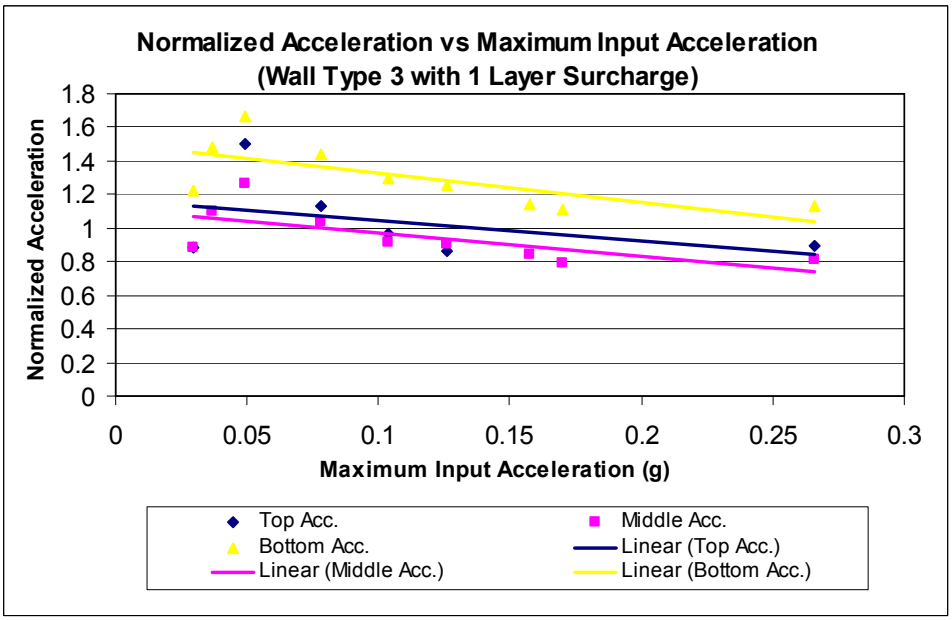

Figure 4.6 Normalized Acceleration versus Maximum Input Acceleration for Wall Type 3 with 1 Layer Surcharge

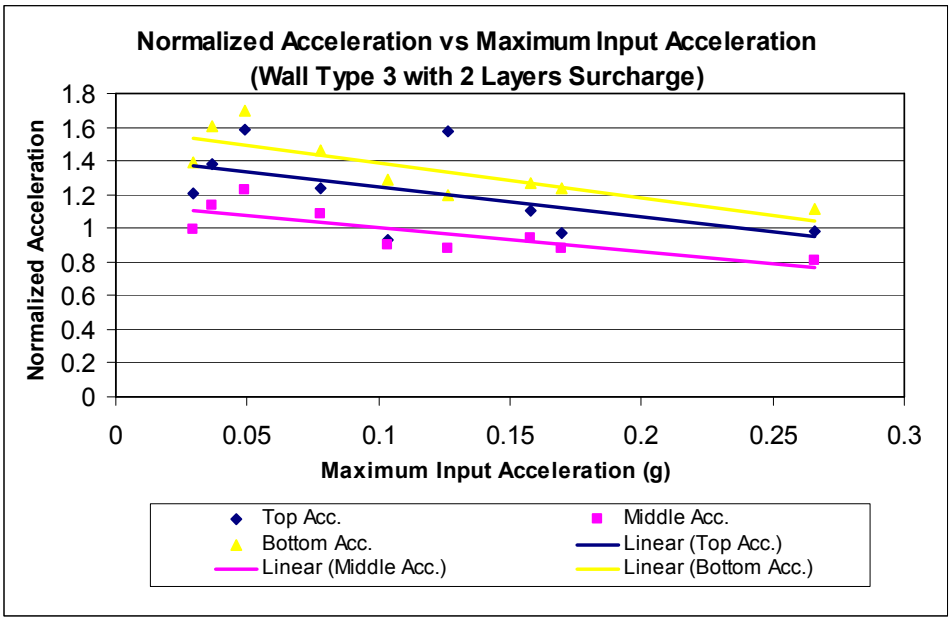

Figure 4.7 Normalized Acceleration versus Maximum Input Acceleration for Wall Type 3 with 2 Layers Surcharge

A labeling system was developed in order to number the individual tests. Table 4.2 shows the explanations of the letters and numbers used in indexing of tests. For example test number TSTA132 means that an input motion having amplitude of 2.9361 mm and a frequency of 3.23 Hz is applied to type 1 wall with 1 layer surcharge on the top of the backfill. For the meaning of the wall types and surcharge layers refer table 4.1.

Table 4.2 Labeling System

First Index		Second Index		Third Index		Fourth Index	
Letter	**Explanation**	**Number**	**Explanation**	**Number**	**Explanation**	**Number**	**Explanation**
A	Wall Type 1	1	1 Layer Srchr.	1	Amp=0.6844mm	1	Frq=2.94 Hz
B	Wall Type 2	2	2 Layer Srchr.	2	Amp=1.8103mm	2	Frq=3.23 Hz
C	Wall Type 3			3	Amp=2.9361mm	3	Frq=3.70 Hz

Table 4.3 Registered Maximum Accelerations

Test No.	Amplitude of Input Motion (mm)	Frequency of Input Motion (Hz)	Maximum Input Acceleration (g)	Max Top Acc. (g)	Max Middle Acc. (g)	Max Bottom Acc. (g)
TSTA111	0.6844	2.94	0.0297	0.0391	0.0347	0.0662
TSTA112	0.6844	3.23	0.0369	0.0519	0.0548	0.0484
TSTA113	0.6844	3.70	0.0490	0.0695	0.0616	0.0438
TSTA121	1.8103	2.94	0.0779	0.1056	0.0995	0.0802
TSTA122	1.8103	3.23	0.1034	0.1361	0.1297	0.0863
TSTA123	1.8103	3.70	0.1576	0.2088	0.1891	0.1222
TSTA131	2.9361	2.94	0.1262	0.1551	0.1419	0.1063
TSTA132	2.9361	3.23	0.1700	0.2295	0.2096	0.1470
TSTA133	2.9361	3.70	0.2661	0.3142	0.2910	0.1954
TSTA211	0.6844	2.94	0.0297	0.0398	0.0320	0.0317
TSTA212	0.6844	3.23	0.0369	0.0580	0.0474	0.0418
TSTA213	0.6844	3.70	0.0490	0.0668	0.0580	0.0421
TSTA221	1.8103	2.94	0.0779	0.1104	0.0940	0.0929
TSTA222	1.8103	3.23	0.1034	0.1317	0.1174	0.0843
TSTA223	1.8103	3.70	0.1576	0.2091	0.1976	0.1378
TSTA231	2.9361	2.94	0.1262	0.1762	0.1681	0.1155
TSTA232	2.9361	3.23	0.1700	0.2346	0.2197	0.1369
TSTA233	2.9361	3.70	0.2661	0.3139	0.2803	0.2017
TSTB111	0.6844	2.94	0.0297	0.0260	0.0261	0.0177
TSTB112	0.6844	3.23	0.0369	0.0324	0.0259	0.0229
TSTB113	0.6844	3.70	0.0490	0.0467	0.0400	0.0321
TSTB121	1.8103	2.94	0.0779	0.1175	0.2069	0.0776
TSTB122	1.8103	3.23	0.1034	0.1751	0.1434	0.1160
TSTB123	1.8103	3.70	0.1576	0.2377	0.1881	0.1550
TSTB131	2.9361	2.94	0.1262	0.1743	0.3032	0.1218
TSTB132	2.9361	3.23	0.1700	0.2440	0.2077	0.1600
TSTB133	2.9361	3.70	0.2661	0.3592	*****	0.2341
TSTB211	0.6844	2.94	0.0297	0.0246	0.0193	0.0182
TSTB212	0.6844	3.23	0.0369	0.0351	0.0286	0.0244
TSTB213	0.6844	3.70	0.0490	0.0491	0.0406	0.0335
TSTB221	1.8103	2.94	0.0779	0.1420	0.1176	0.0972
TSTB222	1.8103	3.23	0.1034	0.1821	0.1543	0.1213
TSTB223	1.8103	3.70	0.1576	0.2688	0.2252	0.1738
TSTB231	2.9361	2.94	0.1262	0.1705	*****	0.1156
TSTB232	2.9361	3.23	0.1700	0.2300	*****	0.1504

Table 4.3 (continued) Registered Maximum Accelerations

Test No.	Amplitude of Input Motion (mm)	Frequency of Input Motion (Hz)	Maximum Input Acceleration (g)	Max Top Acc. (g)	Max Middle Acc. (g)	Max Bottom Acc. (g)
TSTB233	2.9361	3.70	0.2661	0.3829	9.2780	0.2474
TSTC111	0.6844	2.94	0.0297	0.0262	0.0263	0.0364
TSTC112	0.6844	3.23	0.0369	0.1240	0.0408	0.0548
TSTC113	0.6844	3.70	0.0490	0.0738	0.0622	0.0817
TSTC121	1.8103	2.94	0.0779	0.0880	0.0813	0.1123
TSTC122	1.8103	3.23	0.1034	0.1000	0.0945	0.1341
TSTC123	1.8103	3.70	0.1576	0.0771	0.1331	0.1791
TSTC131	2.9361	2.94	0.1262	0.1085	0.1148	0.1578
TSTC132	2.9361	3.23	0.1700	0.3503	0.1350	0.1890
TSTC133	2.9361	3.70	0.2661	0.2376	0.2170	0.3012
TSTC211	0.6844	2.94	0.0297	0.0358	0.0296	0.0412
TSTC212	0.6844	3.23	0.0369	0.0508	0.0418	0.0593
TSTC213	0.6844	3.70	0.0490	0.0779	0.0601	0.0834
TSTC221	1.8103	2.94	0.0779	0.0964	0.0843	0.1140
TSTC222	1.8103	3.23	0.1034	0.0965	0.0929	0.1335
TSTC223	1.8103	3.70	0.1576	0.1745	0.1486	0.2002
TSTC231	2.9361	2.94	0.1262	0.1987	0.1112	0.1515
TSTC232	2.9361	3.23	0.1700	0.1643	0.1490	0.2100
TSTC233	2.9361	3.70	0.2661	0.2618	0.2145	0.2959

4.4 Maximum Dynamic Pressures

Maximum dynamic thrust does not act at the time where maximum dynamic pressures were read at each cell. In other words there is a combination of pressure values where the dynamic thrust is maximum at a time. Therefore tabulating maximum earth pressures is meaningless unless we want to see the variation of the earth pressure with respect to input acceleration at a single cell.

Table 4.3 gives maximum registered dynamic earth pressures in each test and figure 4.8 gives the variation of the normalized dynamic earth pressures with respect to intensity of input acceleration. The dynamic earth pressure values were normalized with respect to static earth pressure measurements.

Table 4.4 Maximum Registered Earth Pressures

	Amplitude of Input Motion (mm)	Frequency of Input Motion (Hz)	Maximum Input Acceleration (g)	Max Press. Cell 4 (kPa)	Max Press. Cell 3 (kPa)	Max Press. Cell 2 (kPa)	Max Press. Cell 1 (kPa)
TSTA111	0.684	2.94	0.030	0.075	0.044	0.012	0.092
TSTA112	0.684	3.23	0.037	0.034	0.030	0.009	0.049
TSTA113	0.684	3.70	0.049	0.071	0.078	0.022	0.096
TSTA121	1.810	2.94	0.078	0.154	0.091	0.058	0.206
TSTA122	1.810	3.23	0.103	0.190	0.106	0.082	0.259
TSTA123	1.810	3.70	0.158	0.298	0.121	0.138	0.432
TSTA131	2.936	2.94	0.126	0.242	0.041	0.047	0.401
TSTA132	2.936	3.23	0.170	0.338	0.057	0.175	0.666
TSTA133	2.936	3.70	0.266	0.333	0.033	0.187	1.216
TSTA211	0.684	2.94	0.030	0.036	0.058	0.010	0.036
TSTA212	0.684	3.23	0.037	0.052	0.072	0.015	0.115
TSTA213	0.684	3.70	0.049	0.053	0.092	0.022	0.111
TSTA221	1.810	2.94	0.078	0.175	0.125	0.052	0.218
TSTA222	1.810	3.23	0.103	0.218	0.148	0.090	0.271
TSTA223	1.810	3.70	0.158	0.296	0.220	0.160	0.555
TSTA231	2.936	2.94	0.126	0.252	0.043	0.149	0.751
TSTA232	2.936	3.23	0.170	0.330	0.019	0.270	1.071
TSTA233	2.936	3.70	0.266	0.442	0.011	0.206	1.590
TSTB111	0.684	2.94	0.030	0.028	0.027	0.016	0.058
TSTB112	0.684	3.23	0.037	0.023	0.022	0.019	0.033
TSTB113	0.684	3.70	0.049	0.014	0.014	0.023	0.044
TSTB121	1.810	2.94	0.078	0.035	0.034	0.148	0.073
TSTB122	1.810	3.23	0.103	0.071	0.068	0.209	0.071
TSTB123	1.810	3.70	0.158	0.046	0.044	0.189	0.078
TSTB131	2.936	2.94	0.126	0.044	0.043	0.159	0.137
TSTB132	2.936	3.23	0.170	0.033	0.031	0.359	0.012
TSTB133	2.936	3.70	0.266	0.062	0.060	0.445	0.155
TSTB211	0.684	2.94	0.030	0.014	0.013	0.011	0.024
TSTB212	0.684	3.23	0.037	0.027	0.026	0.019	0.050
TSTB213	0.684	3.70	0.049	0.037	0.035	0.034	0.029
TSTB221	1.810	2.94	0.078	0.095	0.091	0.099	0.090
TSTB222	1.810	3.23	0.103	0.173	0.165	0.198	0.032
TSTB223	1.810	3.70	0.158	0.086	0.082	0.316	0.108
TSTB231	2.936	2.94	0.126	0.062	0.059	0.256	0.187
TSTB232	2.936	3.23	0.170	0.076	0.073	0.349	0.161

Table 4.4 (continued) Maximum Registered Earth Pressures

	Amplitude of Input Motion (mm)	Frequency of Input Motion (Hz)	Maximum Input Acceleration (g)	Max Press. Cell 4 (kPa)	Max Press. Cell 3 (kPa)	Max Press. Cell 2 (kPa)	Max Press. Cell 1 (kPa)
TSTB233	2.936	3.70	0.266	0.045	0.043	0.512	0.204
TSTC111	0.684	2.94	0.030	0.023	0.013	0.008	0.069
TSTC112	0.684	3.23	0.037	0.077	0.036	0.012	0.093
TSTC113	0.684	3.70	0.049	0.090	0.084	0.019	0.097
TSTC121	1.810	2.94	0.078	0.160	0.126	0.056	0.121
TSTC122	1.810	3.23	0.103	0.172	0.138	0.056	0.088
TSTC123	1.810	3.70	0.158	0.272	0.194	0.103	0.121
TSTC131	2.936	2.94	0.126	0.186	0.158	0.068	0.140
TSTC132	2.936	3.23	0.170	0.265	0.235	0.148	0.232
TSTC133	2.936	3.70	0.266	0.303	0.378	0.317	0.107
TSTC211	0.684	2.94	0.030	0.043	0.050	0.016	0.037
TSTC212	0.684	3.23	0.037	0.077	0.054	0.027	0.076
TSTC213	0.684	3.70	0.049	0.116	0.079	0.034	0.064
TSTC221	1.810	2.94	0.078	0.200	0.144	0.033	0.128
TSTC222	1.810	3.23	0.103	0.225	0.153	0.080	0.039
TSTC223	1.810	3.70	0.158	0.360	0.290	0.164	0.083
TSTC231	2.936	2.94	0.126	0.116	0.148	0.162	0.119
TSTC232	2.936	3.23	0.170	0.229	0.232	0.281	0.049
TSTC233	2.936	3.70	0.266	0.337	0.473	0.416	0.112

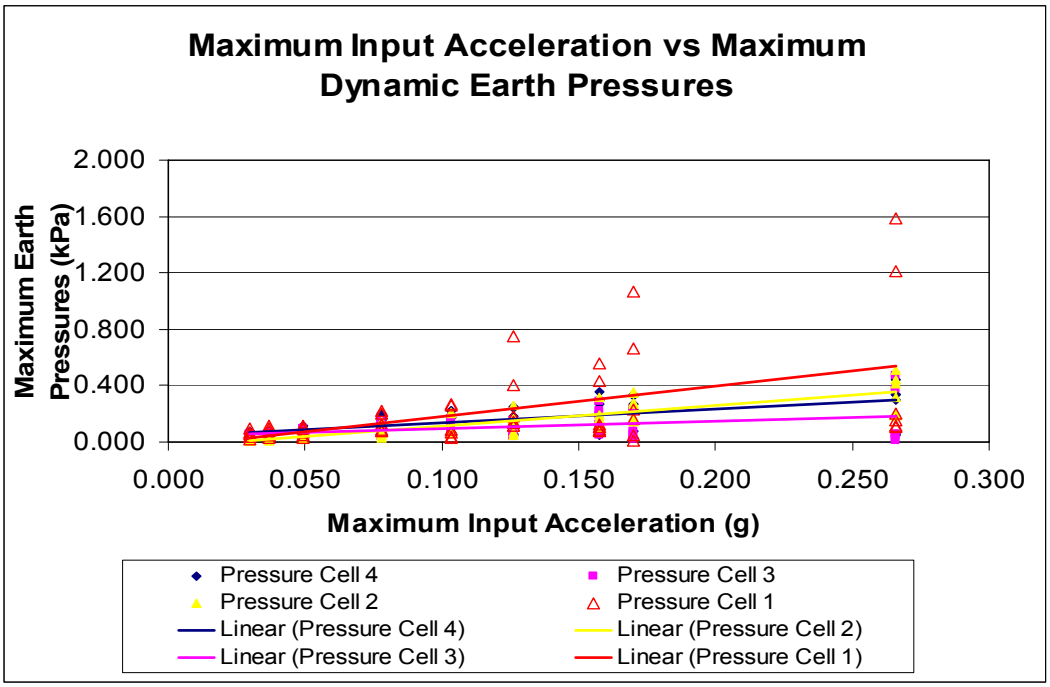

Figure 4.8 Maximum Registered Earth Pressures versus Maximum Input Acceleration

4.5 Maximum Dynamic Thrust

MS-EXCEL spreadsheet program was used to calculate total dynamic thrust. Since a measured pressure value in one cell may either be negative or positive there are 2^4 possibilities for calculating total dynamic thrust. The sheet is designed so that it can compute 16 possible stress distribution patterns, either positive or negative.

In addition to measured maximum dynamic thrust values, Wood (1973) and Mononobe-Okabe solutions were also compared with the results in tables 4.4 and 4.5. In calculating maximum thrust values by M-O method, internal friction angle was taken as 37° and 47° respectively in order to make a comparison.

Maximum dynamic thrust values found by Yunatçı (2003) for laterally braced sheet pile wall having a thickness of 3.2 mm is also compared with the results of this study in figures 4.11 and 4.12.

Table 4.5 Maximum dynamic earth pressures corresponding to maximum dynamic thrust and dynamic thrust magnitudes

Test No.	Maximum Input Acceleration (g)	Maximum Earth Pressures Corresponding to Maximum Dynamic Thrust (kPa)				Measured Maximum Dynamic Thrust (kN)
		Cell 1	Cell 2	Cell 3	Cell 4	
TSTA111	0.030	0.067	-0.007	-0.016	-0.060	0.015
TSTA112	0.037	-0.051	0.011	0.038	0.037	0.015
TSTA113	0.049	-0.096	0.019	0.083	0.072	0.030
TSTA121	0.078	-0.207	0.062	0.072	0.149	0.056
TSTA122	0.103	-0.284	0.078	0.117	0.219	0.078
TSTA123	0.158	-0.433	0.138	0.121	0.296	0.114
TSTA131	0.126	0.372	-0.045	-0.035	-0.221	0.073
TSTA132	0.170	0.513	-0.138	-0.032	-0.226	0.108
TSTA133	0.266	1.153	-0.166	0.011	-0.336	0.198
TSTA211	0.030	-0.047	0.004	0.058	0.039	0.016
TSTA212	0.037	-0.082	0.008	0.019	0.031	0.016
TSTA213	0.049	-0.114	0.014	0.089	0.053	0.031
TSTA221	0.078	-0.218	0.051	0.122	0.174	0.063
TSTA222	0.103	0.295	-0.097	-0.150	-0.220	0.087
TSTA223	0.158	-0.555	0.159	0.220	0.292	0.145
TSTA231	0.126	-0.741	0.144	-0.044	0.267	0.142
TSTA232	0.170	0.987	-0.233	-0.028	-0.290	0.189
TSTA233	0.266	1.422	-0.196	0.015	-0.349	0.238
TSTB111	0.030	-0.056	-0.015	-0.015	-0.028	0.013
TSTB112	0.037	-0.035	-0.014	-0.033	-0.051	0.014
TSTB113	0.049	-0.042	-0.023	-0.012	-0.056	0.014
TSTB121	0.078	-0.073	-0.157	-0.047	-0.173	0.055
TSTB122	0.103	-0.076	-0.191	-0.060	-0.189	0.065
TSTB123	0.158	0.094	0.184	-0.040	0.163	0.061
TSTB131	0.126	0.141	0.155	0.013	0.194	0.060
TSTB132	0.170	0.001	0.358	0.070	0.341	0.097
TSTB133	0.266	-0.094	0.384	-0.053	0.239	0.105
TSTB211	0.030	0.021	-0.007	-0.012	0.002	0.005
TSTB212	0.037	0.001	0.018	0.020	0.020	0.007

Table 4.5 (continued) Maximum dynamic earth pressures corresponding to maximum dynamic thrust and dynamic thrust magnitudes

Test No.	Maximum Input Acceleration (g)	Maximum Earth Pressures Corresponding to Maximum Dynamic Thrust (kPa)				Measured Maximum Dynamic Thrust (kN)
		Cell 1	Cell 2	Cell 3	Cell 4	
TSTB213	0.049	-0.019	-0.017	-0.033	-0.060	0.013
TSTB221	0.078	0.090	0.098	0.090	0.201	0.054
TSTB222	0.103	-0.014	-0.154	-0.142	-0.199	0.061
TSTB223	0.158	0.091	-0.316	-0.073	-0.279	0.097
TSTB231	0.126	0.164	0.230	0.053	0.212	0.083
TSTB232	0.170	-0.151	-0.367	-0.057	-0.321	0.115
TSTB233	0.266	0.039	0.508	-0.037	0.323	0.125
TSTC111	0.030	-0.051	0.010	0.024	0.066	0.015
TSTC112	0.037	0.103	-0.013	-0.046	-0.092	0.027
TSTC113	0.049	-0.097	0.019	0.084	0.089	0.032
TSTC121	0.078	-0.121	0.056	0.126	0.159	0.051
TSTC122	0.103	-0.085	0.053	0.138	0.149	0.047
TSTC123	0.158	0.121	-0.101	-0.189	-0.270	0.075
TSTC131	0.126	-0.149	0.069	0.148	0.160	0.060
TSTC132	0.170	0.109	-0.136	-0.233	-0.275	0.085
TSTC133	0.266	-0.087	0.317	0.377	0.303	0.136
TSTC211	0.030	-0.037	0.015	0.044	0.040	0.015
TSTC212	0.037	-0.095	0.025	0.051	0.040	0.025
TSTC213	0.049	-0.064	0.034	0.079	0.115	0.031
TSTC221	0.078	-0.128	0.033	0.144	0.198	0.053
TSTC222	0.103	0.038	-0.079	-0.150	-0.224	0.052
TSTC223	0.158	0.083	-0.162	-0.289	-0.359	0.099
TSTC231	0.126	0.112	-0.154	-0.127	-0.104	0.065
TSTC232	0.170	0.012	-0.280	-0.231	-0.228	0.097
TSTC233	0.266	-0.019	0.416	0.473	0.337	0.160

Table 4.6 Maximum thrust calculations by M-O and Wood's methods

Test No.	Maximum Input Acceleration (g)	Measured Maximum Thrust (kN)	Maximum Thrust Calculated by Wood's Method Using Max. Input Acc. (kN)	Maximum Thrust Calculated by M-O Method Using Max. Input Acc. (kN)	
				Φ=37°	Φ=47°
TSTA111	0.030	0.015	0.072	0.056	0.043
TSTA112	0.037	0.015	0.090	0.070	0.055
TSTA113	0.049	0.030	0.119	0.094	0.073
TSTA121	0.078	0.056	0.190	0.154	0.120
TSTA122	0.103	0.078	0.252	0.210	0.164
TSTA123	0.158	0.114	0.383	0.339	0.264
TSTA131	0.126	0.073	0.307	0.262	0.204
TSTA132	0.170	0.108	0.413	0.371	0.288
TSTA133	0.266	0.198	0.647	0.652	0.501
TSTA211	0.030	0.016	0.072	0.056	0.043
TSTA212	0.037	0.016	0.090	0.070	0.055
TSTA213	0.049	0.031	0.119	0.094	0.073
TSTA221	0.078	0.063	0.190	0.154	0.120
TSTA222	0.103	0.087	0.252	0.210	0.164
TSTA223	0.158	0.145	0.383	0.339	0.264
TSTA231	0.126	0.142	0.307	0.262	0.204
TSTA232	0.170	0.189	0.413	0.371	0.288
TSTA233	0.266	0.238	0.647	0.652	0.501
TSTB111	0.030	0.013	0.072	0.056	0.043
TSTB112	0.037	0.014	0.090	0.070	0.055
TSTB113	0.049	0.014	0.119	0.094	0.073
TSTB121	0.078	0.055	0.190	0.154	0.120
TSTB122	0.103	0.065	0.252	0.210	0.164
TSTB123	0.158	0.061	0.383	0.339	0.264
TSTB131	0.126	0.060	0.307	0.262	0.204
TSTB132	0.170	0.097	0.413	0.371	0.288
TSTB133	0.266	0.105	0.647	0.652	0.501
TSTB211	0.030	0.005	0.072	0.056	0.043
TSTB212	0.037	0.007	0.090	0.070	0.055
TSTB213	0.049	0.013	0.119	0.094	0.073

Table 4.6 (continued) Maximum thrust calculations by M-O and Wood's methods

Test No.	Maximum Input Acceleration (g)	Measured Maximum Thrust (kN)	Maximum Thrust Calculated by Wood's Method Using Max. Input Acc. (kN)	Maximum Thrust Calculated by M-O Method Using Max. Input Acc. (kN)	
				Φ=37°	Φ=47°
TSTB221	0.078	0.054	0.190	0.154	0.120
TSTB222	0.103	0.061	0.252	0.210	0.164
TSTB223	0.158	0.097	0.383	0.339	0.264
TSTB231	0.126	0.083	0.307	0.262	0.204
TSTB232	0.170	0.115	0.413	0.371	0.288
TSTB233	0.266	0.125	0.647	0.652	0.501
TSTC111	0.030	0.015	0.072	0.056	0.043
TSTC112	0.037	0.027	0.090	0.070	0.055
TSTC113	0.049	0.032	0.119	0.094	0.073
TSTC121	0.078	0.051	0.190	0.154	0.120
TSTC122	0.103	0.047	0.252	0.210	0.164
TSTC123	0.158	0.075	0.383	0.339	0.264
TSTC131	0.126	0.060	0.307	0.262	0.204
TSTC132	0.170	0.085	0.413	0.371	0.288
TSTC133	0.266	0.136	0.647	0.652	0.501
TSTC211	0.030	0.015	0.072	0.056	0.043
TSTC212	0.037	0.025	0.090	0.070	0.055
TSTC213	0.049	0.031	0.119	0.094	0.073
TSTC221	0.078	0.053	0.190	0.154	0.120
TSTC222	0.103	0.052	0.252	0.210	0.164
TSTC223	0.158	0.099	0.383	0.339	0.264
TSTC231	0.126	0.065	0.307	0.262	0.204
TSTC232	0.170	0.097	0.413	0.371	0.288
TSTC233	0.266	0.160	0.647	0.652	0.501

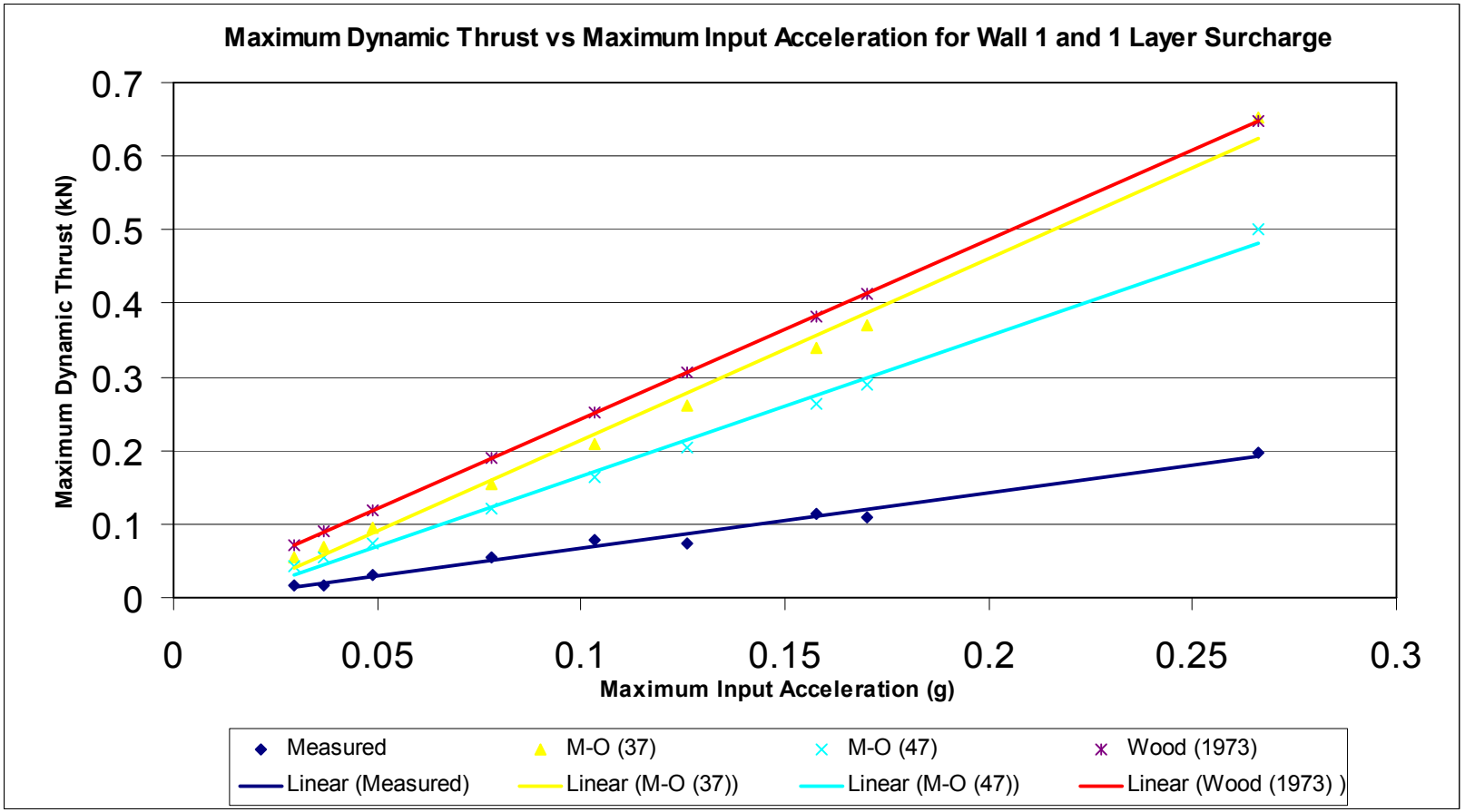

Figure 4.9 Variation of maximum horizontal dynamic thrust with respect to maximum input acceleration for Wall 1 and 1 layer surcharge

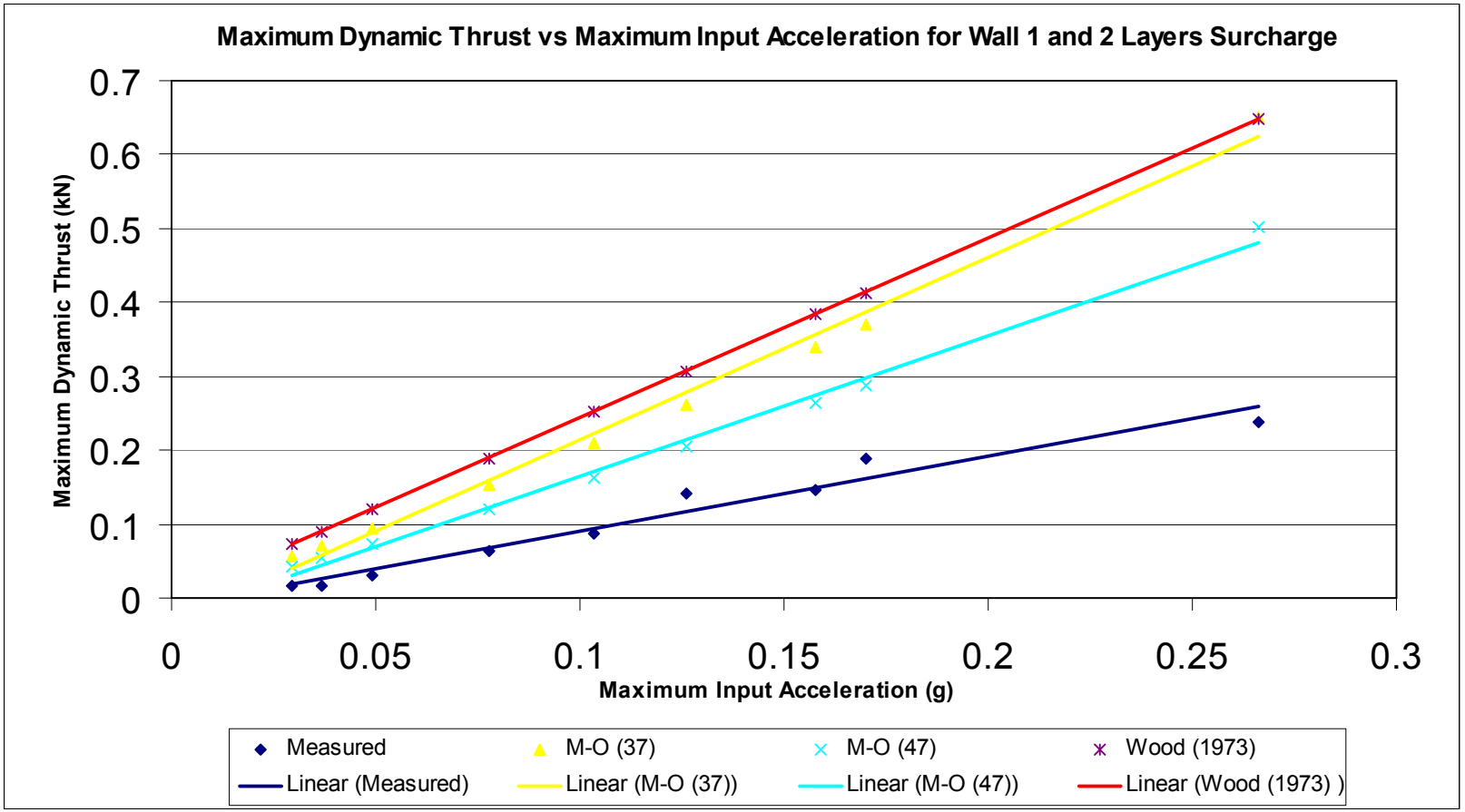

Figure 4.10 Variation of maximum horizontal dynamic thrust with respect to maximum input acceleration for Wall 1 and 2 layers surcharge

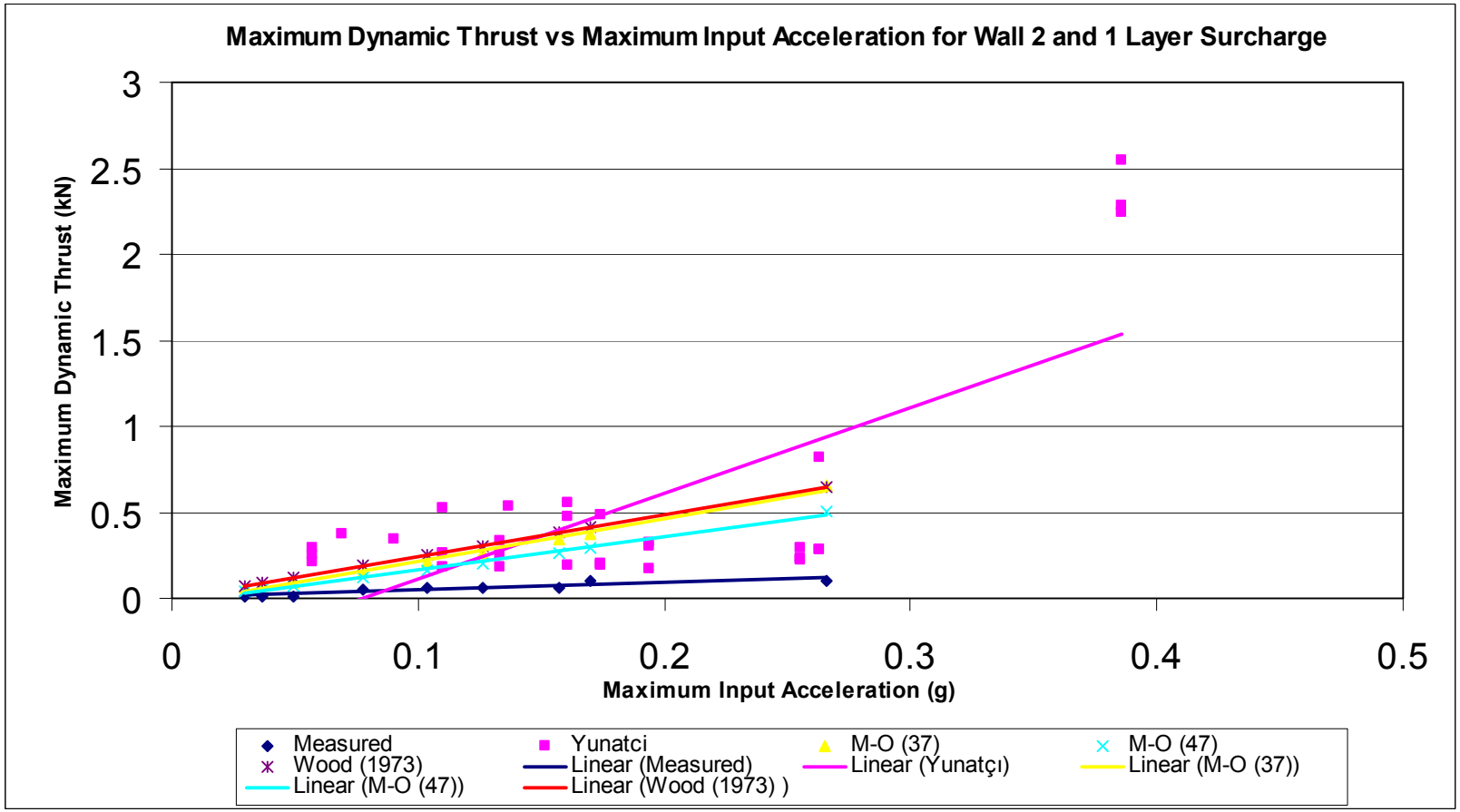

Figure 4.11 Variation of maximum horizontal dynamic thrust with respect to maximum input acceleration for Wall 2 and 1 layer surcharge

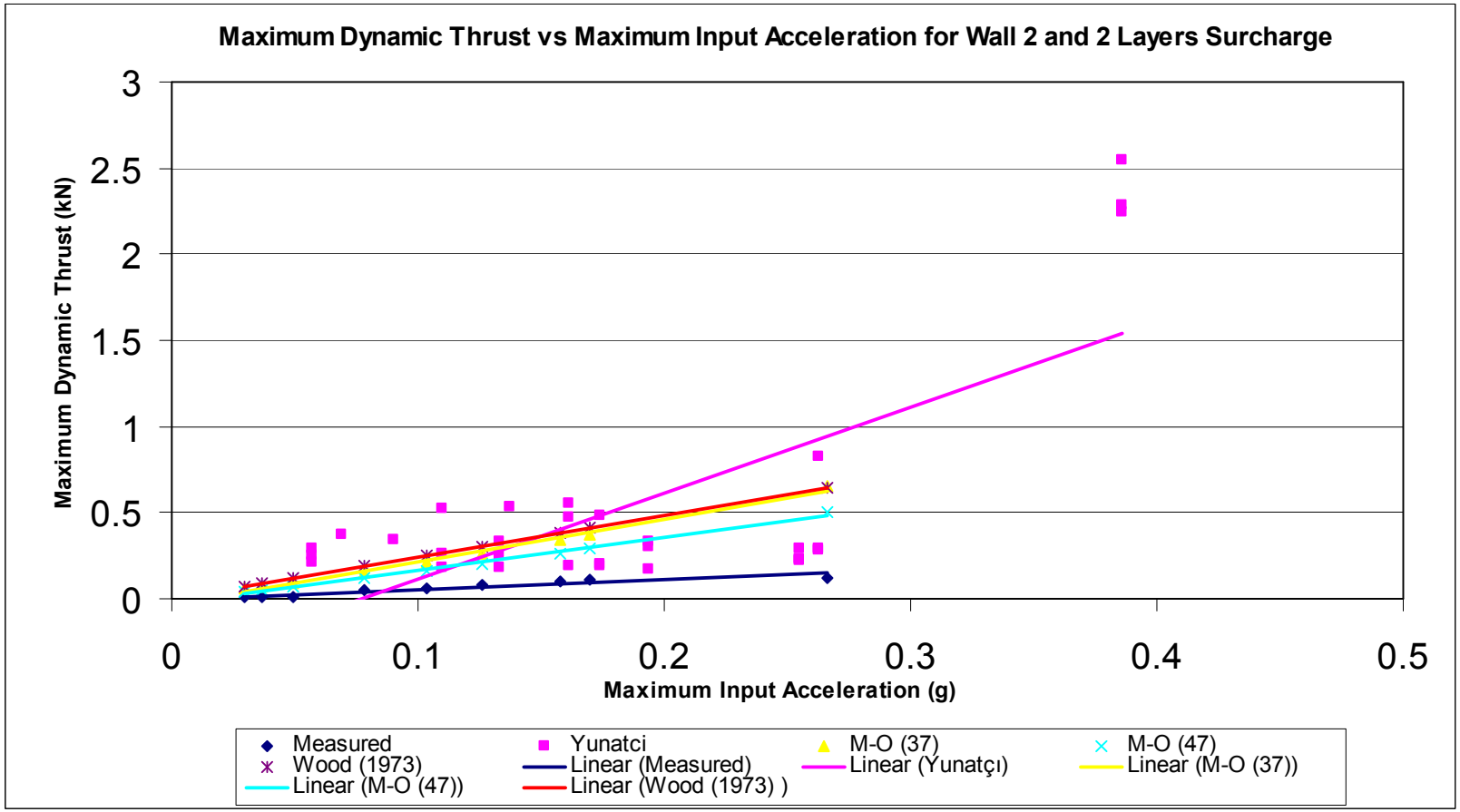

Figure 4.12 Variation of maximum horizontal dynamic thrust with respect to maximum input acceleration for Wall 2 and 2 layers surcharge

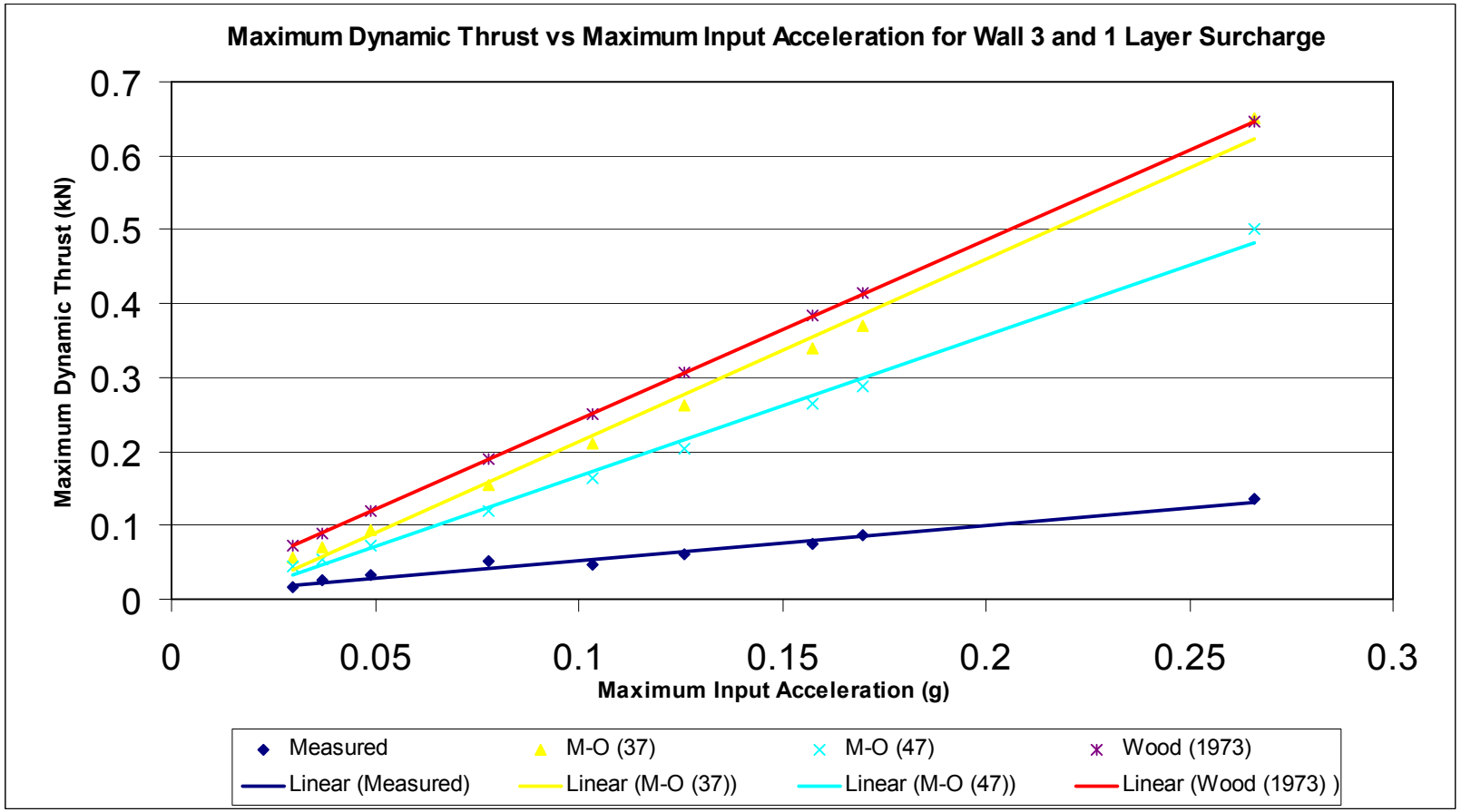

Figure 4.13 Variation of maximum horizontal dynamic thrust with respect to maximum input acceleration for Wall 3 and 1 layer surcharge

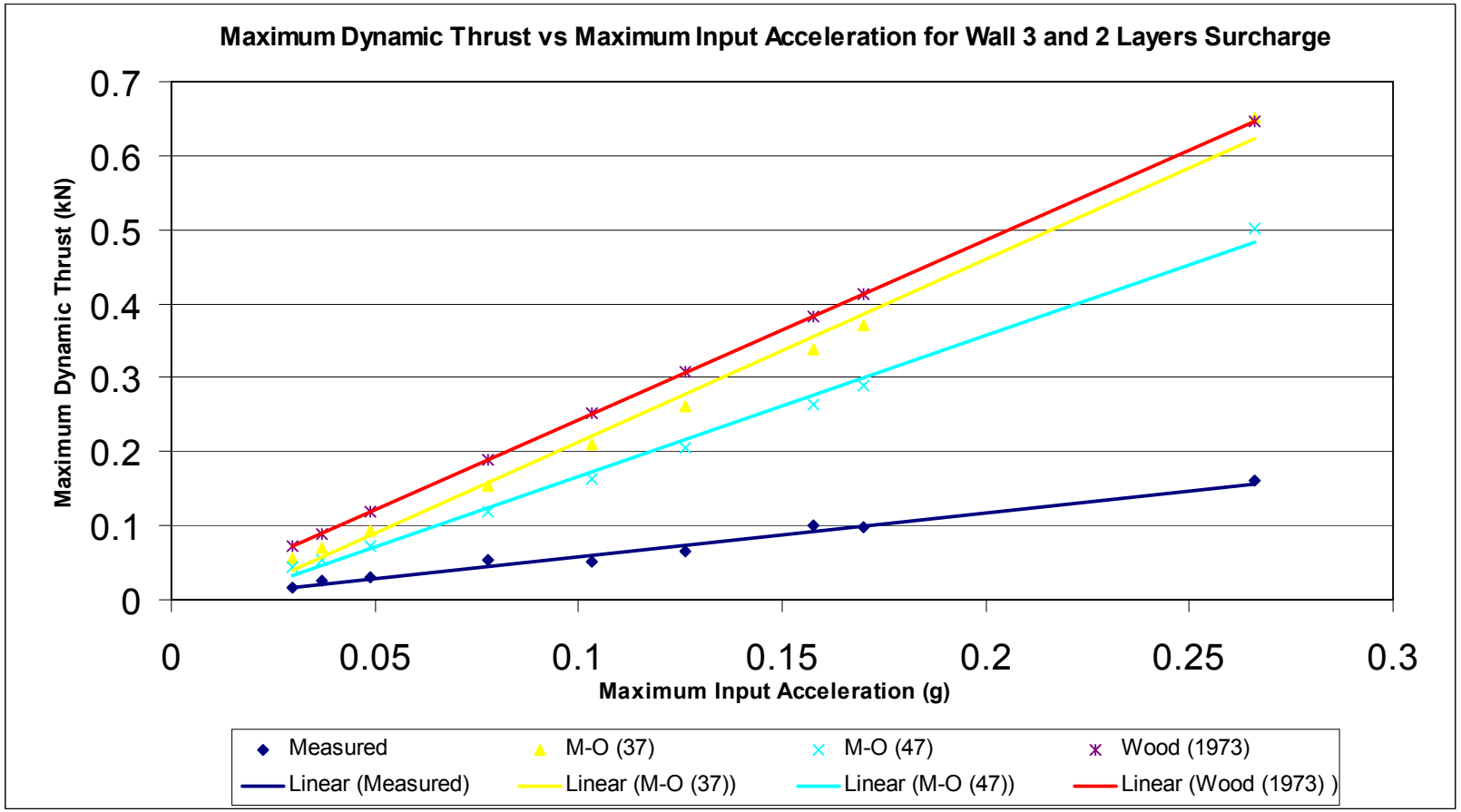

Figure 4.14 Variation of maximum horizontal dynamic thrust with respect to maximum input acceleration for Wall 3 and 2 layers surcharge

4.6 Application Point of Maximum Horizontal Dynamic Thrust

The application point of the resultant dynamic thrust is found by dividing total moment of the dynamic earth pressure with respect to the bottom of the wall with the maximum total thrust. Height of the application point from the bottom of the soil bin is drawn against maximum input accelerations for different wall types and surcharge combinations (Figure 4.15).

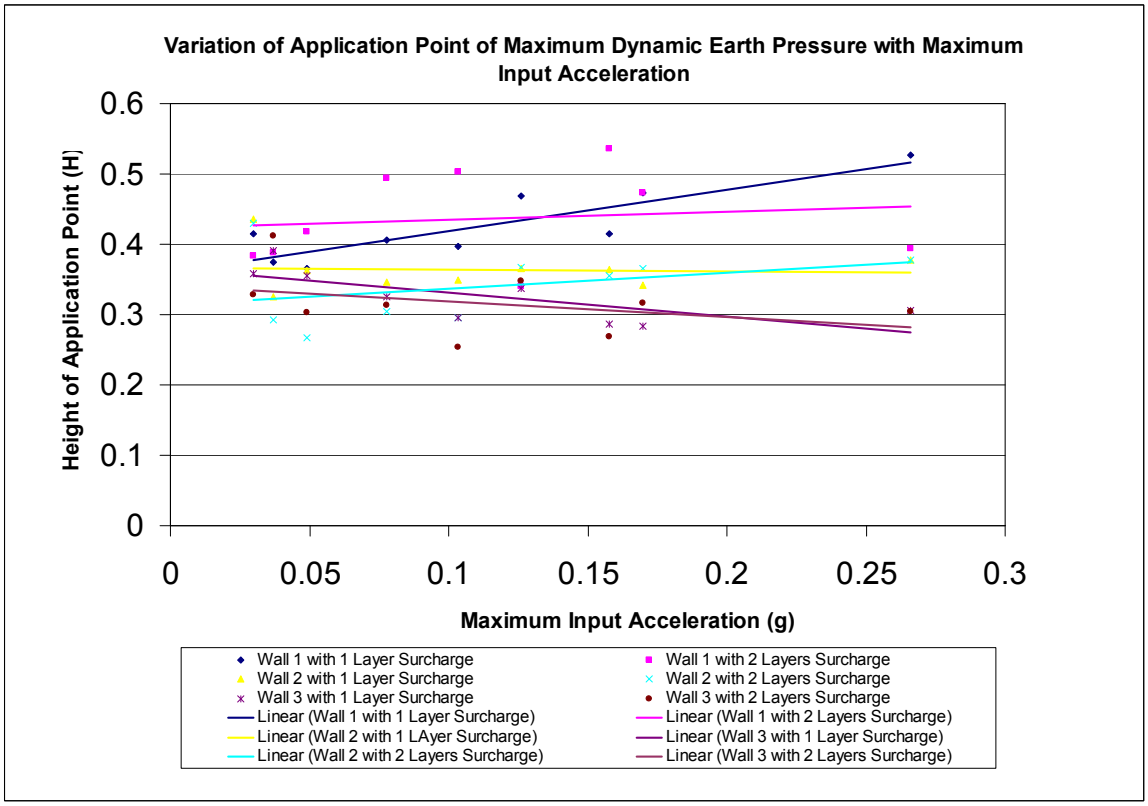

Figure 4.15 Variation of application point of maximum thrust with respect to maximum input acceleration

4.7 Effect of Wall Stiffness on Maximum Dynamic Thrust

Effect of wall stiffness on maximum dynamic thrust is investigated by changing the wall thicknesses. In addition, values obtained by this study are compared with the results obtained by Yunatçı (2003) who used a third bracing at the bottom of the model wall as shown in figure 4.1. Relative stiffness values were obtained by using SAP® finite element program. Walls with different thicknesses were modeled as beam elements having a unit length and thicknesses of 6.6, 3.2 and 2.0 mm respectively. Backfill was modeled with springs with changing stiffness values with respect to depth.

Modulus of subgrade reaction values were needed to be found to assign stiffness values to the horizontal springs. Lateral load – displacement behavior of a soil can be represented using following formula (Birand, 2001):

$$p = k_0 z^n y \tag{4.1}$$

where

k_0 = coefficient of subgrade reaction
z = depth
p = load
y = displacement
n = coefficient used to define the behavior of load – displacement curve. For granular soils it is 1 (Birand, 2001)

Therefore the stiffness values assigned to the springs can be given as:

$$k(z) = k_0 z^n \tag{4.2}$$

Birand (2001) suggests a k_0 value between 9600 and 80000 (kN/m^3) for medium dense sands. The relative density of the sand used in the experiments is 64% therefore it can be classified as medium dense sand (Lambe & Whitman, 1979).
An average value of 44800 kN/m^3 is used for k_0. Figure 4.16 shows the analysis model.

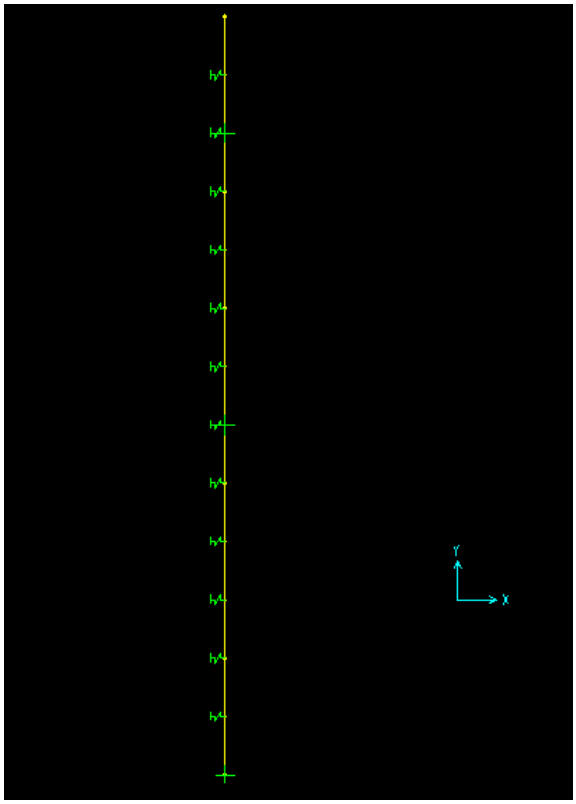

Figure 4.16 Finite element model used for the relative stiffness calculations

As the relative stiffness values of different walls were computed, a unit load is applied at the top of the model and its deflection was measured. The stiffness value for the thinnest wall is taken as unity (1 k). Stiffness values of other walls were computed and tabulated in table 4.6. Figure 4.17 and figure 4.18 show maximum thrust versus maximum input acceleration graphs for different wall models and compare them with the results obtained by Yunatçı (2003) and Çalışan (1999). Experiment layouts were also sketched on the graph. Çalışan had tested a braced rigid gravity wall in his experiments. The rigid gravity type wall had a mass of 483.49 kg and its height was 70 cm. It was braced at two levels.

Table 4.7 Relative stiffness values for different wall types

Wall Setup	Relative Stiffness Values (k)
Wall 1 (Thickness = 6.6 mm)	11.95121951
Wall 2 (Thickness = 3.2 mm)	2.327790974
Wall 3 (Thickness = 2.0 mm)	1

Figure 4.19 shows the variation of Maximum Seismic Thrust / Maximum Input Acceleration ratio with respect to relative stiffness values of different walls used in this study. Note that the stiffness of the model with thinnest wall section (Wall type 3 [T=2.0 mm]) is taken as unity (1 k).

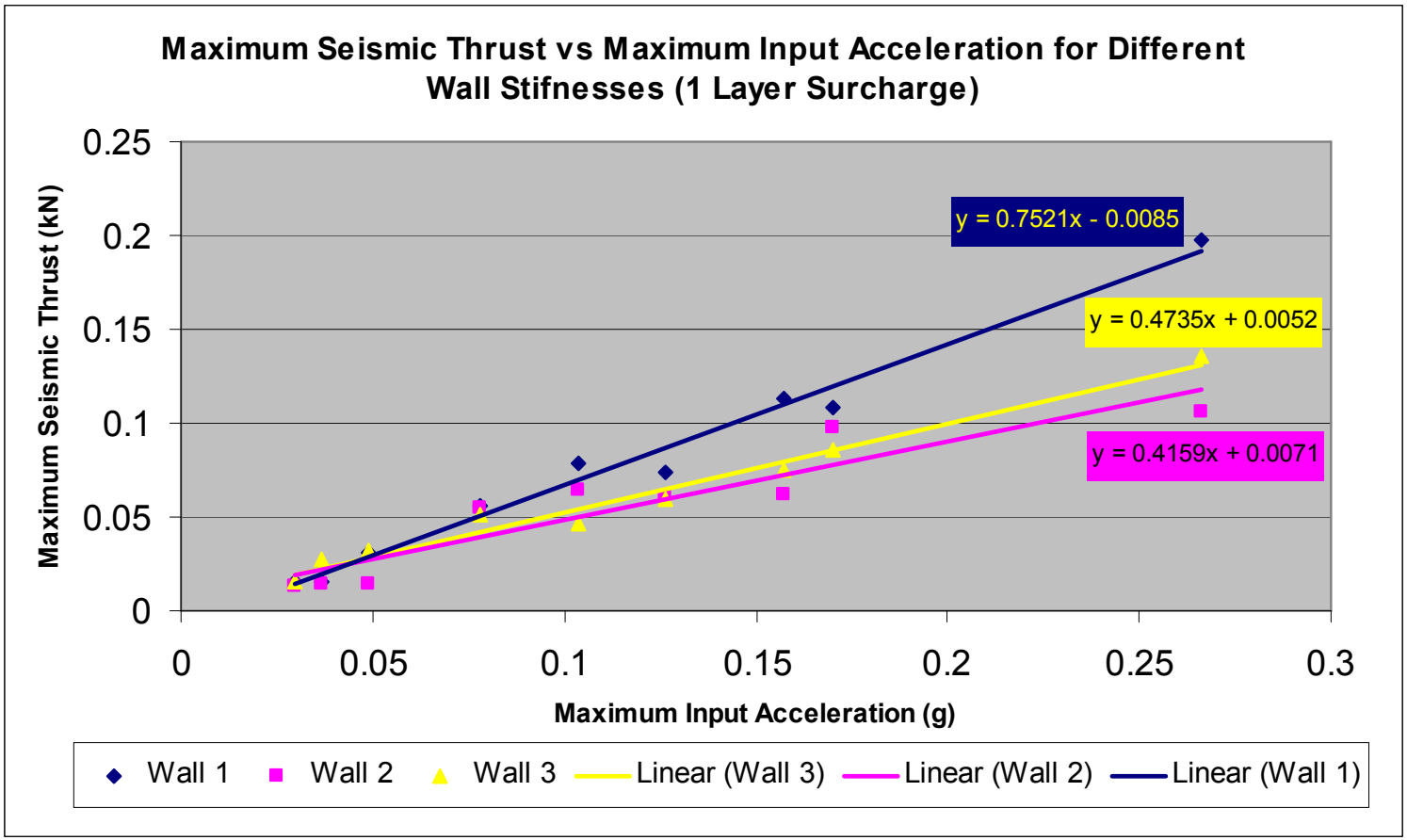

Figure 4.17 Variation of maximum horizontal dynamic thrust with respect to maximum input acceleration for 1 Layer Surcharge

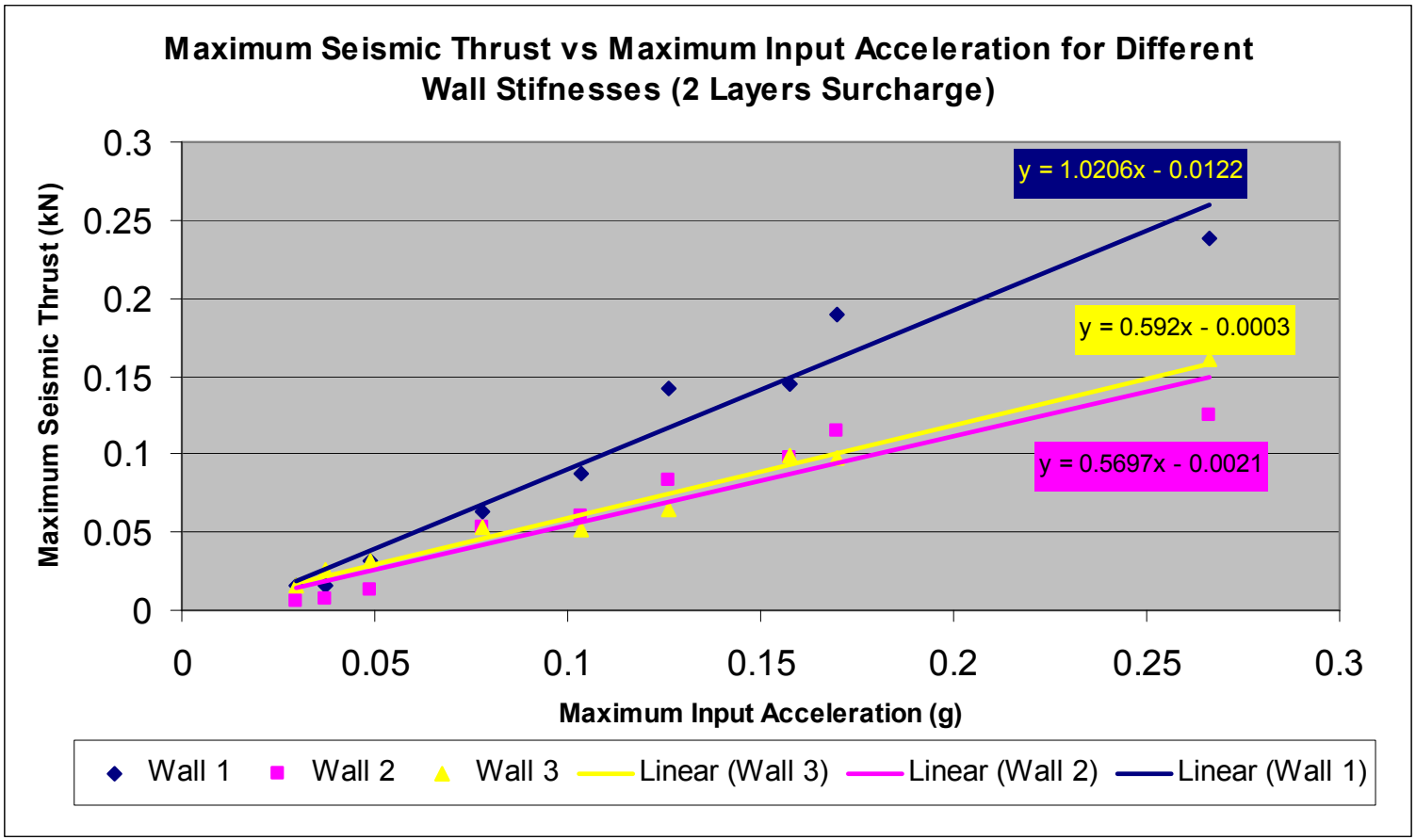

Figure 4.18 Variation of maximum horizontal dynamic thrust with respect to maximum input acceleration for 2 Layers Surcharge

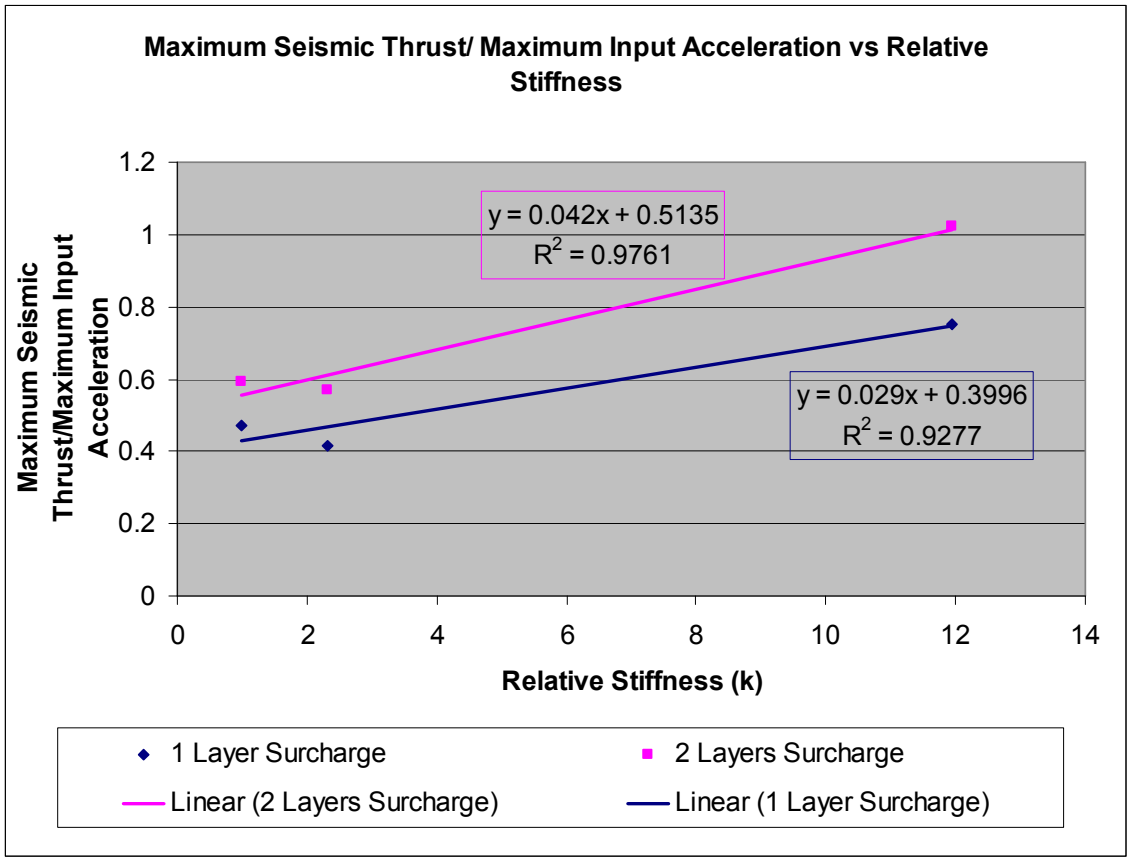

Figure 4.19 Variation of Maximum Seismic Thrust/Maximum Input Acceleration ratios with respect to Relative Stiffness

4.8 Effect of Surcharge on Maximum Dynamic Thrust

Following figure (Figure 4.20) shows the variation of maximum dynamic thrust against maximum input acceleration for different surcharge values.

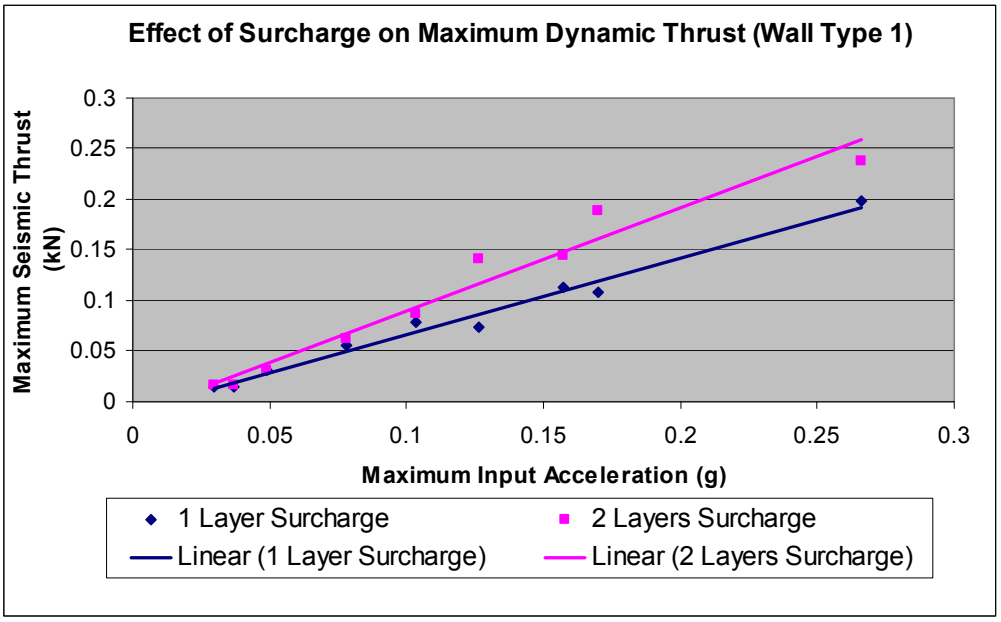

Figure 4.20 Variation of maximum dynamic thrust against maximum input acceleration for different surcharge values (Wall Type 1)

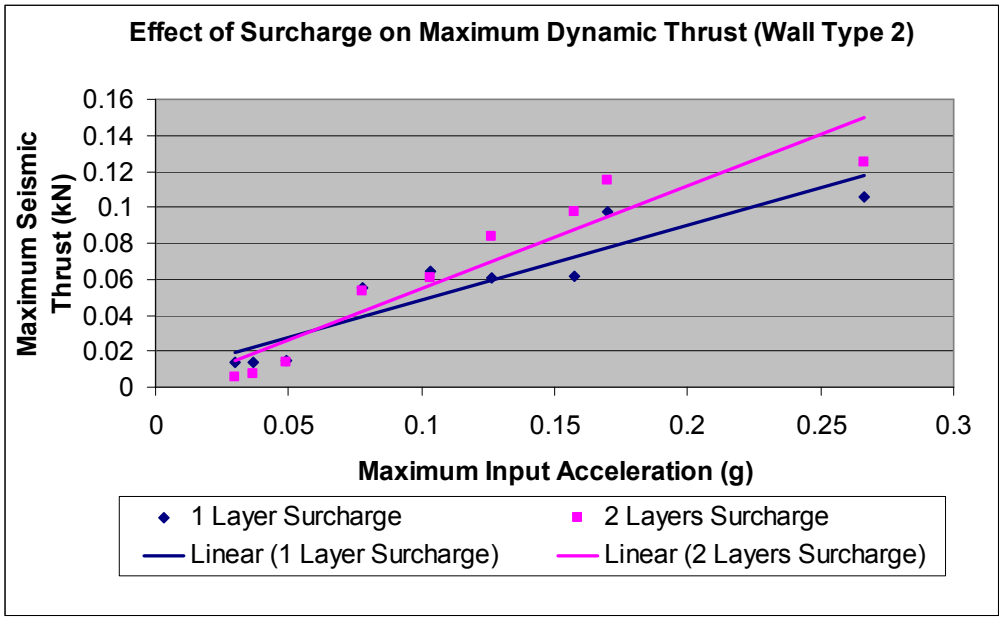

Figure 4.21 Variation of maximum dynamic thrust against maximum input acceleration for different surcharge values (Wall Type 2)

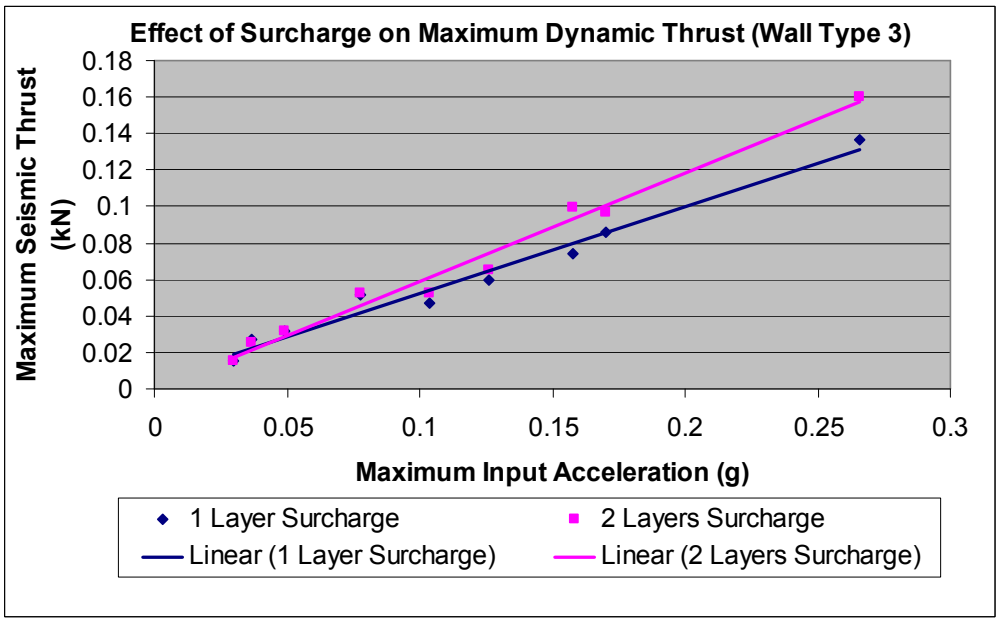

Figure 4.22 Variation of maximum dynamic thrust against maximum input acceleration for different surcharge values (Wall Type 3)

4.9 Dynamic Displacements

Following three figures shows the variation of dynamic displacements with respect to maximum input accelerations for different wall types.

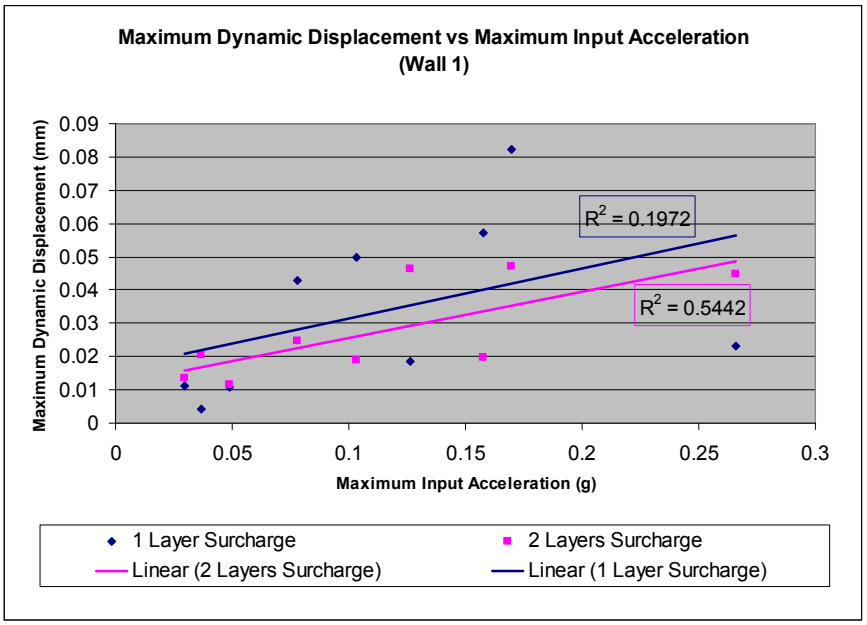

Figure 4.23 Variation of dynamic displacements with respect to maximum input accelerations for wall 1

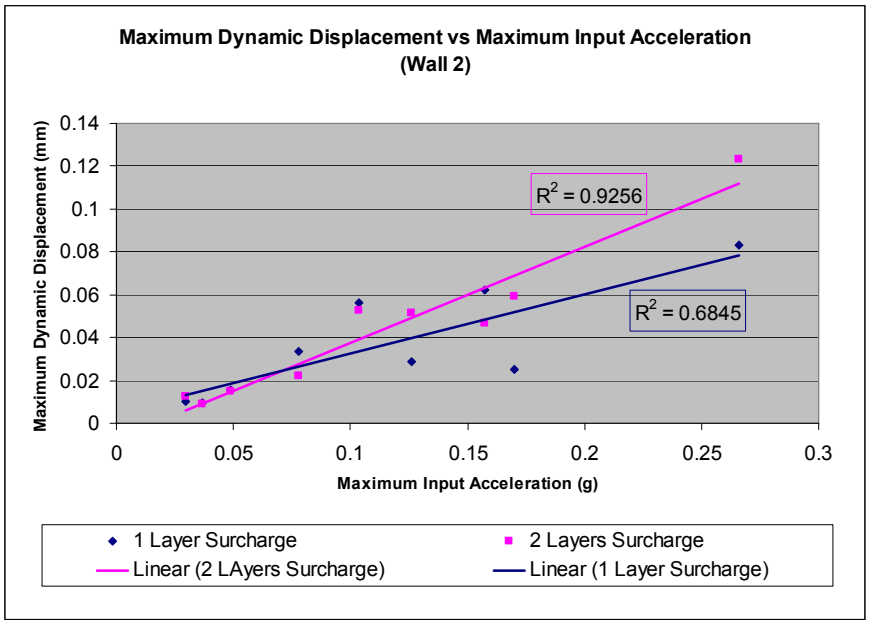

Figure 4.24 Variation of dynamic displacements with respect to maximum input accelerations for wall 2

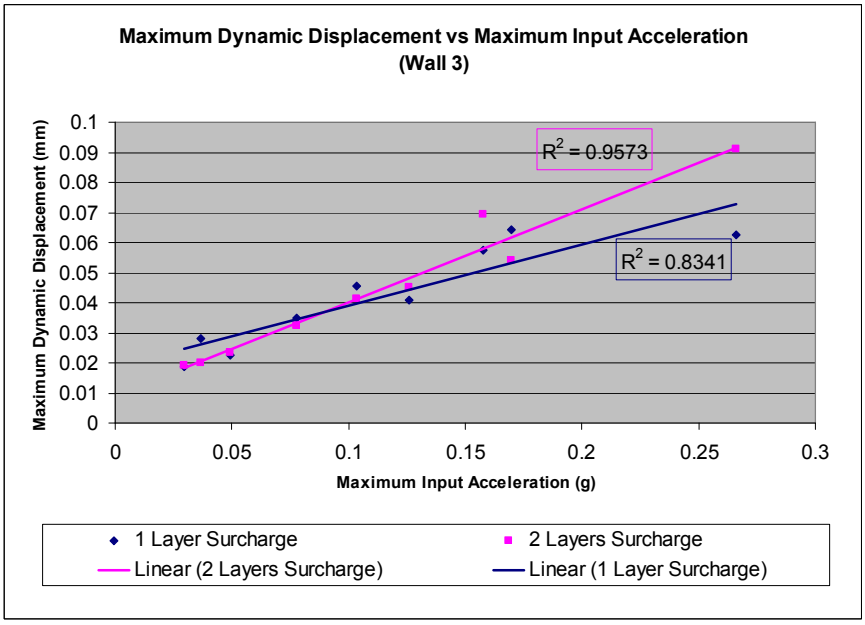

Figure 4.25 Variation of dynamic displacements with respect to maximum input accelerations for wall 3

CHAPTER 5

DISCUSSION OF THE TEST RESULTS

5.1 General

In this study, a series of shaking table tests had been performed in order to investigate the seismic behavior of laterally braced sheet pile walls. The study mainly focused on the effects of stiffness and surcharge on dynamic pressures developed on a sheet pile wall when small input motion accelerations are concerned. This chapter focuses on the interpretation of the test results obtained from shaking table tests. Discussion will be about acceleration amplification, maximum dynamic thrust and its point of application, effect of wall stiffness and surcharge on maximum dynamic thrust developed behind the wall and variation of maximum dynamic wall displacements with respect to maximum input accelerations.

5.2 Discussion of the Test Results

5.2.1 Acceleration Amplification

The accelerations were measured at three different levels, approximately 10 cm behind the back of the wall. Results obtained from accelerometers show that the relationship between input and backfill acceleration is not distinctive. On the other hand, as you can see in related figures (Figure 4.2 to 4.7), best lines drawn for the data pairs are nearly horizontal; indicating there is no clear amplification effect. In addition to that, at small input accelerations, normalized acceleration is very close to one. The results for the amplification effect were also compared with those obtained by Yunatcı (2003) for wall type 2 on the same graphs. For high accelerations such as 0.39g, measured top acceleration is almost 2.6 times greater than the input acceleration showing a clear amplification effect for Yunatcı (2003).

5.2.2 Maximum Dynamic Pressures

Although maximum registered pressure values at each cell do not have any meaning as the wall stability is concerned, it gives an idea about the variation of the pressure values with respect to input accelerations. Figure 4.8 clearly shows that pressure values increase with increasing input motion. In addition to that it tells us that pressure values in the vicinity of bracings (Pressure cell 1 near the top bracing and pressure cell 2 near second bracing) and at the bottom of the wall, where there is no movement, are greater than the one without any lateral support (Pressure cell 3).

5.2.3 Maximum Dynamic Thrust

Measured maximum seismic thrust values were compared with Wood's (1973) elastic solution for L/H value present in the model setup, M-O method for the angle of internal friction values of 37° and 47°, Yunatçı's (2003) study on laterally braced sheet pile wall with a thickness of 3.2 mm (See Figure 4.11 and 4.12). In every case, the seismic thrust increases with increasing input acceleration.

As the measured values were compared with Wood's solution it had been seen that they are larger than the results obtained in this study. But they are closer than those obtained by Yunatcı (2003) for 3.2 mm thick wall. M-O solutions for 37° and 47° internal friction angles are close to Woods (1973) solution and again larger than those obtained in this study.

5.2.3.1 Effect of Wall Stiffness on Maximum Dynamic Thrust

As you can see from figures 4.17 and 4.18 the magnitude of the maximum dynamic thrust significantly increases with increasing stiffness of the wall. In this study, wall type 1 (Thickness = 6.6 mm) has the greatest relative stiffness and exhibits larger magnitudes of seismic thrust.

Figure 4.19 shows the variation of the maximum seismic thrust to maximum input acceleration ratio with respect to changing relative stiffness values. As the wall gets stiffer this ratio increases.

5.2.3.2 Effect of Surcharge on Maximum Dynamic Thrust

Two different surcharge values (1.57 kPa and 3.14 kPa) were used in this study in order to investigate its effect on dynamic pressures. From figures 4.20 to 4.22 it can be seen that surcharge increases maximum dynamic thrust significantly.

5.2.4 Point of Application of Maximum Dynamic Thrust

No clear relationship between point of application of seismic thrust and maximum input acceleration was observed as you can see in figure 4.15. Values of point of application vary between 0.3H to 0.5H. On the other hand, it can be concluded that as the wall gets stiffer point of application of seismic pressure also increases approaching to 0.5H; hence to Wood's theoretical value (0.63H). There could be no clear relationship between surcharge values and point of application of seismic thrust observed. For the wall type 3 (the thinnest wall with thickness of 2.0 mm) the results are in close agreement with M-O.

5.2.5 Maximum Dynamic Displacements

The data for maximum dynamic displacements (Figure 4.21 to 4.23) is very scattered and does not show any clear relationship with respect to both surcharge and wall stiffness values. But it is obvious that with increasing acceleration the dynamic displacement values increase too.

CHAPTER 6

CONCLUSIONS

The results of the shaking table tests on laterally braced sheet pile walls with varying input acceleration levels, wall rigidness and surcharge yield the following conclusions:

1. A clear amplification effect is not observed during the tests. This result may be due to two reasons: (1) The input motion always remained at small acceleration levels and whole system moved as a single body with almost same accelerations in the backfill . In addition, the earth pressures levels were low, therefore the internal friction angle of the backfill was high (almost 55°). This can be interpreted as the soil body experiences very small shear deformations, and behaves in a rigid way. As Wood (1973) stated, for rigid systems no amplification was expected. (2) The height of the wall is small, therefore it was difficult to observe any amplification effect at small acceleration levels even it was present.
2. The variation of the dynamic earth pressures shows that at the points where almost no lateral wall displacements occurred (braced or fixed against lateral movement) the amount of earth pressures was higher. At the bottom, the wall was restricted against lateral displacements.. Therefore the dynamic earth pressures at the bottom cell were measured to be higher.
3. It was observed that the seismic thrust increases with increasing input acceleration. The maximum dynamic thrust values obtained always remained smaller than those found by using Wood's (1973) theoretical solution. It can be said that Wood's solution comprises a thoretical limit for the dynamic thrust values obtained in elastic excitation.
4. The results of the tests showed that the application point of seismic thrust moves upwards with increasing stiffness of the wall as Velestos and Younan (1997) stated. They approach to 0.5 H for a wall having a thichness of 6.6mm.
5. It was also seen that with increasing stiffness the maximum dynamic thrust values increase as Velestos and Younan (1997) and Gazetas (2004) stated. The ratio of

maximum dynamic thrust to maximum input acceleration also increases with increasing stiffness.

6. As the surcharge on top of the backfill is increased maximum dynamic thrust increases. It was observed that the amount of surcharge affects the ratio of maximum dynamic thrust to maximum input acceleration. As surcharge increases, this ratio increases. The amount of surcharge also affects the lateral dynamic wall displacements. Displacement values get higher for larger surcharge values.

REFERENCES

Birand, A. A., “Kazıklı Temeller”, Teknik Yayınevi, 2001

Bock, R.K. (1998, April), “Discrete Cosine Transform”, Retrieved June 15, 2005, from http://rkb.home.cern.ch/rkb/AN16pp/node61.html#SECTION00061000000000000000

Caltabiano, S., Cascone, E. and Maugeri M., “Seismic Stability of Retaining Walls with Surcharge”, Soil Dynamics and Earthquake Engineering, Volume 20, Issues 5-8, December 2000, pp. 469-476

Çalışan, O., “A Model Study On The Seismic Behavior of Gravity Retaining Walls”, Ph.D Dissertation, Middle East Technical University, Ankara, Turkey, January 1999

Das, B. M., “Fundementals of Soil Dynamics”, Elsevier Science Publishing Co. Inc., New York, 1983

Fukuoka, M., and Imamura, Y., “Researches on Retaining Walls During Earthquakes”, Proceedings of the Eight World Conference on Earthquake Engineering, San Francisco, 1984, pp. 501 – 508

Gazetas, G., Psarropoulos, P. N., Anastasopoulos, I. and Gerolymos, N., “Seismic behaviour of flexible retaining systems subjected to short-duration moderately strong excitation”, Soil Dynamics and Earthquake Engineering, Volume 24, Issue 7, September 2004, pp. 537-550

Ichihara, M. and Matsuzawa, H., “Earth Pressure During Earthquake”, Soils and Foundations, Japanese Society for Soil Mechanics and Foundation Engineering, Vol.13, No.4, Dec. 1973, pp. 75-85

Ishii, Y., Arai, H., Tsuchida, H., ”Lateral Earth Pressure in an Earthquake”, Proceedings Second World Conference on Earthquake Engineering, Vol.2, 1960, pp.211-230

Kramer, S.L., “Geotechnical Earthquake Engineering”, Prentice Hall, 1996

Lambe, T.W., Whitman, R.V., “Soil Mechanics”, John Wiley and Sons, 1979

Matuo, H. and Ohara, S., “Lateral Earth Pressure and Stability of Quay Walls During Earthquakes”, Proceedings Second World Conference on Earthquake Engineering, Vol.2, 1960, pp. 165-181

Murphy, V.A., “The Effect of Ground Characteristics on the Aseismic Design of Structures”, Proceedings Second World Conference on Earthquake Engineering, Vol.1, 1960, pp.231-236

Nadim, F. and Whitman, R.V., “Coupled Sliding and Tilting of Gravity Retaining Walls During Earthquakes”, Proceedings of the Eight World Conference on Earthquake Engineering, San Francisco, 1984, pp.477-484

Nandakumaran, P. and Joshi, V.H., “Static and Dynamic Active Earth Pressures Behind Retaining Walls”, Paper No.136, Bulletin I.E.S.T., Vol.10, No.3, pp.113-123,Sept. 1973

Nazarian, H.N., and Hadjian, A.H., “Earthquake-Induced Lateral Soil Pressures on Structures”, Journal of Geotechnical Engineering Division, ASCE, No.GT9, September 1979, pp.1049-1066

Prakash, S., and Basavanna, B.M., “Earth Pressure Distribution Behind Retaining Wall During Earthquake”, Proceedings, Third Symposium on Earthquake Engineering, Nov.1966

Rad, N.S., Tümay, M.T., “Factors Affecting Sand Specimen Preparation by Raining”, Geotechnical Testing Journal, Vol.10, No.1, pp.31-37

Richards, R.Jr., and Elms, D.G., “Seismic Behavior of Gravity Retaining Walls”, Journal of Geotechnical Engineering Division, ASCE, No.GT4, April 1979, pp.449-465

Saran, S., and Prakash, A., “Seismic Pressure Distribution in Earth Retaining Walls”, Proceedings of the Third European Symnposium on Earthquake Engineering, Sofia, September 1970, pp.355-362

Scott, R.F., “Earthquake Induced Earth Pressures on Retaining Walls”, Proceedings of the Fifth World Conference on Earthquake Engineering, Rome, 1973, Session 4D, 202

Seed, H.B. and Whitman, R.V., “Design of Earth Retaining Structures for Dynamic Loads”, Lateral Stresses in the Ground and Design of Earth Retaining Structures, ASCE, 1970, pp.103-147

Sherif, M.A., Ishibashi,I. and Lee, C.D., “Earth Pressures Against Rigid Retaining walls”, Journal of Geotechnical Engineering Division, ASCE, No.GT5, May 1982, pp.679-695

Velestos, A. S., Younan A. H., “Dynamic Response of Cantilever Retaining Walls”, ASCE Journal of Geotechnical and Geoenvironmental Engineering, Vol.123, No.2, February 1997, pp.83-88

Yunatcı, A. A., “A Model Study on the Seismic Behavior of Laterally Braced Sheet Pile Walls”, M.Sc. Thesis, Middle East Technical University, Ankara, Turkey, January 2003

APPENDIX A

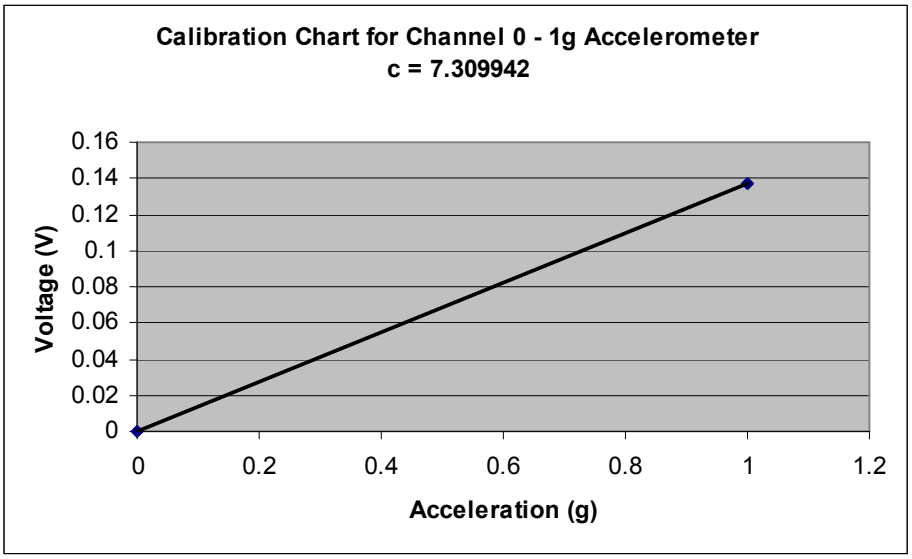

Figure A.1 Calibration Chart for 1-g Capacity Accelerometer

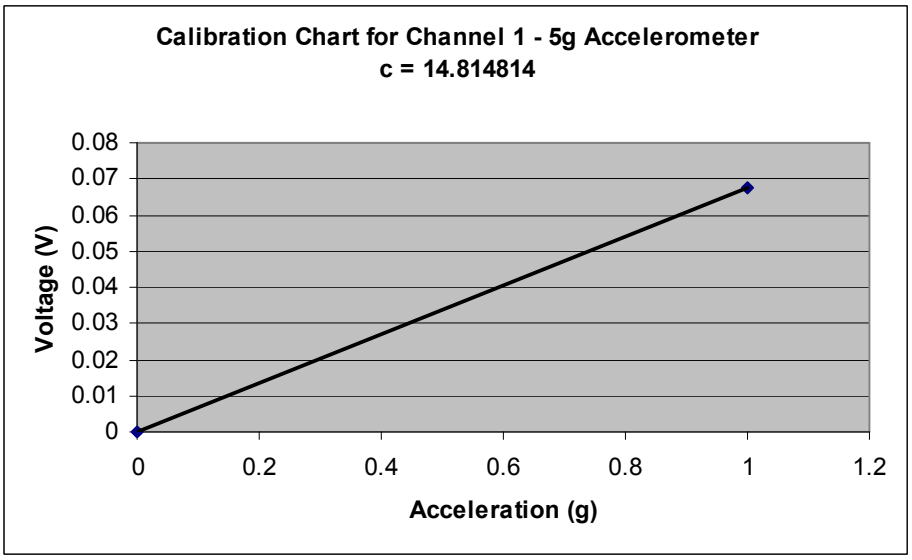

Figure A.2 Calibration Chart for 5-g Capacity Accelerometer

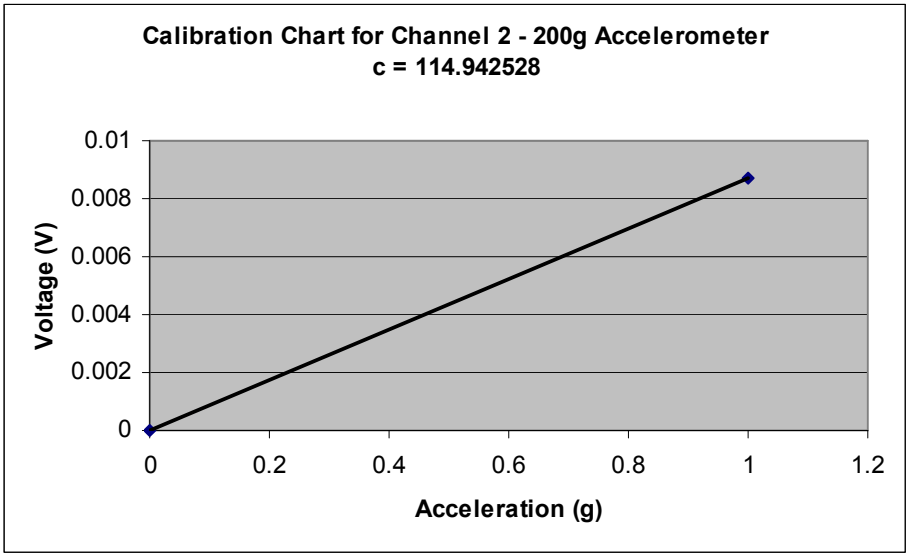

Figure A.3 Calibration Chart for 200-g Capacity Accelerometer

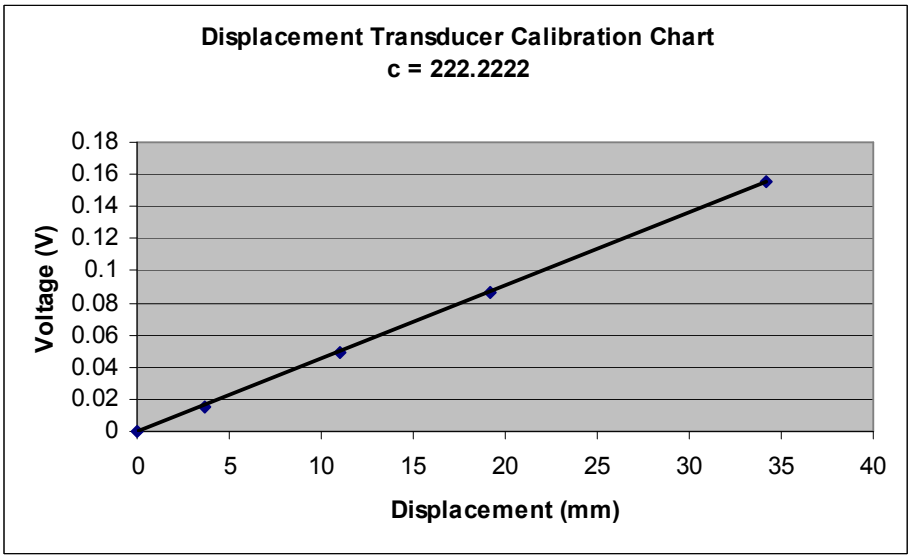

Figure A.4 Calibration Chart for Displacement Transducer

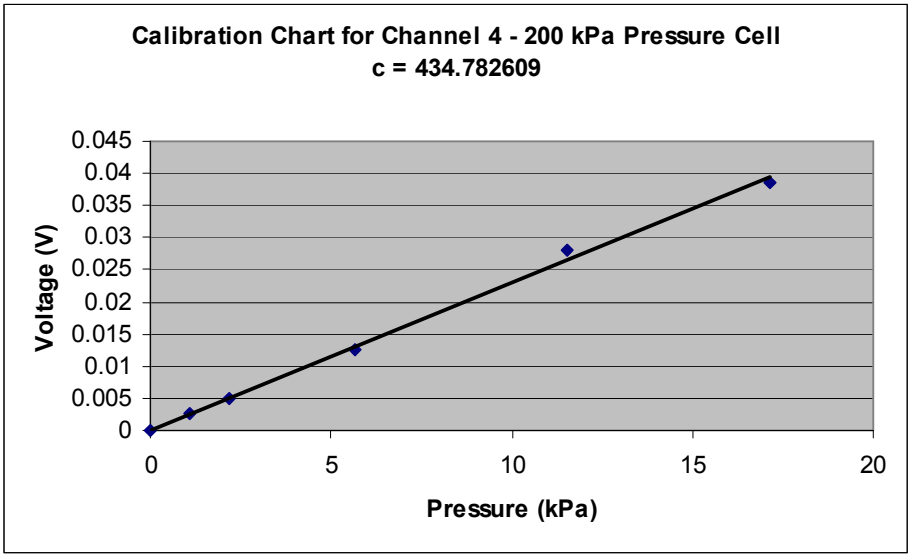

Figure A.5 Calibration Chart for Channel 4 – 200 kPa Earth Pressure Transduces (Ser. No: BP7332)

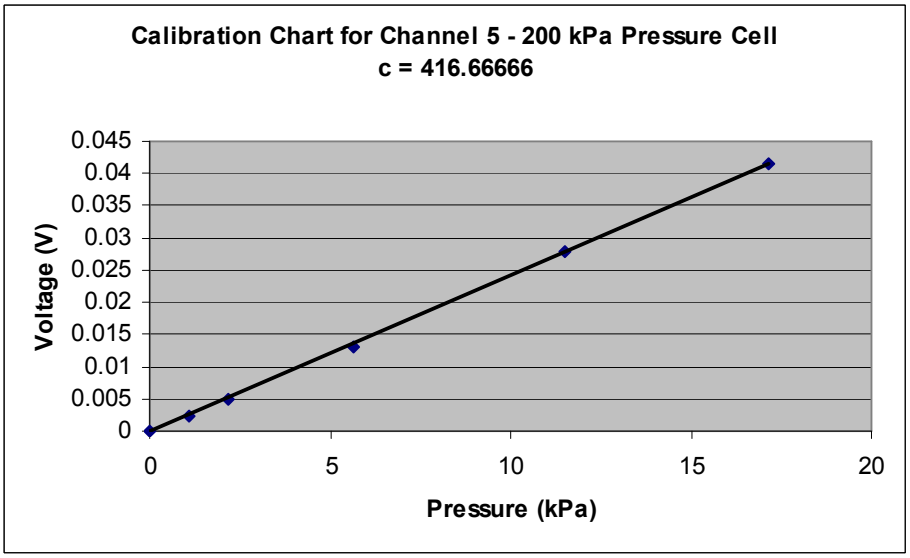

Figure A.6 Calibration Chart for Channel 5 – 200 kPa Earth Pressure Transduces (Ser. No: BP6324)

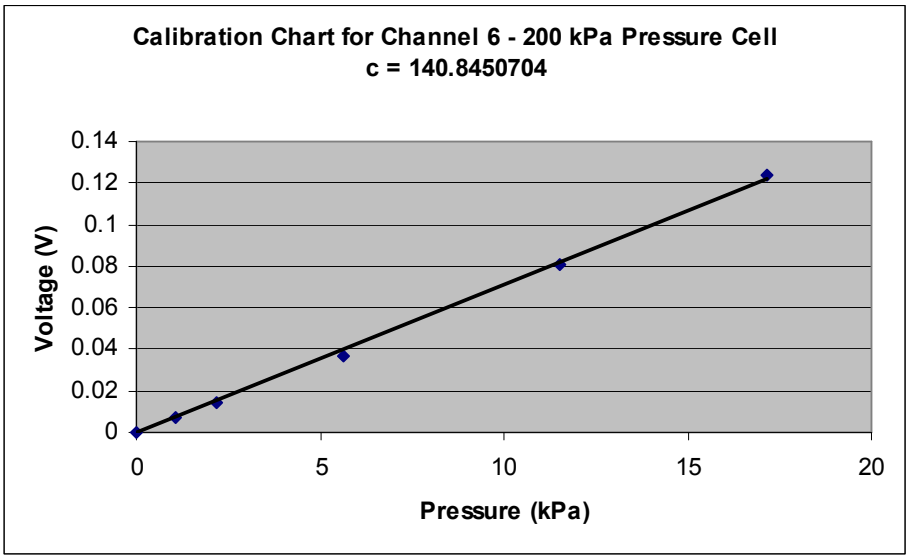

Figure A.7 Calibration Chart for Channel 6 – 200 kPa Earth Pressure Transduces (Ser. No: BP2455)

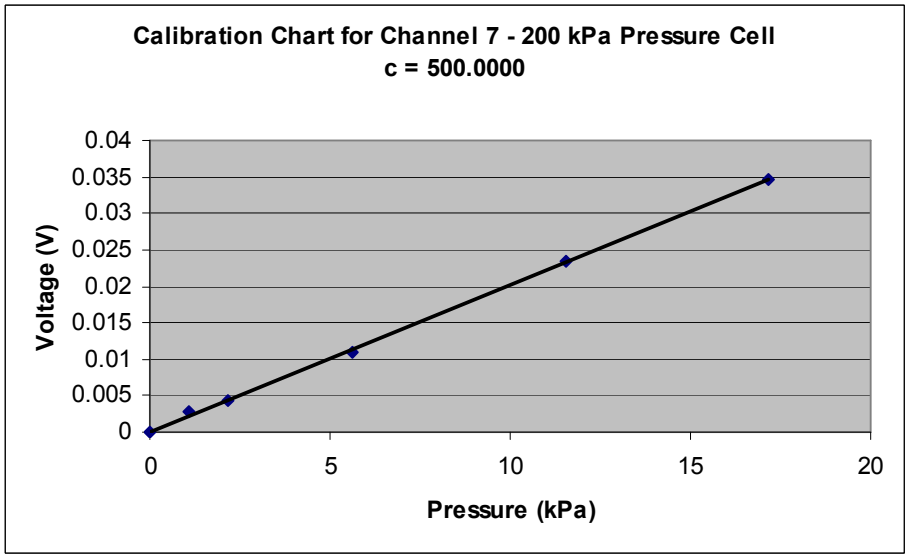

Figure A.8 Calibration Chart for Channel 7 – 200 kPa Earth Pressure Transduces (Ser. No: BP5297)

APPENDIX B

B.1 TECHNICAL SPECIFICATIONS FOR TRANSDUCERS

- EARTH PRESSURE CELLS (SER. NO. 7332, 5297, 6324, 2455)

TML (Tokyo Sokki Kenkjuyo, LTD) KDF-200 kPa

Capacity	: 200 kPa
Rated Output	: 0.3mV/v
Non – linearity	: 2% RO
Temperature range Allowable	: -20 ~+60° C
Resistance	: 350 Ω
Exciting Voltage Recommended	: less than 3 V
Exciting Voltage Allowable	: 10 V
Weight	: 160 g

- ACCELERATION TRANSDUCERS

TML ARF – 50 A (83105)

Capacity	: 50 m/s^2
Rated Output	: 0.5mV/v
Non – linearity	: 1% RO
Frequency Response	: 120 Hz
Temperature range Allowable	: 0 ~+50° C
Overload	: 300 %
Resistance	: 120 Ω
Exciting Voltage Recommended	: less than 2 V
Exciting Voltage Allowable	: 5 V
Weight	: 13 g

B.1 TECHNICAL SPECIFICATIONS FOR TRANSDUCERS

- DISPLACEMENT TRANSDUCER

TML SDP – 100C

Capacity	: 100 mm
Rated Output	: 2.5 mV/v +/- 0.2 %
Sensitivity	: 50 x 10^{-6} mm
Non – linearity	: 0.2% RO
Spring Force	: 5.9 N
Frequency Response	: 1 Hz
Temperature range Allowable	: 0 ~+ 50° C
Resistance	: 350 Ω
Exciting Voltage Recommended	: less than 2 V
Exciting Voltage Allowable	: 5 V

Technical specifications for 1-g and 200-g accelerometer are not listed here.

APPENDIX C

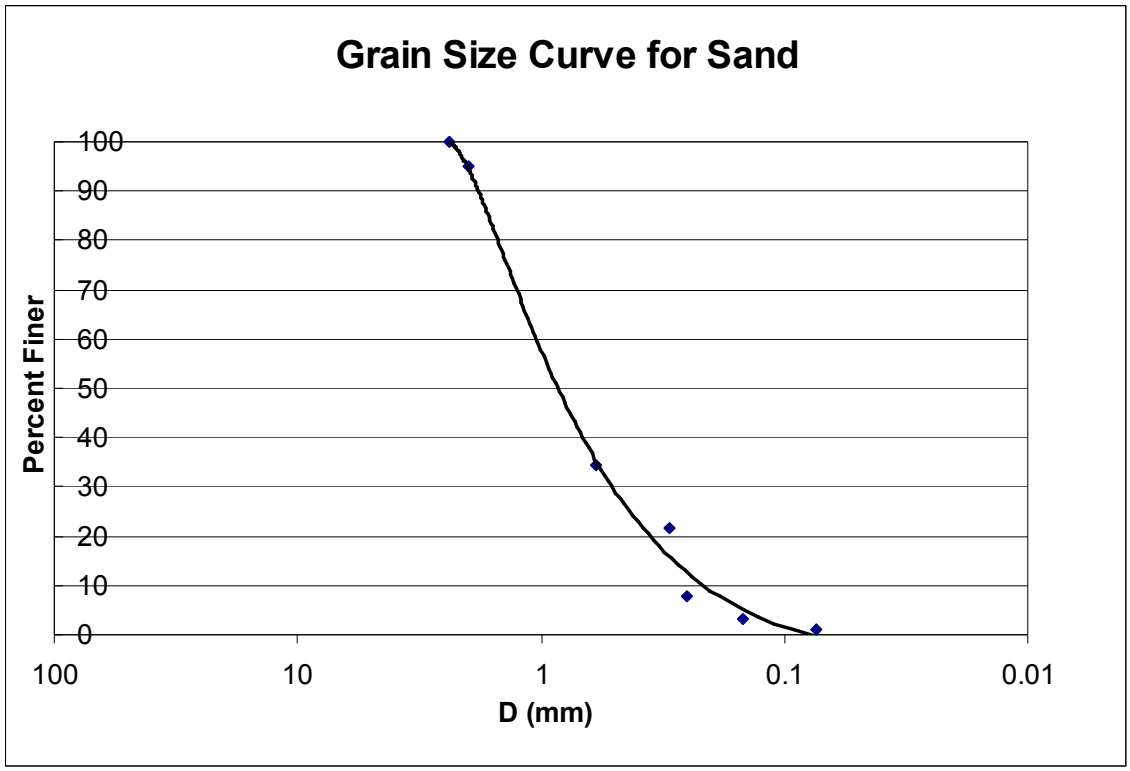

Figure C.1 Grain size distribution curve for sand

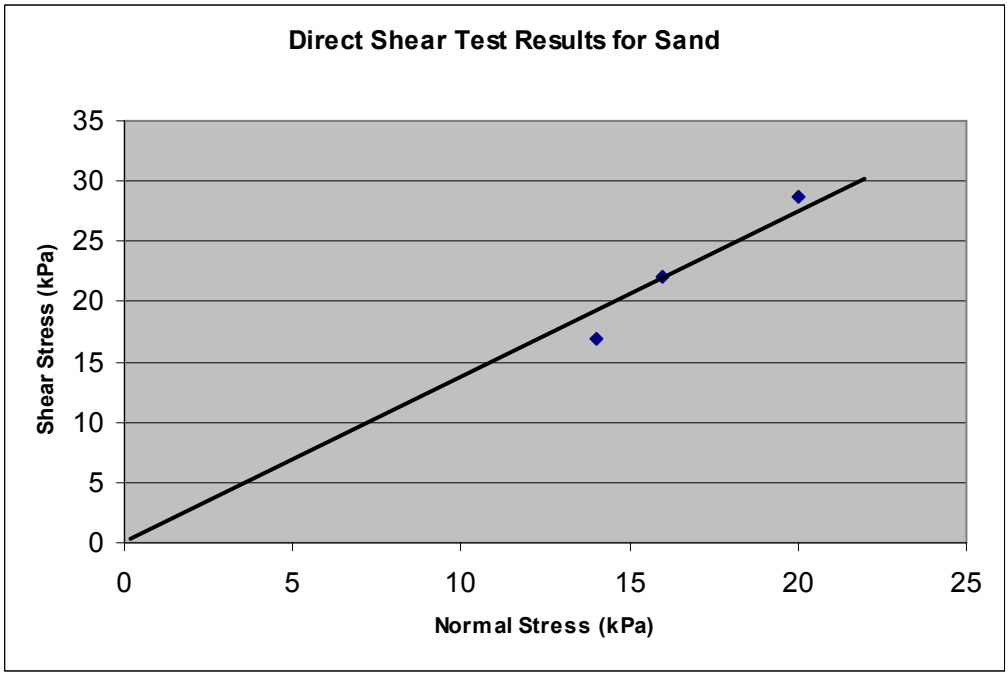

Figure C.2 Direct shear test results for sand